MSc. Thesis

Tyre parameter identification from road tests on a complete vehicle

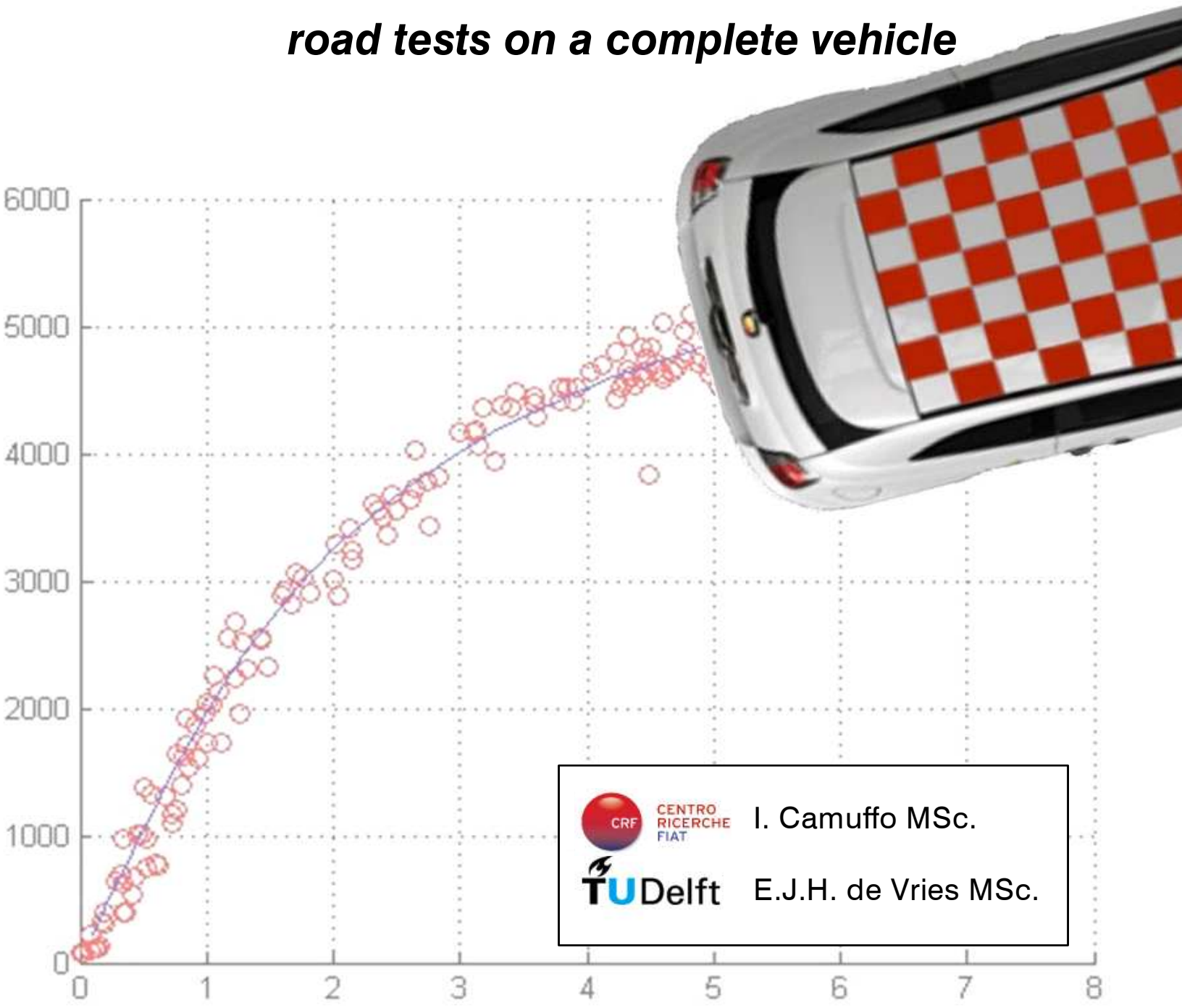

CRF CENTRO RICERCHE FIAT — I. Camuffo MSc.

TU Delft — E.J.H. de Vries MSc.

D. Lo Conte

Delft, April 2010

Abstract

Vehicle manufacturers notice a difference between the tyre behaviour observed in road tests with a complete vehicle and the behaviour of the tyre as provided by the tyre manufacturers. To improve the tyre characterization and avoid appointing its behaviour each time using trial-and-error, Centro Ricerche Fiat requests the development of an application that can identify the tyre parameters consistently and automatically.

This thesis describes the process of developing the TyreEstimator, the application written for the identification of the tyre parameters. The application is built to minimize the difference between the vehicle model data and the experimental data using an optimization algorithm. Two vehicle models are implemented to identify the tyre parameters. The tyre behaviour is described using the Magic Formula tyre model. Due to the sensitivity of the optimization problem, the application is constructed to cope with different options for finding the tyre parameters.

Afterwards an empirical analysis, using the TyreEstimator, is performed. This results in an option set for each vehicle model, which approaches the tyre behaviour best.

Acknowledgements

As customary, I would like to thank here the people without whom this MSc. thesis would not have been possible. First of all I want to thank the Centro Ricerche Fiat for their help and collaboration. In particular I thank I. Camuffo MSc. and the people of the Vehicle Dynamics Group at CRF for giving me the possibility to develop myself academically as well as personally.

Next to that, I am grateful to the TU Delft, and especially my supervisor E.J.H. de Vries MSc. for sharing his extensive knowledge and for his patience. Moreover, I thank D.J. Rixen Prof. Dr. MSc. and P.Th.L.M. van Woerkom Dr. MSc. for introducing me to the wonderful world of dynamics.

Furthermore, I would like to thank my parents, my sister, my girlfriend and the rest of my family for their loving support, their visits and contributions to this thesis. Special thanks go out to the people I have met in Turin, who made my stay an everlasting memory.

Finally, I am grateful to Evert, Noë, Nick and Coen for the criticism while reviewing my thesis. Last but not least, I thank everyone that was there from the beginning of my study together with all the guys of the platform for their help and joyfulness.

Delft, April 2010

Dario Lo Conte
dariolc@yahoo.com

Contents

Nomenclature

General

a_y	lateral acceleration
$C_{F\alpha}$	cornering stiffness
$C_{F\alpha1}$	cornering stiffness at front axle
$C_{F\alpha2}$	cornering stiffness at rear axle
F_y	lateral force
F_{y1}	lateral force at front axle
F_{y2}	lateral force at rear axle
F_z	vertical tyre force
g	gravity constant
I	vehicle inertia
L	vehicle length
m	vehicle mass
P_1	load on front axle
P_2	load on rear axle
r	yaw rate
R	radius of curvature
u	longitudinal velocity at centre of gravity
u_1	longitudinal velocity at front axle
u_2	longitudinal velocity at rear axle
v	lateral velocity at centre of gravity
v_1	lateral velocity at front axle
v_2	lateral velocity at rear axle
V	velocity at centre of gravity
x,y,z	local coordinates
X,Y,Z	global coordinates
x_1	distance between front axle and centre of gravity
x_2	distance between centre of gravity and rear axle
α	slip angle
α_1	slip angle front axle
α_2	slip angle rear axle
β	side slip angle
δ_1	steer wheel angle
η	understeer coefficient
θ	roll angle
λ	root characteristic equation
ψ	yaw angle

Related to the Magic Formula

B_y	lateral stiffness factor
C_y	lateral shape factor
df_z	normalised change in normal load
D_y	lateral peak value
E_y	lateral curvature factor
F_{z0}	nominal tyre load
p	coefficients of Magic Formula
α_y	slip angle
γ_y	camber angle
λ	scaling factors of Magic Formula

Introduction

This research was carried out upon request of the Centro Ricerche Fiat (CRF). At the same time it is my Master thesis for the specialization Engineering Mechanics of the Master Precision & Microsystems Engineering at the faculty of Mechanical Engineering of the Delft University of Technology, the Netherlands.
Within CRF the research was executed for the Vehicle Dynamics Group of the Vehicle Dynamics and Fuel Economy department. My company-tutor was I. Camuffo MSc. and at TU Delft my supervisor was E.J.H. de Vries MSc. The goal of this project is to develop a computer application which can be used for calculating automatically the tyre parameters corresponding to the vehicle behaviour gathered from experimental data.

Background

Centro Ricerche Fiat (CRF) was founded in 1976 as the Fiat Group's major source of expertise in innovation, research and development. It is established as a consortium, whose shareholders are Fiat Group companies. CRF employs more than 850 professionals. The head office, within which this research was performed, is located in Orbassano near Turin in Italy. The other three offices are also located in Italy in Trento, Bari and Foggia. Separately, CRF collaborates with the Centro Studi Sistemi di Trasporto (CSST) of Turin and holds a controlling interest in the Plastics and Optics Research Centre (CRP).
The Centro Ricerche Fiat has achieved significant results, as can be deduced from the total number of patents held (over 2300, with 600 applications still pending). The 50 awarded European projects confirm its significant contribution to European research.

Figure 1 Head office of CRF in Orbassano

CRF's objective is to use innovation as a strategic lever and to enhance the results of its work. The development and implementation of new content makes it possible to produce distinctive and competitive products. The consortium is therefore able to play an active role in the technological growth of the different community areas of the Fiat Group and its partners.

Moreover, CRF is active in the sustainable mobility research field. Their activities focus on investigating innovative solutions that address all aspects of sustainability in transport, among which reducing emissions and noise pollution are significant issues. Furthermore, increasing fuel efficiency by reducing vehicle weight, and improving its dynamics and aerodynamics is being researched thoroughly. The overall aim of CRF is to obtain more ecological, safer and more comfortable vehicles. With respect to the latter two, tyre aspects and thus tyre characterization are of vital importance.

Context

The tyre data supplied by tyre manufacturers is generally not fully representative of the behaviour of tyres on the road. This is due to the different testing conditions; individual testing of a tyre on a roller bench or a flat track as opposed to tyre testing on a complete vehicle on the road. Also the changing conditions due to tyre wear and the different test environments influence this process. Therefore vehicle manufacturers have to modify the tyre data in order to improve the numerical-experimental correlation at vehicle level and are able to validate vehicle models with data coming from experimental tests.

The standard approach for the validation of a vehicle model for handling analysis consists first in the validation of the suspension models. These models are validated using the experimental data from the elasto-kinematic bench tests. For these tests the suspensions and their components are excited and the response is measured. Afterwards the complete vehicle model is validated against the test data coming from road tests. For this validation the model is adjusted by acting upon the parameters of the tyre model.

Until now this last validation has been undertaken by engineers at CRF. They modify the tyre model parameters individually and simulate the behaviour of the vehicle until it matches the behaviour that emerges from the experimental data. This starts

with tuning the parameters that influence the quasi-static lateral behaviour of the vehicle, which are induced by manoeuvres with slow dynamics. The verification is then extended to the parameters that influence the transient behaviour and those influencing the combined behaviour (lateral and longitudinal loads). This trial-and-error method can take up some days of work and reduces the reliability and reproducibility of the validation process. It is clear that this process is time consuming, not consistent and not efficient.

Task

To improve the characterization of tyres from road tests an application needs to be developed that automates the identification of tyre model parameters. The Magic Formula tyre model is used to represent the tyre behaviour. This model is available in literature and used all over the world for this purpose. The application should be capable of taking into account data from experimental manoeuvres and perform simulations with different vehicle models (available within CRF), where the input data is represented by the tyre parameters.

Using optimization algorithms, the application has to minimize the difference between the data obtained by experimentally performed manoeuvre on the test track and the data coming from the simulated manoeuvre using a vehicle model. By obtaining the tyre parameters with the same method every time, the process is better reproducible and has a higher reliability than the manual process. In addition, the employees at CRF need less time to characterize the tyres and can invest their time more effectively. The original assignment formulated by CRF (in Italian) can be found in Appendix A.

Outline

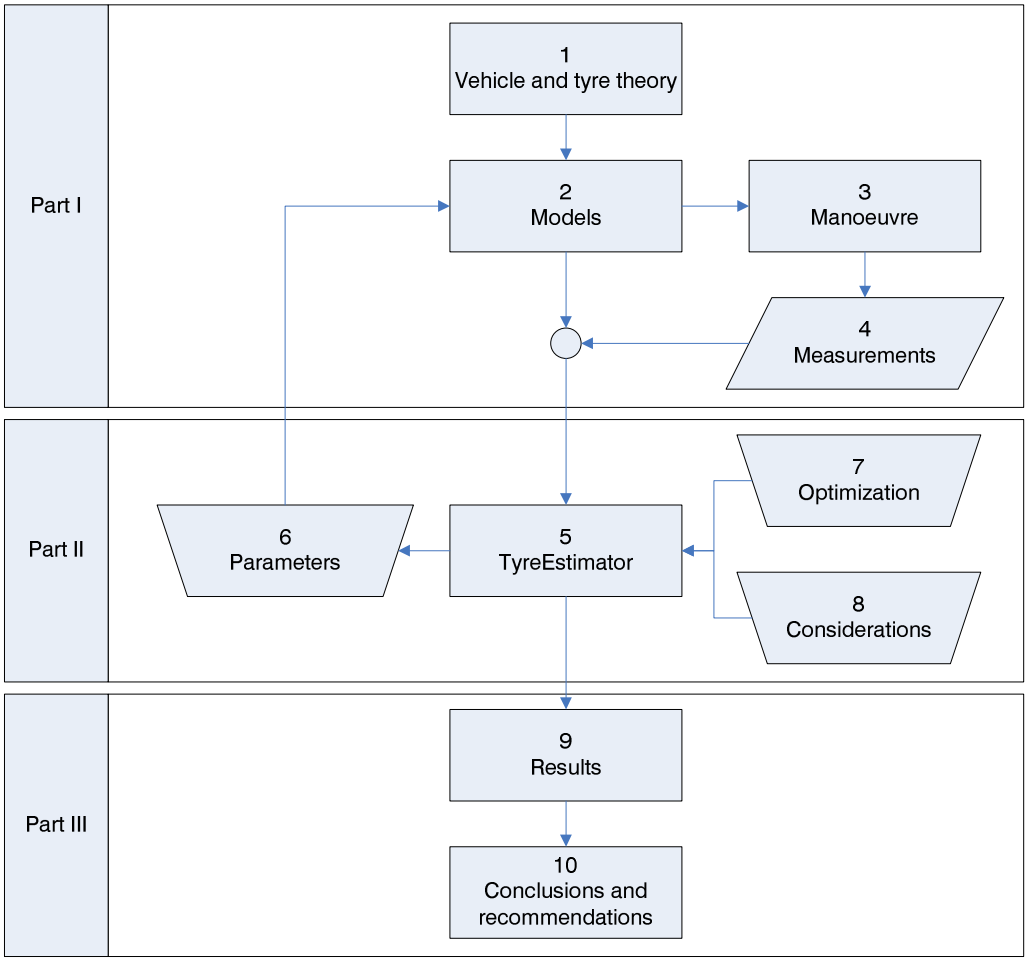

Figure 2 Scheme of tyre parameter identification process corresponding to the structure of this thesis

A schematic representation of the total process for identifying the tyre parameters is given in Figure 2. This scheme covers the whole process from the theory and the models to the results and conclusions. It is divided in three parts, which correspond to the main parts of this thesis. The blocks in each part correspond to the chapters of this thesis.

Seen on a global level, the Part I treats the general theory, the modelling used for the application and the data acquisition. In Part II the designed application for the optimization routine and related topics are discussed. Part III shows the results that the application has produced and contains conclusions and recommendations based on the results.

Part I consists of four chapters. The chapter 1 is an introduction to the vehicle theory and tyre theory. In chapter 2 the vehicle models are introduced. Chapter 3 deals with the manoeuvre. The chapter 4 describes how the experimental data is obtained and processed.

Part II also includes four chapters. In chapter 5 the need and working of the application is explained. In chapter 6 the parameters on which the optimization is based are discussed. Chapter 7 touches upon the optimization procedure itself. Other options that concern the optimization procedure are treated in chapter 8.

In Part III, which consists of two chapters, the results of the optimization using different options for the two vehicle models are shown in chapter 9. Chapter 10 contains a general conclusion of the thesis and a 'best practice' is presented for both vehicle models. This chapter includes recommendations for further research and for the improvement of the application.

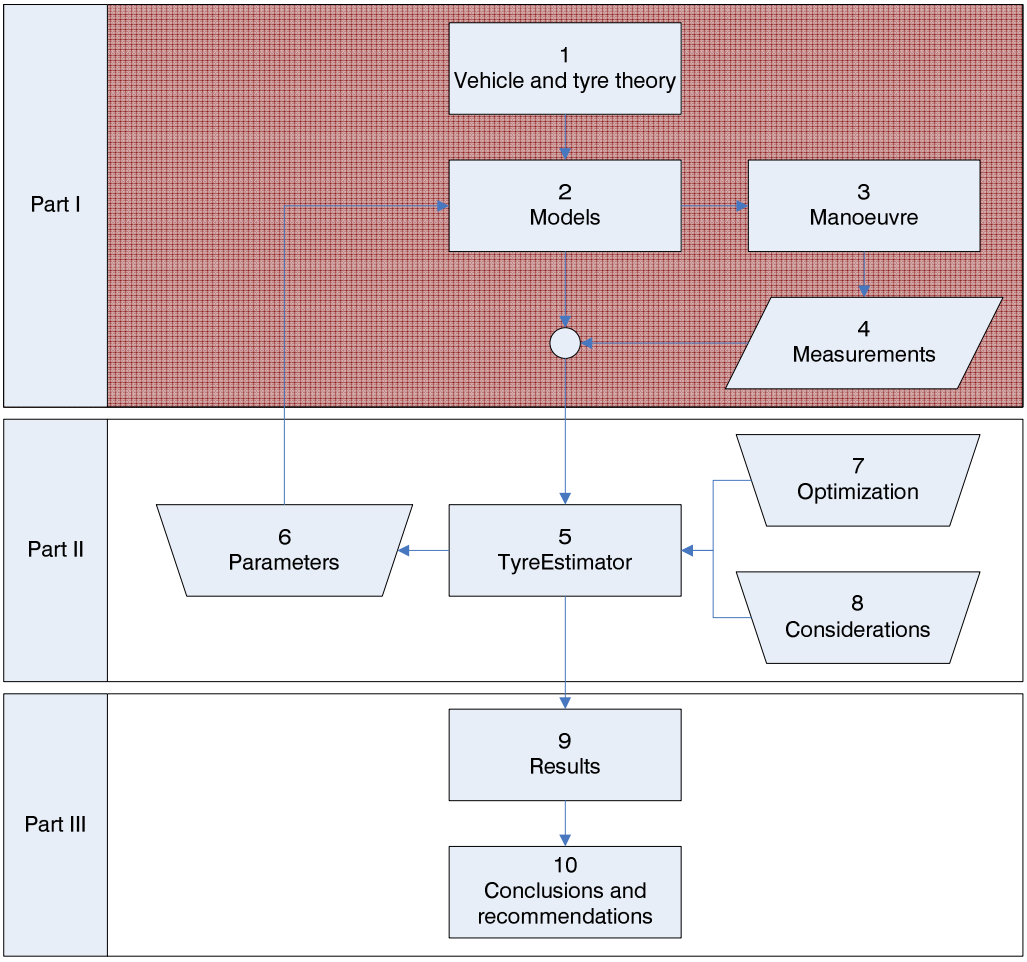

Part I General Theory

"Mathematical tyre models are used to calculate the tyre forces as responses to the wheel motion with respect to the road. The model may be a part of a comprehensive vehicle model that serves to analyse the dynamic behaviour of the vehicle while running over a road surface." – Hans B. Pacejka

The mathematical tyre model introduced by Pacejka is the Magic Formula tyre model. For using the model in an optimization process the understanding of the vehicle behaviour using tyre models is essential.

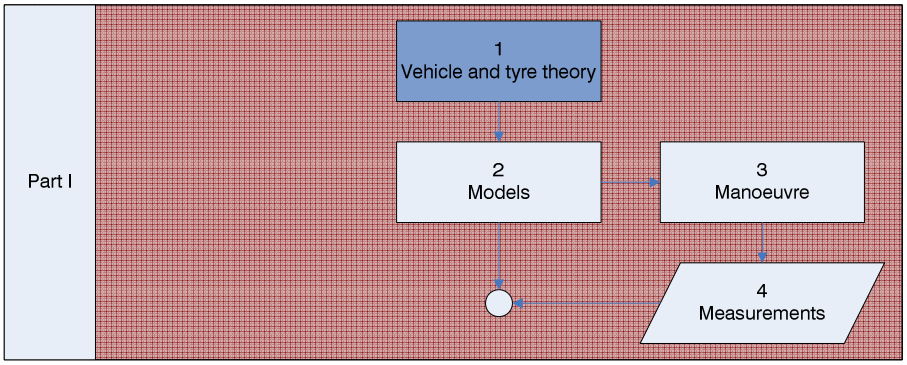

1 Vehicle and tyre theory

The behaviour of a modelled vehicle is based primarily on its tyre model. This makes vehicle and tyre models closely related. For the understanding of this thesis both modelling principles are discussed.

A basic analysis, which is performed in this chapter, uses a slowly cornering vehicle represented by the simplest available model. This analysis covers the fundamental aspects of the vehicle's motions in a horizontal plane. Besides, it provides the basis for the explanation of the vehicle's handling, responsiveness to the driver input or ease of control. The vehicle handling properties are further analysed in accordance with the tyre characteristics.

In section 1.1 a basic introduction is given to vehicles in general and the simple modelling of a vehicle is discussed. Section 1.2 provides a basic introduction to tyres and the modelling thereof.

1.1 Introduction to lateral vehicle dynamics

In subsection 1.1.1 the vehicle-ground interaction and different aspects affecting the behaviour of the vehicle are discussed. Thereafter, in subsection 1.1.2, an important vehicle model is introduced, the bicycle model. In subsection 1.1.3 the model's important vehicle properties are derived and analyzed, among which the equations of motion for steady state cornering. Subsection 1.1.4 treats conclusively the vehicles handling behaviour by making use of the equations derived in subsection 1.1.3.

1.1.1 General vehicle properties

A simplified explanation of the relation between vehicle, tyre and road is given by: the vehicle is supported by the suspensions which connect the tyres, which are

supported by the ground, to the vehicle. The tyres transfer the driving power through the wheel-ground contact. To control the trajectory of the vehicle they provide the required lateral forces. As written in the introduction, the suspensions were validated by means of an elasto-kinematic bench test.

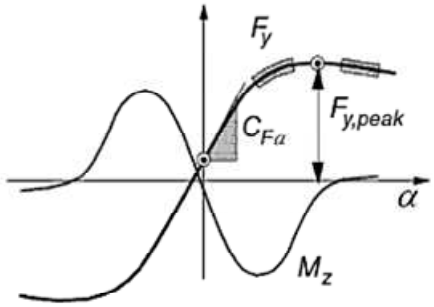

Figure 3 Example of lateral force vs. slip angle curve

Experimental measurements show the lateral force (F_y) development as a function of the slip angle (α). An example of this plot is given in Figure 3. The lateral force represents the horizontal force at road level, while the slip angle is given by the angle between the forward speed and the actual speed of either the wheel or the axle, as drawn in Figure 4. For the F_y-α relation the lateral force first builds up linearly with the slip angle. Then slowly a maximum lateral force is reached, which for higher slip angles then diminishes to a constant lateral force. This is due to the saturation of the tyre and explained further in subsection 1.1.4.

The (linear) slope of the curve is one of the tyre characteristics that determines the basic linear handling and stability behaviour of vehicles. The slope is also referred to as cornering stiffness ($C_{F\alpha}$), while the lateral force is also called cornering force. The non-linear shape of the side force has a considerable effect on the handling characteristics and stability properties of the vehicle at higher lateral accelerations. Load dependency, notably the non-linear behaviour relationship of cornering stiffness with tyre normal load, has a considerable effect on the handling characteristics. This is described in more detail in subsection 1.1.4.

Aside from the slip angle, the camber angles of the wheels cause a lateral force. This angle, pictured in Figure 4, is given by the angle between the symmetry-plane of the wheel and the road normal. Generally, the camber angles for four-wheeled vehicles are small and for simple analyses in the linear range the forces generated by the camber angles are not taken into account. This is explained further in subsection 1.2.3.

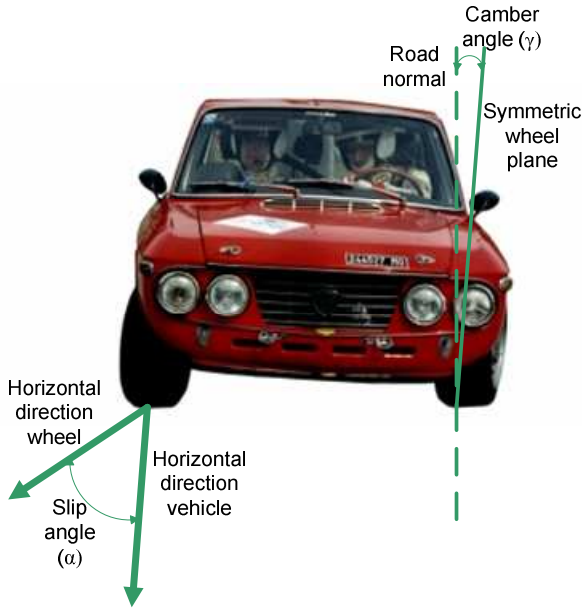

Figure 4 Slip and camber angle drawn schematically

1.1.2 Bicycle model

The steady-state handling analysis adopts a simple single track vehicle model. In this bicycle model, the vehicle is considered as one body to which one front and one rear wheel are attached. The wheels can be chosen to be steerable or fixed. A constant speed, a flat road, and small roll angles are assumed for the model. These assumptions restrict the movement to the horizontal plane. The driving forces to keep a constant velocity are considered small, to prevent longitudinal slip.

For high lateral accelerations, above 0.7 g, the contribution of the roll motion of the vehicle body in addition to the vertical load change on the wheels of the individual axles cannot be disregarded. This can also be deduced from Appendix A. Simple adjustments of parameters of the vehicle model cannot compensate for this. Therefore effective axle characteristics need to be calculated. This is explained further in subsection 2.1.1.

Figure 5 shows the bicycle model, with a steerable front wheel and a fixed rear wheel. The local coordinate system is connected to the centre of gravity. Based on the Society of Automotive Engineers (SAE-) coordinates, x points forward, z points in the direction of gravity and y is perpendicular to x and z and points to the right.

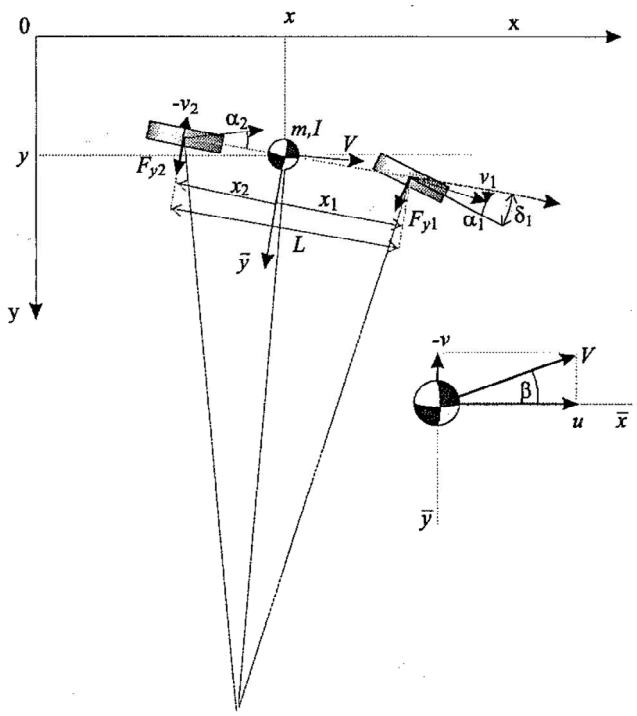

Figure 5 Schematic representation of the bicycle model according to the SAE coordinate system

Generally three degrees of freedom are needed to describe the vehicles dynamic position in the horizontal plane. Degrees of freedom (DOF) are directions or rotations in which the vehicle is free to move. For the horizontal plane, the position in x-direction (x), the position in y-direction (y) and the orientation (ψ) of the vehicle with respect to the x-axis are regarded as such. The constant forward velocity makes it reasonable to disregard the DOF in x-direction, this way a two DOF vehicle model is obtained.

In the figure, the wheelbase of the vehicle is denoted by L. The distance between front axle, recognizable by the subscript 1, and centre of gravity is called x_1. The distance between the rear axle, recognizable by subscript 2, and the centre of gravity is called x_2 and has a negative sign. The steer angle is represented by δ_1, while β represents the sideslip angle given by the difference in angle between forward speed and actual speed of the centre of gravity. The symbols α_1 and α_2, correspond respectively to the front and rear slip angles. These angles are given by the differences between the direction of the velocity of the wheel and the direction of the wheel.

The velocity vector of the centre of gravity is indicated by V. Velocities and forces at the front- and rear axle are separated into a component in x-direction (longitudinal)

and a component in y-direction (lateral). The longitudinal velocities of the two axles are denoted by u_1 and u_2 while the lateral velocities are denoted by v_1 and v_2. It is assumed that the forward speed remains constant; therefore the x-component of the force is neglected. With F_{y1} and F_{y2} the lateral forces are denoted at the front and rear axle, which are perpendicular to the direction of the respective wheel.

To calculate the steer angle and the sideslip angle from the wheel slip angles kinematic terms are introduced, which represents the steer angle and the sideslip angle when the slip angles are zero for low speeds. The calculation of the steer angle and the sideslip angle is shown in Appendix C.

The equations of motion for the bicycle model, for $|\psi|<<1$, now read:

$$m\ddot{y} = F_{y1} + F_{y2} = C_{F\alpha 1}\alpha_1 + C_{F\alpha 2}\alpha_2 \quad \textbf{(1-1)}$$

$$I\ddot{\psi} = F_{y1}x_1 + F_{y2}x_2 = x_1 C_{F\alpha 1}\alpha_1 + x_2 C_{F\alpha 2}\alpha_2 \quad \textbf{(1-2)}$$

The slip angles as functions of y and ψ can be found after simplification and using linearization and are expressed by:

$$\alpha_1 = \delta_1 + \arctan\left(-\frac{v_1}{u_1}\right) \approx \delta + \frac{v_1}{V} \quad \textbf{(1-3)}$$

$$\alpha_2 = \arctan\left(\frac{-v_2}{u_2}\right) \approx \frac{-v_2}{V} \quad \textbf{(1-4)}$$

The track of the model is zero, because it is a bicycle model. Therefore the longitudinal velocity is not affected by the yaw velocity and may be assumed equal to V. The lateral speeds at the front and rear axle, on the contrary, are affected by the yaw velocity. These are equal to the lateral speed of the centre of gravity plus a contribution of the yaw speed times the distance between the respective axle and the centre of gravity. Therefore the lateral velocities are described by:

$$v_1 = v + x_1\dot{\psi}$$
$$v_2 = v + x_2\dot{\psi}$$
$$v = \dot{y} - V\psi$$

Implementing these relations and grouping the terms the equations of motion become:

$$m\ddot{y} + \left(C_{F\alpha 1} + C_{F\alpha 2}\right)\frac{\dot{y}}{V} + \left(C_{F\alpha 1}x_1 + C_{F\alpha 2}x_2\right)\frac{\dot{\psi}}{V} - \left(C_{F\alpha 1} + C_{F\alpha 2}\right)\psi = C_{F\alpha 1}\delta_1 \quad \textbf{(1-5)}$$

$$I\ddot{\psi} + \left(C_{F\alpha 1}x_1^{\,2} + C_{F\alpha 2}x_2^{\,2}\right)\frac{\dot{\psi}}{V} - \left(C_{F\alpha 1}x_1 + C_{F\alpha 2}x_2\right)\psi + \left(C_{F\alpha 1}x_1 + C_{F\alpha 2}x_2\right)\frac{\dot{y}}{V} = C_{F\alpha 1}\delta_1 x_1 \quad \textbf{(1-6)}$$

For shorter writing it is defined that:

$$C = C_{F\alpha 1} + C_{F\alpha 2}$$
$$Cs = C_{F\alpha 1}a + C_{F\alpha 2}b$$
$$Cq^2 = C_{F\alpha 1}a^2 + C_{F\alpha 2}b^2$$

Using the notations introduced above, the equations of motion can be written as:

$$m\ddot{y} + C\frac{\dot{y}}{V} + Cs\frac{\dot{\psi}}{V} - C\psi = C_{F\alpha 1}\delta_1 \tag{1-7}$$

$$I\ddot{\psi} + Cq^2\frac{\dot{\psi}}{V} + Cs\frac{\dot{y}}{V} - Cs\psi = C_{F\alpha 1}\delta_1 x_1 \tag{1-8}$$

These relations are associated with a fourth order system, which implies four solutions. To solve the equations of motion the determinant is written down, set to zero and calculated;

$$\det\begin{vmatrix} m\lambda^2 + \frac{C}{V}\lambda & \frac{Cs}{V}\lambda - C \\ \frac{Cs}{V}\lambda & I\lambda^2 + \frac{Cq^2}{V}\lambda - Cs \end{vmatrix} = 0$$

Leading to the characteristic equation:

$$\lambda^2\left(mI\lambda^2 + \frac{CI + Cq^2m}{V}\lambda + \frac{C^2q^2 - C^2s^2}{V^2} - mCs \right) = 0 \tag{1-9}$$

From the characteristic equation it is deduced that two roots are equal to zero. The other two solutions are obtained from the argument between brackets. Substituting the roots in the standard exponential function, and introducing a polynomial of grade n-1 for all n poles at zero leads to the following response:

$$y = A + Bt + C_1e^{\lambda_1 t} + C_2e^{\lambda_2 t}$$
$$\psi = D + Et + G_1e^{\lambda_1 t} + G_2e^{\lambda_2 t}$$

The first two terms of the response describe the undisturbed straight movement (E=0). These constants don't provide information on the dynamic behaviour; they are only defined by the choice of the coordinate system. Without changing the essence of the problem, it is possible to add an arbitrary value to y and ψ. It is therefore concluded that only the first derivatives of the position in y-direction and the first derivative of the orientation matter. With this knowledge two new variables are now introduced:

$$v = \dot{y} - V\psi$$
$$r = \dot{\psi}$$

The system of equations finally comes to be:

$$m\left(\dot{v}+Vr\right)+C\frac{v}{V}+Cs\frac{r}{V}=C_{F\alpha 1}\delta_1 \tag{1-10}$$

$$I\dot{r}+Cq^2\frac{r}{V}+Cs\frac{v}{V}=C_{F\alpha 1}\delta_1 x_1 \tag{1-11}$$

1.1.3 Linear steady state cornering

During steady state cornering the velocities observed from the vehicle are constant, therefore the time derivatives of equation (1-11) are set to zero. The equations of motion can now be described:

$$mVr+C\frac{v}{V}+Cs\frac{r}{V}=C_{F\alpha 1}\delta_1 \tag{1-12}$$

$$Cq^2\frac{r}{V}+Cs\frac{v}{V}=C_{F\alpha 1}\delta_1 x_1 \tag{1-13}$$

Considering that the vehicle drives an arc with a constant radius R ($\delta \neq 0$), the following relation holds:

$$r=\frac{V}{R}$$

The expression for the lateral velocity is deduced from the first equation of motion and reads:

$$v=\frac{C_{F\alpha 1}\delta_1 V}{C}-\frac{mV^2 r}{C}-sr$$

Substituting this result into the second equation of motion and replacing r in the same equation yields:

$$\frac{Cq^2-mV^2 s-Cs^2}{R}=C_{F\alpha 1}\left(x_1-s\right)\delta_1 \tag{1-14}$$

The track curvature as a function of the steer angle can now be calculated:

$$\frac{1/R}{\delta_1}=\frac{C_{F\alpha 1}\left(x_1-s\right)}{Cq^2-mV^2 s-Cs^2} \tag{1-15}$$

Inverting the relation to get a function of V^2 and using the fact that $a + b = L$ leads to:

$$\frac{\delta_1}{1/R}=\frac{Cq^2-mV^2 s-Cs^2}{C_{F\alpha 1}\left(x_1-s\right)}=L-\frac{mV^2 s}{C_{F\alpha 1}\left(x_1-s\right)}=L+\frac{\eta V^2}{g} \tag{1-16}$$

The symbol η represents the understeer coefficient, which characterizes the handling behaviour of the vehicle. This term is explained further in the next subsection.

1.1.4 Handling

With handling the responsiveness of a vehicle to the driver steer input is denoted. This implies that handling is an overall measure of the combination of driver and vehicle. The combination of driver and vehicle can be considered either as a closed-loop or an open-loop system. If the system is considered as closed-loop, the driver observes the position and direction and acts on it, pictured in Figure 6. On the contrary, if the system is considered as open-loop, the vehicle responds to specific steering inputs. This way the vehicle can be characterized separately. The most important properties for the handling characterization are understeer and oversteer.

Figure 6 A Ferrari California undergoing a handling test

These terms describe the way a vehicle follows the turns on the road. The distinction of these terms is caused by a difference in front and rear slip angle. When the front slip angle exceeds the rear slip angle, the vehicle slides more over its front wheels and makes a larger turn than the direction of the front wheels suggest. This phenomenon is called understeer. On the contrary, oversteer occurs when the vehicle slides more over its rear wheels and a sharper than expected turn is made. The term oversteer originates from the sliding of the back wheels, which tend to 'overtake' the front wheels.

The previously mentioned understeer coefficient provides a basis to explain the same principle using analytical formulas. This coefficient describes the degree of understeer for a vehicle, according to the cornering stiffness ($C_{F\alpha}$) and the front- and rear axle loads (P) in the following way:

$$\eta = \frac{P_1}{C_{F\alpha 1}} - \frac{P_2}{C_{F\alpha 2}}$$

The axle loads at front and rear are calculated using the moment equilibrium. These are given by:

$$P_1 = mg\frac{-x_2}{L}$$

$$P_2 = mg\frac{x_1}{L}$$

Assuming a linear and equal relation of cornering stiffness with axle load for both axles and constant with respect to the slip angle, then the understeer equals zero according to the relation for this coefficient. Such behaviour is referred to as neutral behaviour, which means that the vehicle follows the turn the way it should. This implies that the steer angle can remain constant while following a path with a constant radius for different lateral accelerations.

Assuming a non-linear and equal relation of cornering stiffness with axle load for both axles, as shown in Figure 7, even if still constant with respect to the slip angle, the under- or oversteer behaviour is characterized by the load distribution between front and rear axle. If the load at the front axle is higher than at the rear axle, the front slip angle will be higher during cornering. In that case the ratio of vertical load and cornering stiffness for the front axle is higher than for the rear, which leads to a positive understeer coefficient. An understeered vehicle has to increase linearly the steer angle to maintain a path with constant radius for higher lateral accelerations. This is also valid vice versa; if the vertical load on the rear axle is higher, the rear slip angle will be higher during cornering, resulting in an oversteered vehicle. To maintain the path with a constant radius for higher lateral accelerations the steer angle should be linearly decreased. For an oversteered vehicle it is important to mention that above a certain critical speed the vehicle becomes directionally unstable. Safety reasons therefore induce that all passenger vehicles should have an understeered behaviour in the linear range.

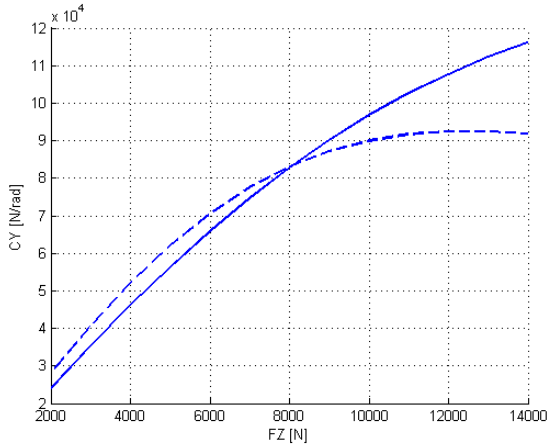

Figure 7 Plot of non-linear relation between cornering stiffness and vertical load for different tyres

The cornering stiffness can be assumed constant with the slip angle only for lateral accelerations below approximately 0.4 g. Therefore, this assumption is restricted to low lateral accelerations. Considering the F_y-α curve, after the part where the linear cornering stiffness is valid, the curve starts to bend away from the initial slope. This is indicated as limit handling and is due to the saturation of the tyre. Saturation means that the build-up of lateral force for an increasing slip angle becomes less and eventually becomes zero or even negative for a further increasing slip angle. If saturation takes place at the front or rear axle the vehicle behaves in a more extreme way.

A more realistic situation is obtained by assuming tyres with the same non-linear relation between lateral force and slip angle for the front and rear axle and with the same non-linear behaviour as a function of the vertical load.

When higher lateral accelerations are considered, due to the non-linear relationship of the lateral force with respect to the vertical load, the effect of vertical load transfer from inner tyre to outer tyre becomes important. This implies that generally the slip angle of the tyres has to be higher to deliver the amount of lateral force required for cornering.

The under- or oversteer behaviour is, especially for higher lateral accelerations, mainly characterized by the vertical load transfer distribution between front and rear axle. If the load transfer on the front axle is higher, the front slip angle will be higher and the saturation will take place at the front axle. The understeered vehicle has to further increase the steer angle to maintain a path with constant radius for higher lateral accelerations.

This is also valid for the opposite circumstance; if the vertical load on the rear axle is higher, the rear slip angle will be higher, resulting in an oversteered vehicle. To maintain the path with a constant radius for higher lateral accelerations the steer angle must be decreased. Safety reasons therefore induce the fact that almost all passenger vehicles have an understeered behaviour also for high lateral accelerations. It is possible that a vehicle shows an understeered behaviour for the linear part of the cornering stiffness, but for limit handling it becomes oversteered. This can happen when static load is higher on the front axle but vertical load transfer between inner and outer wheel is higher at the rear axle than at the front axle.

A comparison of two vehicles, one with limit understeer and one with limit oversteer is shown in Figure 8. These vehicles have the same linear understeer behaviour. The plot displays the steer angles vs. the lateral accelerations of the vehicles driving an arc with a constant radius. For high lateral accelerations, the understeered vehicle needs to increase its steer angle to follow the constant arc radius, where the oversteered vehicle needs to reduce its steer angle.

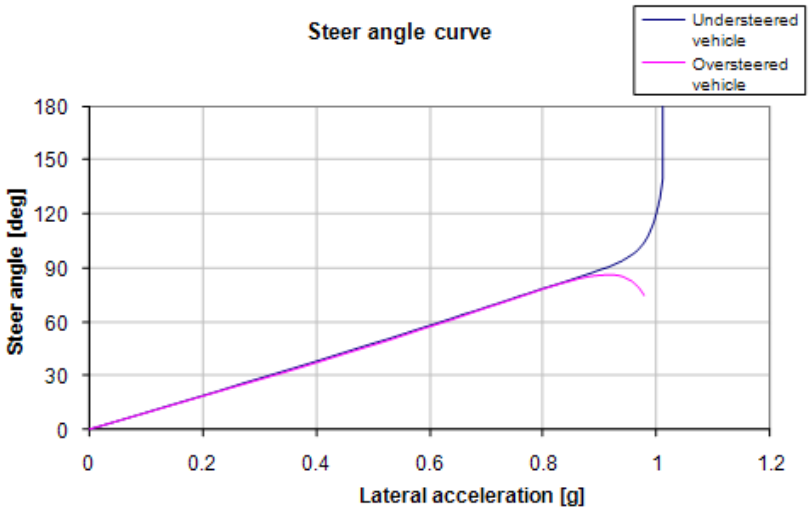

Figure 8 Plot of steer angle vs. lateral acceleration for limit understeered and oversteered vehicle

The sideslip curve shows a reversed pattern. The angle for the limit oversteered vehicle increases progressively, where the angle of the limit understeered vehicle reduces as can be seen in Figure 9. As explained in the previous paragraphs, most passenger vehicles are designed to have an understeered behaviour. This is also because experience shows that this behaviour can be controlled more intuitively by the driver.

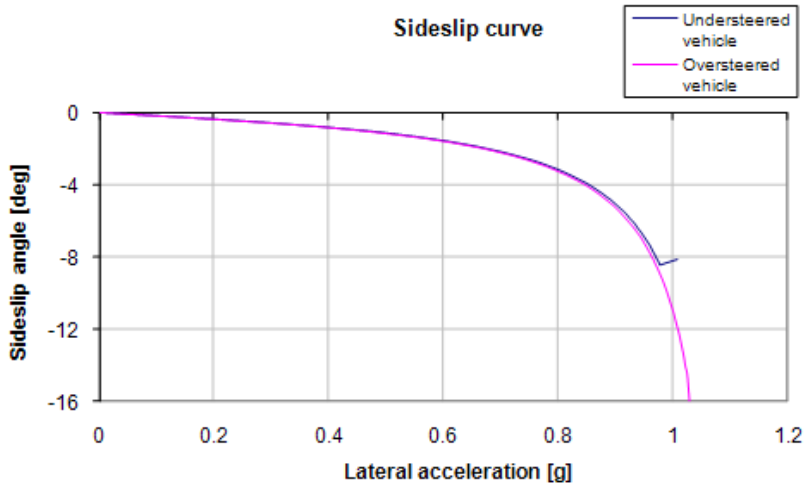

Figure 9 Plot of sideslip angle vs. lateral acceleration for limit understeered and oversteered vehicle

1.2 Introduction to lateral tyre dynamics

Firstly a general tyre description is given in subsection 1.2.1, containing background information on its function and properties. In subsection 1.2.2 the tyre coordinate system is discussed followed by the development of lateral forces for cornering. Moreover, a physical explanation is given of the phenomena that develop the lateral forces in subsection 1.2.3. Subsequently, the different possibilities for tyre modelling are discussed in subsection 1.2.4. Subsection 1.2.5 focuses on the most important model for this thesis, the Magic Formula tyre model.

1.2.1 General tyre properties

Tyres are critical for vehicles because of the three basic functions they have. These functions are:

- Supporting the vertical load, while cushioning against road shocks
- Develop longitudinal forces, for breaking and accelerating
- Develop lateral forces for cornering

At the moment, for passenger vehicles, the standard tyre is the radial-ply tyre. These tyres, shown in Figure 10, were patented and introduced by Michelin in 1946. The higher road comfort, the better handling and the longer tread life compared to the previously standard bias-ply tyres, were reason enough to choose these as a standard.

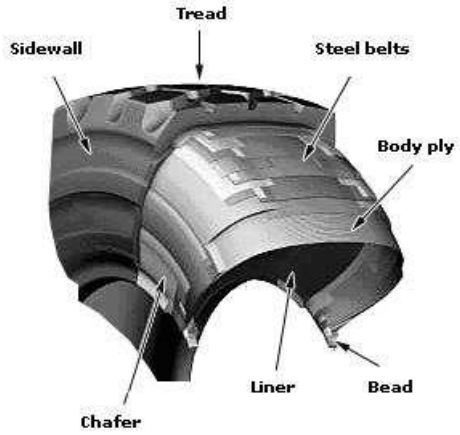

Figure 10 Schematic drawing of radial-ply tyre

A radial-ply tyre is composed of a flexible carcass of high-tensile-strength cords connected to steel cable beads that firmly anchor the assembly to the rim. Internal pressure allows the tyre to maintain its geometry under loading conditions. The radial-ply type of construction makes the sidewall extremely flexible resulting in a soft ride. The directional stability is produced by the cable beads, these keep the tread flat on the road despite the lateral deflection of the tyre caused by cornering.
Some important aspects of the tyre that define its behaviour are material, inflation pressure, vertical load, size, width, speed and camber angle. These aspects contribute all in their own way to the stiffness and the behaviour of the tyre.

1.2.2 Coordinate system and definitions

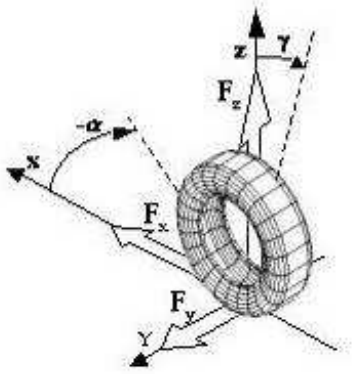

Figure 11 Drawing of coordinate system from TNO Delft tyre user manual

The ISO-coordinate system of the tyre is derived from the Delft tyre user manual. In Figure 11 this system is depicted. This system is not consistent with the definition by SAE in figure 5, but can be obtained with a 180° rotation about the x-axis. A

horizontal road on which the tyre is moving is used as a reference. The origin of the coordinate system, the wheel centre, is located in this plane at the cross-section of the two vertical symmetry axes. The direction of the wheel heading in the horizontal plane is regarded as the x-axis and orthogonal to that is the y-axis pointing to the left. The z-axis is orthogonal to the road plane and points upwards from the wheel centre. The longitudinal force F_x is the component of the force along the x-axis acting in the road plane. F_y is the lateral force component acting along the y-axis in the road plane. The normal force in the direction of the z-axis is denoted by F_z and acts normal to the road plane.

1.2.3 Lateral slip

With slip, the relative motion between the tyre and the road surface on which it moves is denoted. Pure slip can occur in longitudinal (direction of the wheel) or lateral (orthogonal to the wheels direction) direction. When both longitudinal and lateral slip occurs, this is called combined slip. For example when braking during cornering the lateral force decreases and the longitudinal force increases. The resultant of these two forces is then smaller or equal to the pure horizontal slip force, which cannot exceed its maximum value. This value is dictated by the nominal load and the friction coefficient.

The aspects that develop lateral forces are looked at. The lateral forces generated by the tyre are necessary to control the direction of the vehicle and determine the handling behaviour. The origins of these forces, the slip angles and camber angles as stated in subsection 1.1.1, are explained in the next paragraphs.

To define the wheel slip angle, the assumption is made that free straight forward rolling on a flat road at zero sideslip is considered the zero slip condition. The slip angle of the wheel defines the lateral slip. As for the axle slip angle of the bicycle model, the slip angle is the angle between the heading direction and the travel direction of the wheel (x-axis). This angle is considered positive if the travel direction of the wheel has a positive component in y-direction. The angle is thus measured from the wheel plane to the velocity vector.

Physically, slip consists of the build-up of (additional) tyre deformation and possible sliding in the contact patch. This term describes the portion of a vehicle's tyre that is in actual contact with the road surface. The deformations generate lateral forces

acting mostly towards the rear of the contact patch. By convention the lateral force is taken at the centre of contact and an aligning torque is introduced.

The aligning torque is represented by a lateral force at a distance (pneumatic trail) from the wheel centre that generates the same amount of torque. This lateral force provides a limited contribution to the total lateral forces (typically about 1%) and has a limited influence on the vehicle's handling behaviour. Therefore this aspect is not considered for this thesis.

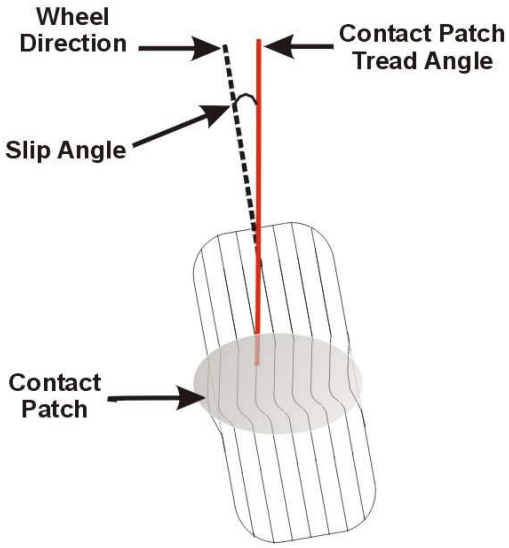

Figure 12 Schematic drawing of tyre deformation due to a slip angle

As stated in subsection 1.1.1, the slope of the curve is known as cornering stiffness. The load and inflation pressure are the main variables that influence this property. Other factors that have influence on the cornering stiffness are the type of tyre, the size and width and the tread design.

The inflation pressure increases the carcass stiffness but reduces the length of the contact patch, so the net influence on cornering stiffness cannot be generalized. It is assumed that increasing the inflation pressure results in a higher cornering stiffness for passenger vehicles. The pressure mostly influences the lateral force generation at high loads. Pressure also has a strong influence on the peak traction level that can be achieved under slip angle conditions.

Cornering forces increase with the vertical load, but not proportionally, due to the saturation of the tyre. This leads to, as mentioned in subsection 1.1.4, relatively higher lateral forces for low vertical loads than for high vertical loads. The understeer gradient is significantly influenced by this property.

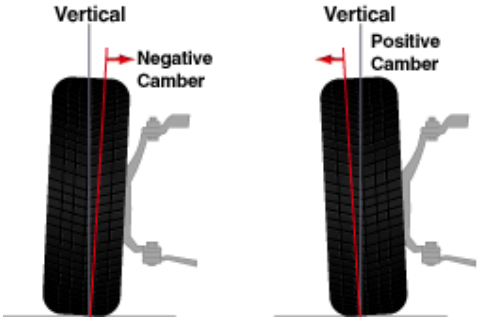

Figure 13 Schematic representation of camber angle

The camber angles, pictured in Figure 13, develop lateral forces as well. With camber angle the lateral inclination of the tyre is denoted, which is defined between the z-axis and the wheel plane. Depending on the initial angle and the roll of the body this property can cause a bigger contact patch. This means that more lateral forces can be developed and the response to steering will be improved. The lateral force produced by the altered wheel-ground configuration is referred to as camber thrust. The camber is characterized by the initial slope of the curve, called camber stiffness. Camber stiffness of radial tyres is typically ten to fifteen times lower than the cornering stiffness of a tyre, as stated in the book by Pacejka. Therefore this contribution is of less importance.

For the camber stiffness the most important variables are the tyre type and the tread design. Other variables that can influence the camber stiffness are the load and the inflation pressure.

1.2.4 Modelling

Considering all tyre modelling procedures, these can be divided in four categories. The first category describes the tyre by a complex physical model. Great details are described in this model and uses computer simulations and finite element models to compute the results.

The second type of modelling for describing tyre characteristics makes use of a simplified physical model. An example is the brush-model. This model uses relatively simple mathematical formulas, while including a lot of important matters for its dynamics. A representation of this model is given in Figure 14.

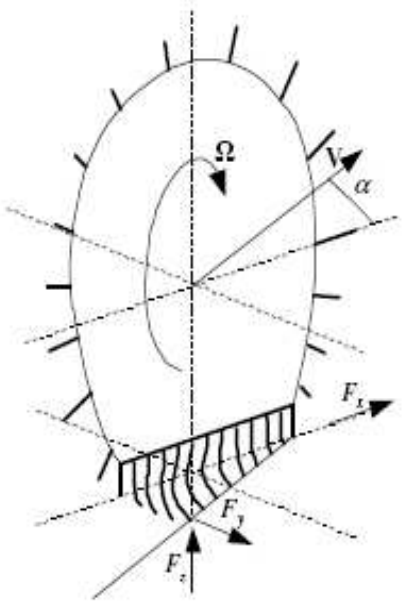

Figure 14 Schematic drawing of brush-model

The similarity approach is the third category, which is based on the use of some basic tyre characteristics typically obtained from measurements. By rescaling, distorting and multiplications new relationships are obtained to describe the conditions. The quick calculations made by this model are an advantage for the use in vehicle simulations.

The last category treats the tyres using a purely empirical approach. For this method the experimental data is fitted with complex mathematical formulas, because simple polynomial fits are not capable to represent reliably the tyre behaviour over the complete range of slip angles. A well known example of this method is the Magic Formula tyre model, used throughout this thesis. In the next section this model is described in more detail.

1.2.5 Magic Formula tyre model

The Magic Formula, or Delft tyre model, is widely used to calculate steady-state force and moment characteristics for the use in vehicle dynamics studies. The development of this empirical model started in the 1980's. In a cooperative effort between the TU Delft and Volvo, various versions (Bakker et al 1987, 1989, Pacejka et al. 1993) as a solution for this problem were produced. In these models the combined slip situation (longitudinal and lateral slip) was still modelled physically. This changed when Michelin introduced a purely empirical model (cf. Bayle et al. 1993).

Further developments were made by DVR, a joint venture of TU-Delft and TNO. The new version incorporates a method for the computation of the aligning torque by accommodating a relatively simple physically based combined slip extension.

Data on which the Magic Formula is based can either come from individual tyre measurements or from complete vehicle tests. Tyre manufacturers base their estimations of the tyre coefficients on individual tyre tests. For CRF it is more important how the tyres respond during a complete vehicle test and what tyre behaviour is shown during the tests.

In this thesis the lateral forces F_y at the front and rear axle are considered. This is a function of vertical force, slip angle camber angle and longitudinal slip. The last property is not taken into account, because the manoeuvre considered is performed at constant speed and does not induce longitudinal slip. The same holds for the camber angles, as their contribution to the cornering stiffness as mentioned in subsection 1.2.3. is low. Moreover, the camber angles of a four-wheeled vehicle are small. For high lateral accelerations this contribution could be more significant, but on the basis of full-vehicle tests this behaviour can hardly be discriminated.

Disregarding the camber angle and longitudinal slip implies that the part of the tyre behaviour, which is dependent on the camber angle and brake slip, can not be changed by altering the parameters therefore meant. Possibly, the vehicle behaviour caused by these aspects can be compensated by altering other parameters in the model. This is acceptable considering their small influences on the vehicle behaviour and if the tyre behaviour matches the experimental data over the whole spectrum.

The Magic Formula defines a curve starting in the origin, which reaches slowly a maximum and then tends to a horizontal asymptote. The formula for the lateral force F_y is defined as:

$$F_y\left(F_z,\alpha_y\right)=D_y\sin\left[C_y\arctan\left\{B_y\alpha_y-E_y\left(B_y\alpha_y-\arctan\left(B_y\alpha_y\right)\right)\right\}\right] \qquad \textbf{(1-17)}$$

α_y = Lateral slip angle

B_y = Lateral stiffness factor

C_y = Lateral shape factor

D_y = Lateral peak value

E_y = Lateral curvature factor

The same relation holds for the front and rear axle curve. For identical front and rear tyres one could expect the axle characteristics to be identical. However, these can

differ considerably because of suspension kinematics and load transfer while cornering. An illustration of the curve generated by the Magic Formula is given in by showing the lateral force as a function of the slip angle for a given vertical load profile.

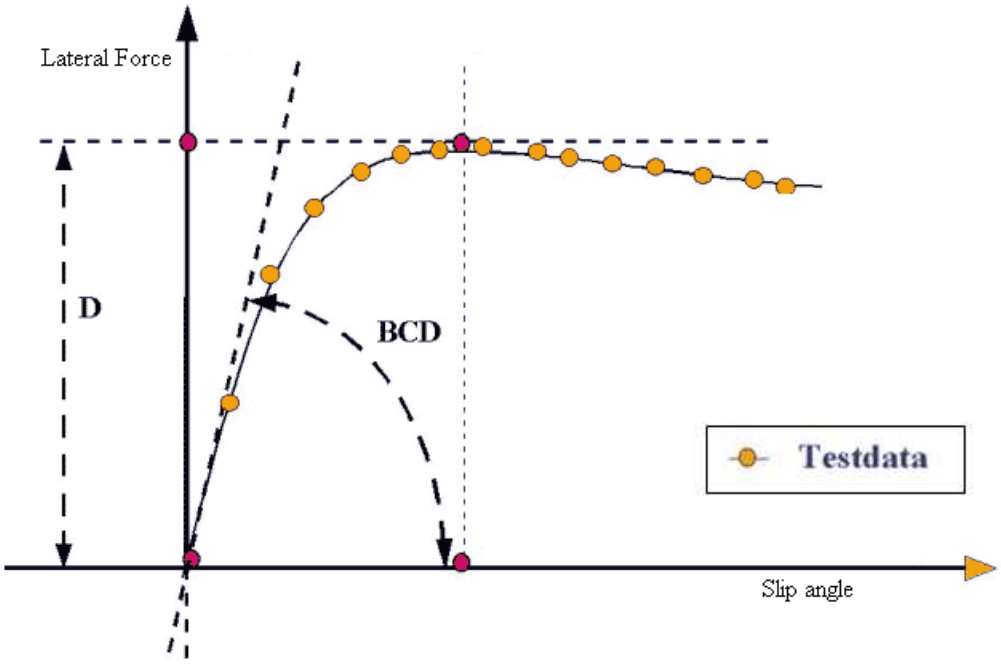

Figure 15 Representation of Magic Formula model

To fit the experimental data with the curve produced by the Magic Formula it might be necessary to shift the diagram horizontally or vertically to make sure the line passes through the origin. The most likely cause of this shift is camber. This effect is not accounted for throughout this thesis and is not considered.

The variables mentioned in the formula are calculated using combinations of coefficients and scaling factors. Considering this aspect, two different ways are considered for resolving the problem of fitting the Magic Formula to the experimental data; either by changing the coefficients or by changing the scaling factors. The scaling factors are originally thought to compensate for deviating curves. The advantage of changing the coefficients instead of the scaling factors is that the components of the Magic Formula can be changed in a more detailed way. Their influence on the shape of the curve is discussed in chapter 6.

The total number of parameters (more than 30) used in the Magic Formula makes it difficult and not effective to change all parameters individually for the identification.

If all parameters are considered the optimization is more vulnerable for finding local minima, this is explained further in chapter 5. The response can also be indifferent to certain parameter changes as for the parameters related to the camber angles. Parameters that describe force responses which are not excited by the manoeuvre, for example parameters describing the longitudinal slip, are not to be considered as well. Therefore the most important coefficients are selected to be used for the optimization process. This is explained in more detail in the subsections 2.1.2 and 2.2.2.

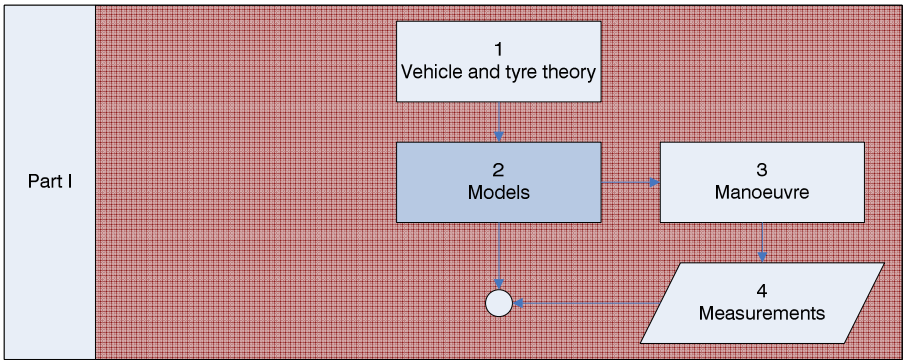

2 Models

In order to compare the experimental data with the data from the simulated vehicle, two vehicle models were made available by CRF. Both models were written and operate in the Matlab/Simulink environment. To finally fit the experimental data the vehicle model is optimized by changing tyre parameters. The models are called by their number of degrees of freedom to protect the official names.

The first model, explained in section 2.1, concerns a simple bicycle model with a rolling coefficient implemented. The advantages of this vehicle model are its simplicity, which gives good insight in the problem, and the quick iterations. It was mainly used to realize the optimization program.

The second model, discussed in section 2.2, is a complete vehicle simulation model developed by CRF. This model was primarily used to find the best optimization model options of the application. An advantage of this model is the more realistic behaviour of the vehicle, leading to more reliable tyre parameters.

2.1 Two-DOF Model

This vehicle model was developed by CRF and used to make quick estimations of vehicle behaviour. The idea of the model for the use in the application was to calculate a good starting point for a second optimization, with a more complex vehicle model, to save time during the optimization process. This advantage arises from the fact that the simple model takes between two and three seconds per simulation, where the complex model requires 30 to 40 seconds. The speed of the calculations for this model made it also suitable for the build-up of the application. The vehicle model is based on the bicycle model, explained in the subsection 1.1.2,

which is considered as two degree of freedom system. In this model the roll of the vehicle is accounted, and the load transfer is accounted by calculating the effective axle characteristics.

2.1.1 Vehicle model

The underlying thought for this model is to calculate a stationary equilibrium for a gradually increasing lateral acceleration. When these outcomes are lined up a range of (stationary) lateral accelerations is obtained. For the equilibrium a slip angle is found that, according to the vertical load on the tyres, generates a lateral force that provides the lateral acceleration of the vehicle. The lateral acceleration starts at zero and a new equilibrium is calculated for every 0.01 g. This evolves until a lateral acceleration of two g is reached or no feasible equilibrium position can be found. The procedure stops at its maximum slip angle, therefore the curve has no decay.

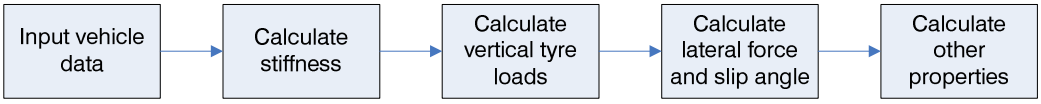

Figure 16 Two-DOF vehicle model scheme

The simple vehicle model is divided in five sub-routines, pictured in Figure 16. These are explained shortly below:

- In the first sub-routine the model data of the vehicle is implemented, like mass, wheel base, mass partitioning, steering ratio, suspension stiffness etc.
- The second sub-routine calculates the roll stiffness of the tyres and suspensions. Hence the total linear stiffness of the suspension system and the vertical translations of the tyres and the suspensions are worked out.
- A calculation of the vertical load (F_z) for every tyre is made in the third sub-routine for every value of a_y, which uses among other vehicle data the roll stiffness calculated in the previous sub-routine.

  The vertical tyre load consists of a static contribution and a quasi-static contribution. The static contribution is calculated using moment equilibrium, this way the total vertical load is divided between front and rear axle. The individual static tyre load is obtained by dividing the load on the axle of the respective tyre by two.

  The quasi-static contribution to the vertical tyre force, different for each lateral acceleration, is due to the lateral cornering forces acting at road level

and thus creating a moment about the centre of gravity. To counteract this moment a couple of vertical forces act at a relative distance of the track width. These effective axle cornering characteristics also represent effects that result from suspension and steering system design factors such as steering compliance and roll steer. In Figure 17 the rolling axis and the centre of gravity is represented showing the different rolling heights at the front.

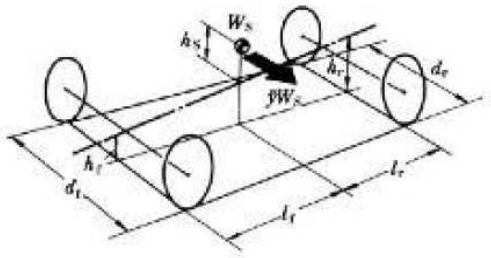

Figure 17 Schematical overview of rolling axis

- Next, in the fourth sub-routine, the required lateral force (F_y) is calculated for the front and rear axle. The lateral force is delivered by the tyres. This lateral force produced by the tyres is calculated using a simplified form of the Magic Formula described in subsection 2.1.2. With the given parameters for the Magic Formula the slip angle is calculated that develops the required lateral force. By dividing the lateral force by the slip angle the approximated linear axle stiffness is worked out for both axles.
- Finally in the fifth sub-routine the total slip stiffness is computed. The rest of the code contains calculations of the other contributions to the total slip. Besides the steer angle and sideslip angle are worked out using the formulas from the Appendix C.

2.1.2 Simple Tyre Model

The tyre model used for this vehicle is based on the Magic Formula. The parameters used in this version are simplified with respect to the original formula. In the next paragraphs these simplifications are explained. In the formulas p refers to a parameter, while λ refers to a scaling constant.

Recalling the Magic Formula for the lateral force from the previous chapter:

$$F_y\left(F_z,\alpha_y\right)=D_y\sin\left[C_y\arctan\left\{B_y\alpha_y-E_y\left(B_y\alpha_y-\arctan\left(B_y\alpha_y\right)\right)\right\}\right] \qquad \textbf{(2-1)}$$

The shape factor C_y is described by:

$$C_y = p_{Cy}\lambda_{Cy} \tag{2-2}$$

Considering the function for C_y, two parameters can be varied (p_{Cy} and λ_{Cy}). These changes will have the same linear effect on C_y.

The Magic Formula defines the peak height D_y of the graph with the formula:

$$D_y\left(F_z,\gamma_y\right) = \mu_y\left(p_{Dy1} + p_{Dy2}df_z\right)\left(1 - p_{Dy3}{\gamma_y}^2\right)\lambda_{\mu y}F_z$$

The relation for df_z is:

$$df_z = \frac{F_z - F_{z0}}{F_{z0}}$$

Considering the function for D_y three parameters are chosen to be variable (p_{Dy1}, p_{Dy2} and $\lambda_{\mu y}$). The other terms in the formula are related to the camber angles of the vehicle, which are not considered. Therefore the terms p_{Dy3} and γ_y are set to zero. This results in the new expression for D_y:

$$D_y\left(F_z\right) = \mu_y\left(p_{Dy1} + p_{Dy2}df_z\right)\lambda_{\mu y}F_z \tag{2-3}$$

In this case it can be seen that with p_{Dy1} and p_{Dy2} the individual contributing terms can be changed, while $\lambda_{\mu y}$ only changes the total value.

E_y according to the Magic Formula defines the curvature factor with:

$$E_y\left(F_z,\gamma_y\right) = \left(p_{Ey1} + p_{Ey2}df_z\right)\left\{1 - \left(p_{Ey3} + p_{Ey4}\gamma_y\right)\operatorname{sgn}\alpha_y\right\}\lambda_{Ey} \qquad (\leq 1)$$

The same relation for df_z holds as before. As for the function for D_y of the Magic Formula only three parameters are chosen to be variable (p_{Ey1}, p_{Ey2} and λ_{Ey}). The other parameters (p_{Ey3}, p_{Ey4} and γ_y) are set to zero. The E_y contribution can not have a value higher than one. If this may happen a restriction is built in the model that will change the E_y parameter to one. The expression for E_y now reads:

$$E_y\left(F_z\right) = \left(p_{Ey1} + p_{Ey2}df_z\right)\lambda_{Ey} \qquad (\leq 1) \tag{2-4}$$

K_y, used to calculate stiffness factor B_y, is according to Magic Formula defined by:

$$K_y\left(F_z,\gamma_y\right) = p_{Ky1}F_{z0}\sin\left[2\arctan\left\{\frac{F_z}{p_{Ky2}F_{z0}\lambda_{F_{z0}}}\right\}\right]\left(1 - p_{Ky3}\left|\gamma_y\right|\right)\lambda_{F_{z0}}\lambda_{Ky}$$

Again the camber angle is not considered, thus p_{Ky3} equals zero. The scaling factors and coefficients which are chosen to be variable are λ_{Ky}, p_{Ky1} and p_{Ky2}. Scaling factor λ_{Fz0}, which allows the tyres to be scaled according to their rated loads, is not considered for it has a complex influence on the curve. The relation for K_y for this model is:

$$K_y(F_z) = p_{Ky1} F_{z0} \sin\left[2 \arctan\left\{\frac{F_z}{p_{Ky2} F_{z0}}\right\}\right] \lambda_{Ky} \quad \textbf{(2-5)}$$

To calculate the stiffness factor B_y is calculated by:

$$B_y(F_z) = \frac{K_y}{C_y D_y} \quad \textbf{(2-6)}$$

2.2 Fourteen-DOF Model

This vehicle model is entirely written and developed by CRF, and is distributed inside the Fiat Group. The model is more complex then the Two-DOF vehicle model, especially because of the higher number of degrees of freedom. This explains the higher computation time per simulation. The aim with this model is to calculate accurately the tyre parameters that reproduce the behaviour of the experimental vehicle.

The fourteen degrees of freedom of this model are linked to real DOF of the vehicle and its components. Six are given by the body, three translations and three rotations. Four other DOF are given by the four suspension deflections and the last four are given by the individual wheel speeds.

2.2.1 Vehicle Model

On the grounds that the model is meant for internal use, not much can be disclosed about this model. However it can be reported that the model consists of various modules that can be changed to represent the vehicle behaviour. The modules are not structural, but look-up table based. By changing the data in the tables the chassis, the front and rear suspension, the powertrain, the steering system or the tyres can be adapted. Moreover, a driver model is available which simulates the behaviour of different drivers.

The test manoeuvres performed in experimental tests by CRF are made available in the model as well as a tool to extract data from the model simulation. The output of this tool is consistent with the extracted data from the experimental manoeuvres. The model is used to simulate the vehicle's behaviour and to optimize vehicle handling as well as ride comfort.

2.2.2 Complete Tyre Model

The tyre model used by this vehicle model to simulate the vehicles behaviour is based on the complete Magic Formula. The difference between this model and the tyre model from the Two-DOF vehicle model is that all the parameters of the model are considered, but most of them are kept constant. These parameters come from the tyre manufacturer and should describe properly the behaviour of the tyre. Like in the simple tyre model the vertical and horizontal offset is not considered. For consistency reasons, the same parameters as mentioned for the Two-DOF model are chosen to be variable. The procedure to identify the behaviour of the tyre corresponding to the experimental data for both models is then similar and can be easily compared.

Recalling the formula for the lateral force, which was represented by the Magic Formula, was denoted in the previous chapter by:

$$F_y\left(F_z,\alpha_y\right)=D_y\sin\left[C_y\arctan\left\{B_y\alpha_y-E_y\left(B_y\alpha_y-\arctan\left(B_y\alpha_y\right)\right)\right\}\right] \qquad \textbf{(2-7)}$$

The shape factor C_y is described according to:

$$C_y=p_{Cy}\lambda_{Cy} \qquad \textbf{(2-8)}$$

Considering the function for C_y, two parameters can be varied (p_{Cy} and λ_{Cy}), but these changes will have the same linear effect on C_y.

According to the Magic Formula the peak height of the graph is defined by D_y. Originally this relation is given by:

$$D_y\left(F_z,\gamma_y\right)=\mu_y\left(p_{Dy1}+p_{Dy2}df_z\right)\left(1-p_{Dy3}\gamma_y{}^2\right)\lambda_{\mu y}F_z \qquad \textbf{(2-9)}$$

Considering the function for D_y of the Magic Formula three parameters can be varied (p_{Dy1}, p_{Dy2} and $\lambda_{\mu y}$). The other parameters and scaling constants are not variable. Therefore their influence in this case remains present, but using the other parameters to base the optimization on the result is equally valuable.

E_y according to the Magic Formula defines the curvature factor with:

$$E_y\left(F_z,\gamma_y\right)=\left(p_{Ey1}+p_{Ey2}df_z\right)\left\{1-\left(p_{Ey3}+p_{Ey4}\gamma_y\right)\operatorname{sgn}\alpha_y\right\}\lambda_{Ey}\qquad(\le 1)\qquad\textbf{(2-10)}$$

In this equation of the Magic Formula only three parameters are varied (p_{Ey1}, p_{Ey2} and λ_{Ey}). The rest of the values are held constant. This makes the change of the influence of the camber angle zero.

K_y, used to calculate stiffness factor B_y, is according to Magic Formula defined by:

$$K_y\left(F_z,\gamma_y\right)=p_{Ky1}F_{z0}\sin\left[2\arctan\left\{\frac{F_z}{p_{Ky2}F_{z0}\lambda_{F_{z0}}}\right\}\right]\left(1-p_{Ky3}\left|\gamma_y\right|\right)\lambda_{F_{z0}}\lambda_{Ky}$$

Because the camber angle is still not considered p_{Ky3} is constant. The scaling factors and coefficients on which the fitting is based are λ_{Ky}, p_{Ky1} and p_{Ky2}. The λ_{Fz0} is disregarded like in subsection 2.1.2. This leads to the following relation for stiffness factor B_y:

$$B_y\left(F_z\right)=\frac{K_y}{C_yD_y}$$

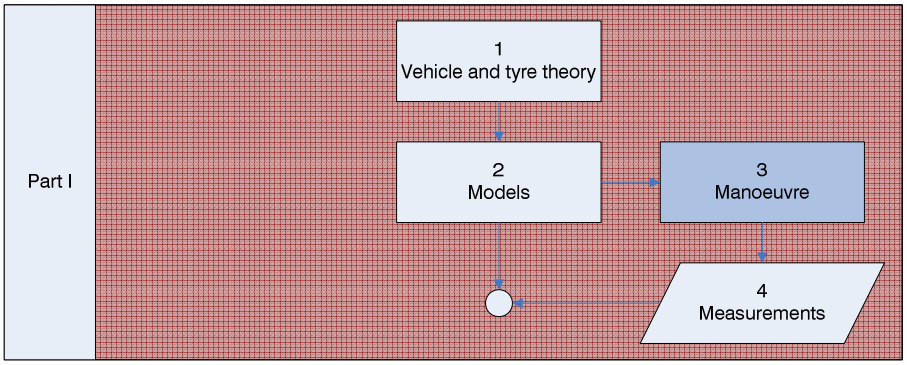

3 Manoeuvre

A vehicle manoeuvre is a planned movement of the vehicle, dictated by location and/or time. Manoeuvres are operated to characterize vehicle handling aspects. In section 3.1 of this chapter an introduction is given to the different manoeuvres used for experimental tests. Section 3.2 deals with the manoeuvres 'performed' by the simulation models, which approach the experimental tests.

3.1 Introduction to vehicle manoeuvres

The most important standard steering manoeuvres are discussed in this section. These manoeuvres are useful to characterize the behaviour of the vehicle and tyres, and have all their own purpose, with its advantages and disadvantages. Manoeuvres are divided in two categories; stationary and transitory manoeuvres. Stationary manoeuvres adopt slowly applied variations, while transitory manoeuvres adopt quickly applied variations. Examples of the manoeuvres of the two categories are given in the subsections 3.1.1 and 3.1.2. All are ISO-standard procedures. More information can be found by reading the manuals of the manoeuvres.

3.1.1 Stationary manoeuvres

- Slow ramp steer (ISO-4138)

  Steering manoeuvre in which the steer angle of the vehicle is increased slowly with a maximum of 60 deg/s up to 180 degrees. This can be done either at constant speed or constant throttle in simulation. Generally the experiments are performed with constant throttle, because when performed at constant speed also longitudinal slip is introduced. For constant throttle this effect can

be neglected. By means of this manoeuvre the whole range of lateral accelerations can be explored, from 0 to the limit of lateral acceleration.

- Steering pad (ISO-4138)
  This manoeuvre prescribes the radius of a circle the vehicle has to follow. During the manoeuvre the speed is increased gradually and the driver is required to change the steer angle to pursue the circular path. The amplitude of the steering wheel deflection depends on the behaviour of the vehicle.

The manoeuvres considered above, if performed on the same vehicle, can yield relatively big differences in the results. These influences may be caused by the different approaches to the manoeuvres and the heavy wear on the tyres.

3.1.2 Transitory manoeuvres

- Step steer (ISO-7401)
  This procedure is similar to the slow ramp steer. Only now the increase of the steer angle will be much faster, about 250 degrees/s up to a certain steer angle. Then the steer angle is held constant and the vehicle is stabilized. By increasing the maximum steer angle higher lateral accelerations are explored up to the point where the vehicle can not be stabilized anymore.
- Frequency response/Sweep (ISO-7401)
  At a constant speed, above 10 m/s, a sine movement with constant amplitude is assigned to the steering wheel with a slowly increasing frequency. The lateral accelerations caused by the sweep are measured, so that the maximum cannot exceed a certain value, for example 0.7 g. During the sweep the frequency is increased from 0 to 4 Hz. The data is analysed in the frequency domain.

3.2 Manoeuvre model

The manoeuvre performed to obtain the experimental data is a slow ramp steer manoeuvre. Due to the very slow transition of this manoeuvre it is considered as a steady state manoeuvre. This implies that the transient behaviour is not excited during this manoeuvre.

The reason for performing this steady state manoeuvre is the fact that the dynamic behaviour of the vehicle can not be simulated using the Two-DOF model. As explained in section 2.1, based on the gradually increasing lateral acceleration, the Two-DOF vehicle model calculates a stationary equilibrium. A range of stationary lateral equilibriums is then produced, excluding the possibility to convene the dynamic behaviour.

The Fourteen-DOF, which does consider the dynamic behaviour, simulates the slow ramp steer manoeuvre like in the experimental test. By using this manoeuvre the transient behaviour modelled in the vehicle model is not excited. Therefore the results from the two models and the experimental data are equivalent.

Moreover the necessity to perform a steady state manoeuvre is given by the Magic Formula tyre model. The parameters under consideration affect the quasi static tyre behaviour. To excite this behaviour, and be able to discriminate the parameters that induce this behaviour, the (stationary) slow ramp steer is the appropriate manoeuvre.

Figure 18 Bird's eye view of the CRF test track near Balocco, Italy

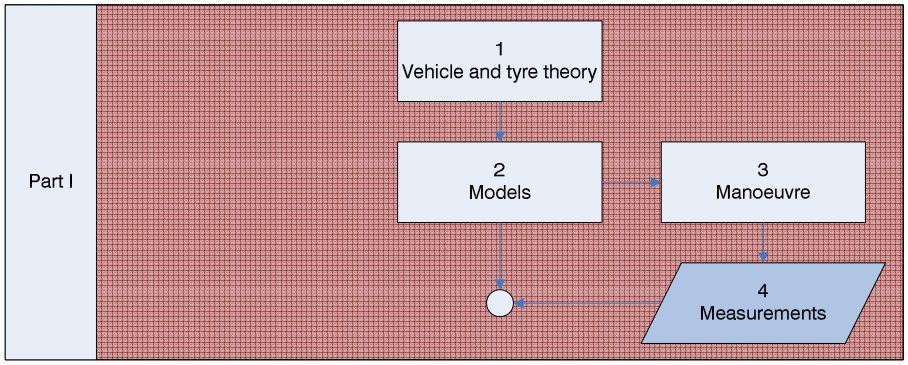

4 Measurements

The measurements coming from the experiments with a complete vehicle were already available at CRF. These tests were performed at the CRF test track near Balocco, Italy. In Figure 18 a bird's eye view of the test track is shown.

For the thoroughness of this thesis, an outline of the signal acquisition procedure performed by CRF is given in section 4.1. In section 4.2 the elaboration of the signals to obtain the data are presented.

4.1 Signal acquisition

The signal acquisition is explained for the slow ramp steer manoeuvre. The goal of the slow ramp steer manoeuvre is the characterization of vehicle behaviour up to the limit in quasi-steady state condition. At CRF the measured signals and filters used for all manoeuvres comply with ISO DIS 15037, in which the general conditions of the test methods for passenger car vehicle dynamic are described. During the test the following variables are measured:

- Steering wheel angle
- Steering wheel torque
- Lateral acceleration
- Yaw rate
- Roll rate
- Sideslip angle
- Vehicle speed
- Longitudinal acceleration

Figure 19 Photo of a gyrometric box that measures lateral acceleration and speed attached to a vehicle

The process of acquisition consists of at least three runs, to obtain reliable data. The manoeuvres are performed according to the described procedure.

4.2 Elaboration

After the experiments have been completed the acquired signal must be elaborated, to extract useable data. This procedure implies resampling of the data at the standard frequency, and filtering and scaling of the data. If there is some offset in the measurements this is then eliminated.

The gyrometric box is not placed at the centre of gravity of the vehicle. In order to calculate the lateral acceleration of the centre of gravity from the measured lateral acceleration, compensations for different factors have to be applied. In Figure 20 this procedure is shown schematically. First the contribution induced by the vehicle roll is eliminated. This compensation of the g-component is deducted from a_y, with:

$$a_y = a_{y,meas} - g \cdot \sin\theta \tag{4-1}$$

Then the position compensation is applied for the offset in z-direction. The compensation in z-direction is necessary to account for the acceleration caused by the roll acceleration at the gyrometric box. This compensation in z-direction is given by:

$$a_y = a_{y,meas} + dz \cdot \ddot{\theta} \tag{4-2}$$

Next the compensation of the y-direction is required to account for the roll speed at the gyrometric box. This compensation in y-direction is given by:

$$a_y = a_{y,meas} + dy \cdot \dot{\theta}^2 \tag{4-3}$$

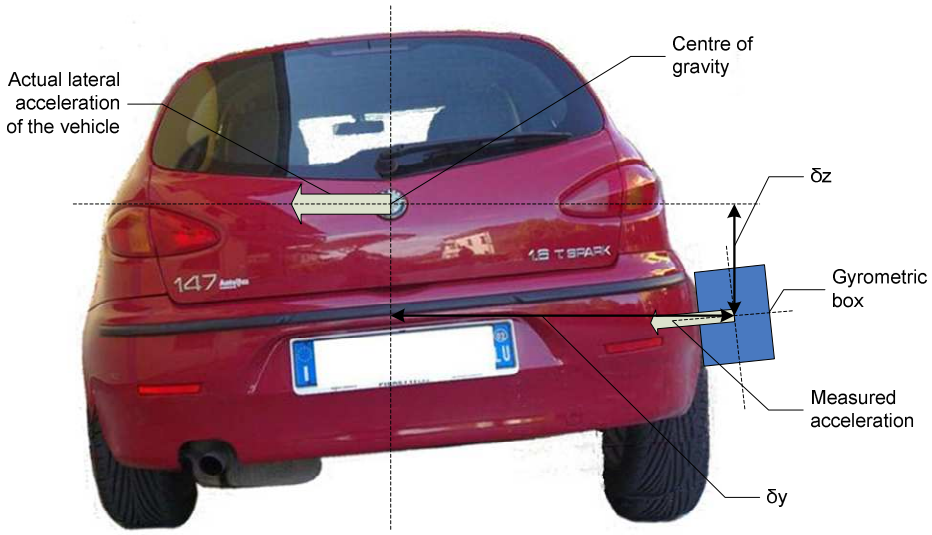

Figure 20 Representation of lateral acceleration compensation due to sensor position

Then using a linear bicycle model with non-linear cornering stiffness characteristics is identified from the measured data. The graph in which the results are synthesised shows different plots and parameters. The most important ones are:

- Slip angle and gradient at front axle and rear axle using the formula's from Appendix C
- Lateral forces, by multiplying the lateral acceleration with the load on the respective axle and therewith the cornering stiffness at front axle and rear
- Steering wheel angle and gradient vs. lateral acceleration, calculated at reference speed (100 km/h) and nominal radius
- Sideslip angle and gradient vs. lateral acceleration, calculated at reference speed (100 km/h) and nominal radius

The resulting number of data points for front and rear axle is the same.

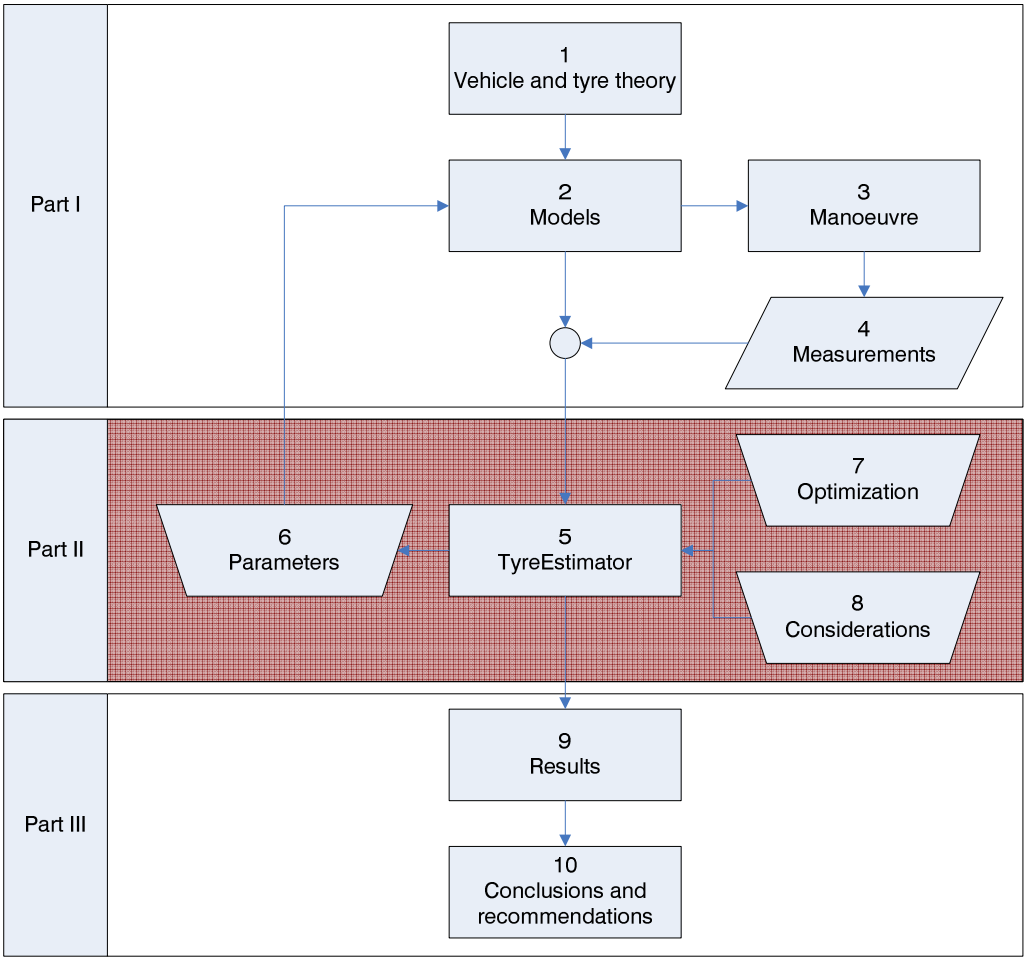

Part II Optimization process

"Optimization is the determination of values for design variables, which minimize (maximize) the objective function, while satisfying the constraints" - P.Y. Papalambros

Design variables are the parameters of the optimization that are allowed to change and influence the objective function. The constraints define the domain of the design variables. For this problem, a simplified description is: "Minimize the difference between the experimental data and the model data by changing parameters of the Magic Formula".

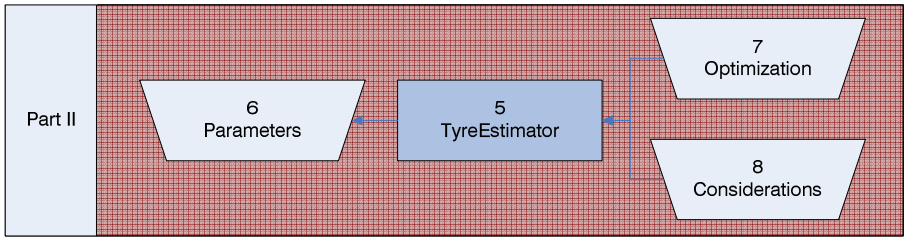

5 TyreEstimator

To identify the tyre parameters, given in the subsections 2.1.2 and 2.2.2, an optimization has to be performed that minimizes the difference between model and experimental data. To execute this optimization a computer application is developed, named TyreEstimator, which operates in the Matlab/Simulink environment. This application is built to perform the optimization according to the chosen options and shows the results.

Section 5.1 is an introduction to the application. In section 5.2 the need for the different options of the application is discussed. Section 5.3 shows how the computer application works and is operated.

5.1 Introduction

The goal of the application is thus to minimize the difference between measured and modelled data using an optimization routine. To get comparable data to base the application on, the vehicle models perform a manoeuvre consistent with the experimentally performed manoeuvre. The specifications of this manoeuvre are featured in section 3.2. The vehicle models used for this optimization are described in subsection 2.1.1 and 2.2.1 of this thesis. The different parts of the vehicle, such as body and suspensions, were validated for the use in simulation models by CRF. These validations and their procedures are beyond the scope of this thesis, meanwhile the data from the validations is assumed to be correct. Though inaccurate validations may lead to inconsistencies between the experimental model and the simulation models, it is very plausible that these are caused by the tyre model.

The Magic Formula tyre model, described in subsection 1.2.5 of this thesis, is used to model the tyre responses. For the Two-DOF model a simplified form of the Magic Formula is used. The vertical loads applied to the tyres are resulting from the vehicle model.

5.2 Options

Optimization has the purpose to find the global minimum of a function, by defining this function as the difference between measured and modelled data this is a good method to identify the tyre parameters of the Magic Formula. A drawback of using optimization is that while searching the global minimum the possibility exists that a local minimum is found. A local minimum is a point, which locally may be considered as a minimum, but observing the whole domain does not necessarily need to correspond to a global minimum, as pictured in Figure 21. This can be visualized by the algorithm standing on a mountain and wanting to find the deepest valley. If it comes across a small valley, it may not be able to 'see' the deep valley anymore. Therefore it will converge to the local minimum within the small valley instead of trying to find the global minimum.

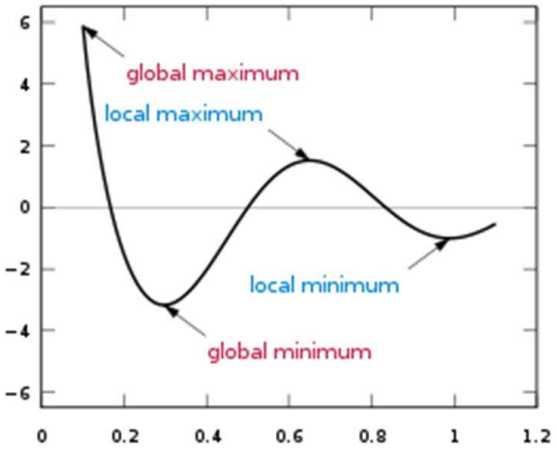

Figure 21 Schematic explanation of local and global minima

Some aspects that influence the finding of local minima are:

- Algorithms: Various algorithms exist to compute the best result for an optimization procedure. Algorithms differ from each other in approach and speed. Because of boundary conditions and the objective function not all can be applied for every case. Although the global optimum should be found by all applicable algorithms, the algorithm could get stuck in a local minimum.
- Objective function: The function that has to be minimized is called objective- or cost function. The function establishes a relation between the experimental and the model data. Altering this relation, for example by giving more or less importance to certain parts of the data, changes the outcome of the optimization routine.

- Starting point: To influence the outcome of the optimization, and to avoid finding a local minimum, the starting point can be changed. Beginning the optimization close to the 'deepest valley' improves the results significantly and avoids finding local minima. Generally, the starting point is given by the parameters given by the tyre manufacturers. A better starting point is difficult to find without going into detail.
- Averaging: This is the name for the clustering of points of the dataset, by calculating their mean values. By reducing the number of points that have to be evaluated, less weight is given to the outliers and local minima caused by the outliers may be avoided.

To find the global minimum, application options are included to deal with these issues. The individual options are discussed in the chapters 7 and 8. In the next subsection the application itself is discussed.

5.3 Application

The TyreEstimator application is developed in the Matlab environment and is able to identify the parameters corresponding to a vehicle behaviour using an optimization procedure. When the application is started the window from Figure 22 appears. This Graphic User Interface (GUI) allows the user to plot figures and to select different optimization options.

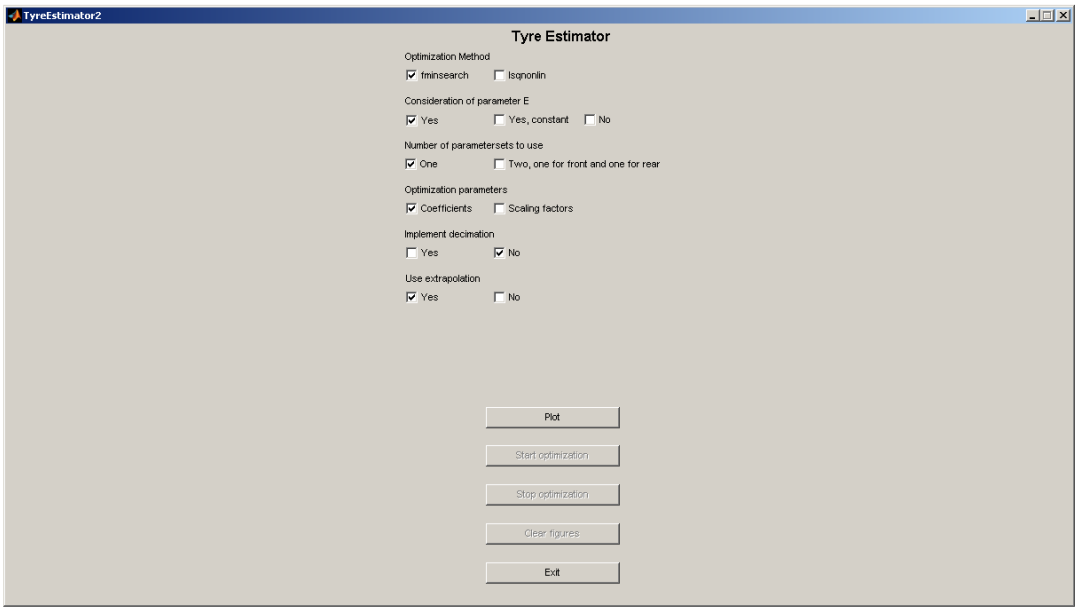

Figure 22 TyreEstimator opening window

At the start of the application only the 'Plot'- and 'Exit'-button are enabled. By clicking the 'Plot'-button a dialog box appears which permits the user to choose the starting parameters or use the standard starting parameters. The chosen parameters are then used for a simulation with the vehicle model. The results are then shown in the GUI as can be seen in Figure 23.

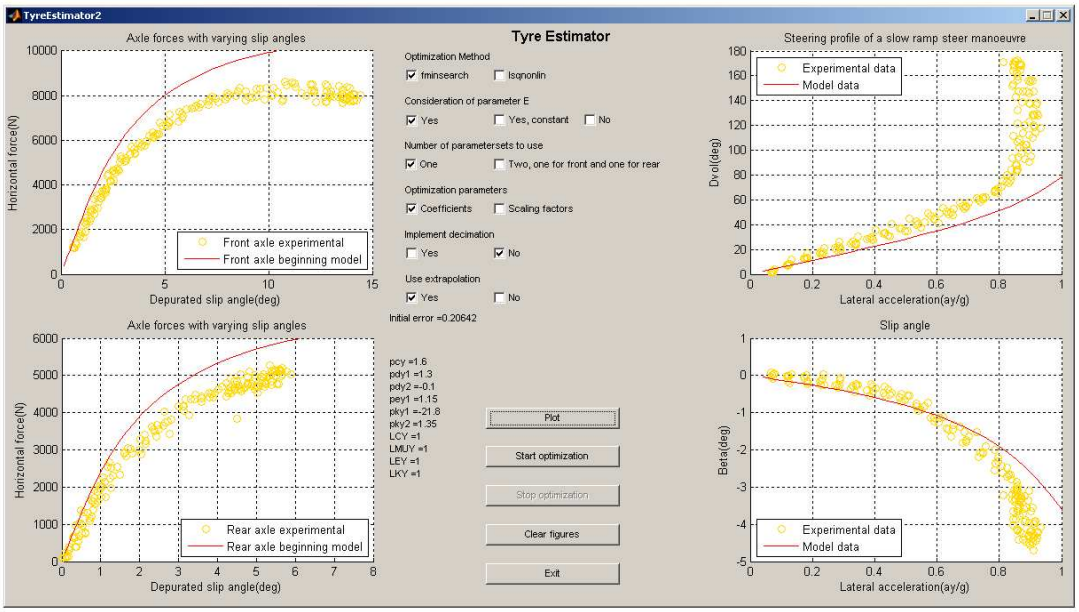

Figure 23 TyreEstimator window after plotting initial conditions

In the left part of the GUI the front and rear axle characteristics are plotted, while in the right part the steer wheel angle and the side slip angle as a function of the lateral acceleration are plotted. The initial mean error and the initial parameters are now shown as well in the GUI.

By clicking 'Start optimization' the optimization is started using the options from the GUI and the initial parameters from the plot. The working and motivations for the options are discussed in the chapters 6, 7 and 8. The optimization is stopped when the optimizer finds a minimum or by pressing the 'Stop optimization'-button at any time during the optimization. The latter command implies that a final simulation with the vehicle model using the last parameter set is performed. Otherwise the application is programmed to show the results at the end of the optimization cycle in the GUI of the TyreEstimator. These results are shown in the same graphs as the initial plots, like in Figure 24.

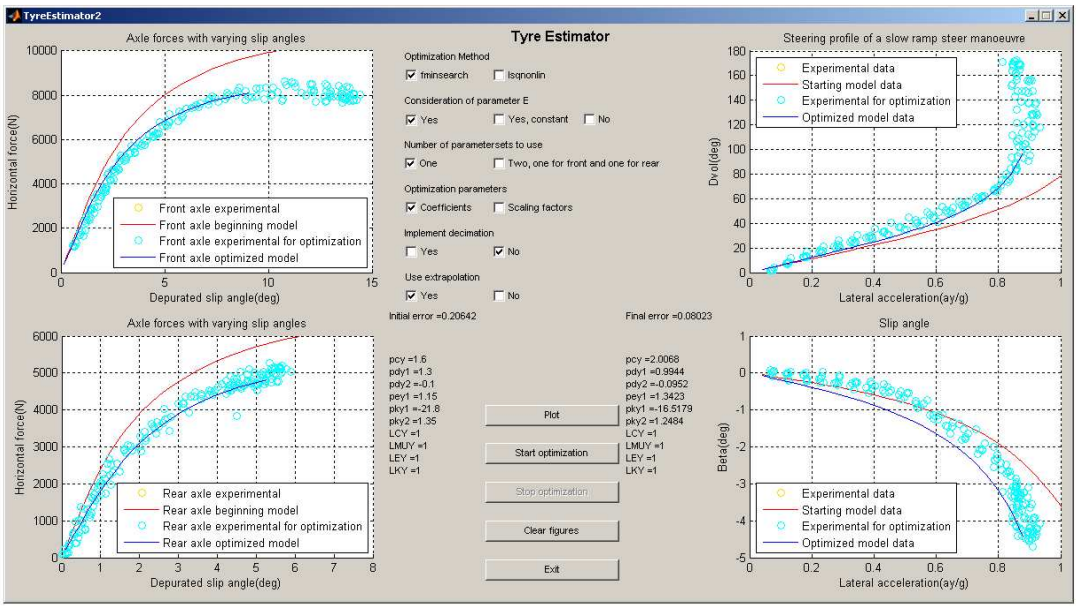

Figure 24 TyreEstimator window showing complete optimization

The final mean error is shown as well as the final parameters. Next a new optimization with new options can be started using parameters that resulted from the previous optimization, standard initial parameters or customized parameters. More information on the programming steps behind the application and a more theoretical explanation on how to use the application are given in Appendix D.

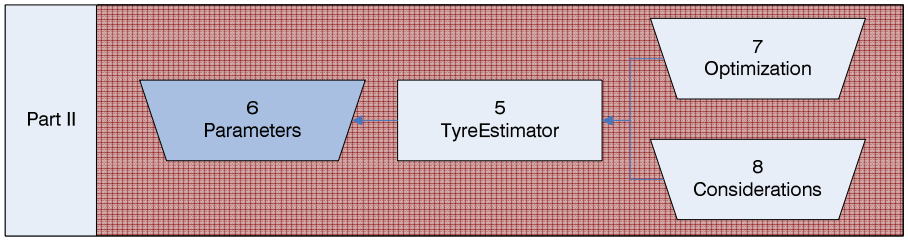

6 Parameters

The parameters, subdivided in coefficients and scaling factors, which are considered for this optimization are mentioned earlier in the subsections 2.1.2 and 2.2.2. The effects of these parameters on the objective curves will be considered in more detail in this section. The effects of the two sets of design variables are considered separately because of their mutual influence.

Scaling factors were created with the purpose to fit different experimental data without altering the coefficients. This may be ideal to fit the experimental data, although changing individual parameters could change the curve more accurately.

To get some feeling with the coefficients and the scaling factors all the parameters were changed individually and the effects on the model were analyzed. The initial parameters are taken from a tyre model supplied by CRF. The simulations were performed with the Two-DOF vehicle model because of the simplicity and the speed.

In the section 6.1 and 6.2 the results of the analysis are described. Section 6.3 concentrates on a special case; the parameters concerning E_y. Conclusively in section 6.4 an evaluation of the issues involving parameters is given.

6.1 Coefficients

To evaluate the influence of each coefficient, higher and lower values with respect to the initial coefficient have been arbitrarily chosen. These values are located within the common variable range of the respective coefficients, with an equal positive and negative deviation the difference in value from the initial coefficient is approximately the same. The complete results show the different ways in which the parameters tend to affect the objective curve. These, together with the used values, can be found in Appendix E. In the results dataset 1 is obtained using the lowest value, dataset 2 using the initial value and dataset 3 by means of the highest value. A summary of the results is given by:

- The C_y component determines together with the E_y component the shape of the curve. Especially the amount of decay after the peak is reached is determined by p_{Cy}, although this is not visible for the simulations with the Two-DOF vehicle model. The change in shape also alters the horizontal and vertical position of the peak. When p_{Cy} is increased the peak shifts horizontally to the left. This is shown in Figure 25,

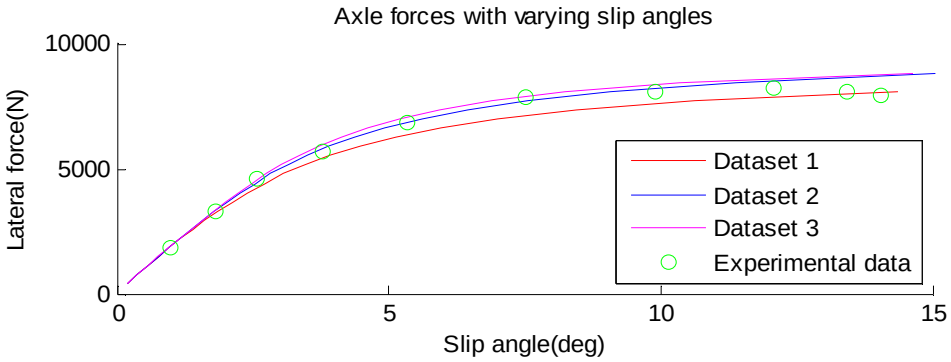

Figure 25 Influence of p_{Cy} on front axle curve

- The D_y component defines the peak value as well as the maximum slip angle, as can be deduced from the Magic Formula. Although in the formula p_{Dy2} is related to the load, the overall effect for this configuration of parameters is approximately the same for p_{Dy1} and p_{Dy2}.
- Together with C_y, the E_y parameter defines the shape of the curve. In particular the shape of the peak is given by E_y. Under given values of D_y and K_y it allows adjustments of the location of the maximum. For a lower p_{Ey1} coefficient the peak is reached rapidly and afterwards the curve may even descend a bit, while for higher values the peak is reached slowly and the curve will not descend. The p_{Ey2} coefficient is designed to have an influence related to the load. In Figure 26 it is shown that this effect is negligible.

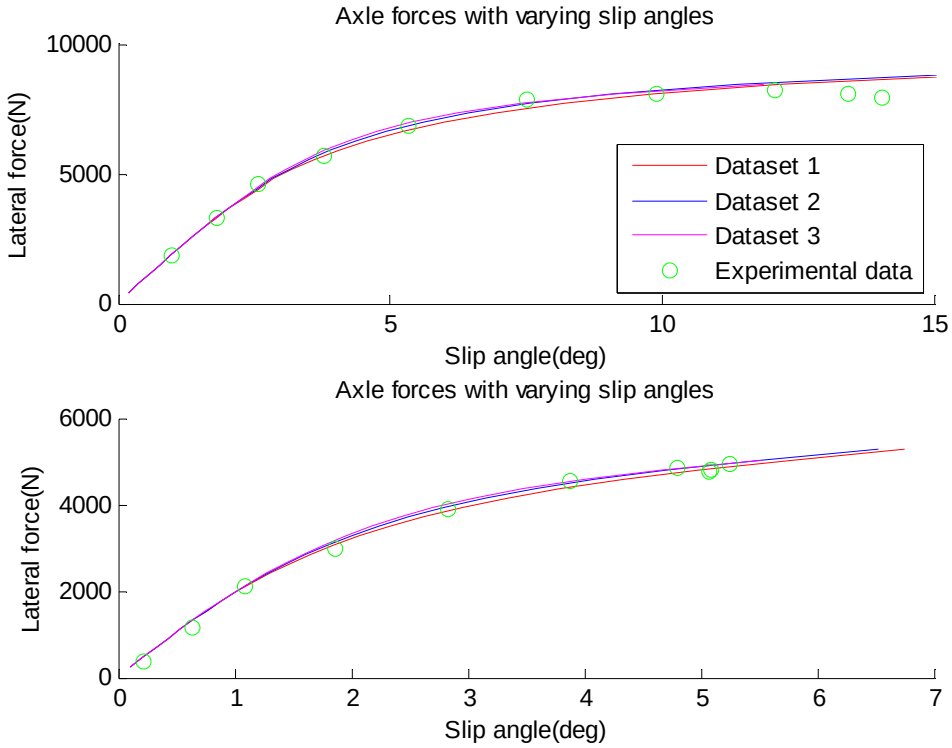

Figure 26 Influence of p_{Ey2} on front and rear axle curve

- The K_y component defines the stiffness factor of the curves. This is the initial angle of the graph with respect to the horizontal axis. Increasing p_{Ky1}, a greater initial angle and thus a higher stiffness is obtained. The other coefficient, p_{Ky2}, influences the graph in the opposite way; as p_{Ky2} is increased, the stiffness decreases.

6.2 Scaling factors

The same analysis is performed for the scaling factors. For the analysis the scaling factors are increased and decreased by one third. All the results, which can be found in Appendix E, show the different ways in which the scaling factors tend to affect the objective curves. The conclusions that can be drawn from this analysis are:

- The λ_{Cy} scaling factor shows the same influence on the C_y component as the p_{Cy} coefficient. This is obvious because of their linear relationship in the Magic Formula.
- The $\lambda_{\mu y}$ scaling factor affects the D_y component linearly. It affects the vertical position of the peak as well as the maximum slip angle. In Figure 27 these effects on the front and rear axle curve are visible.

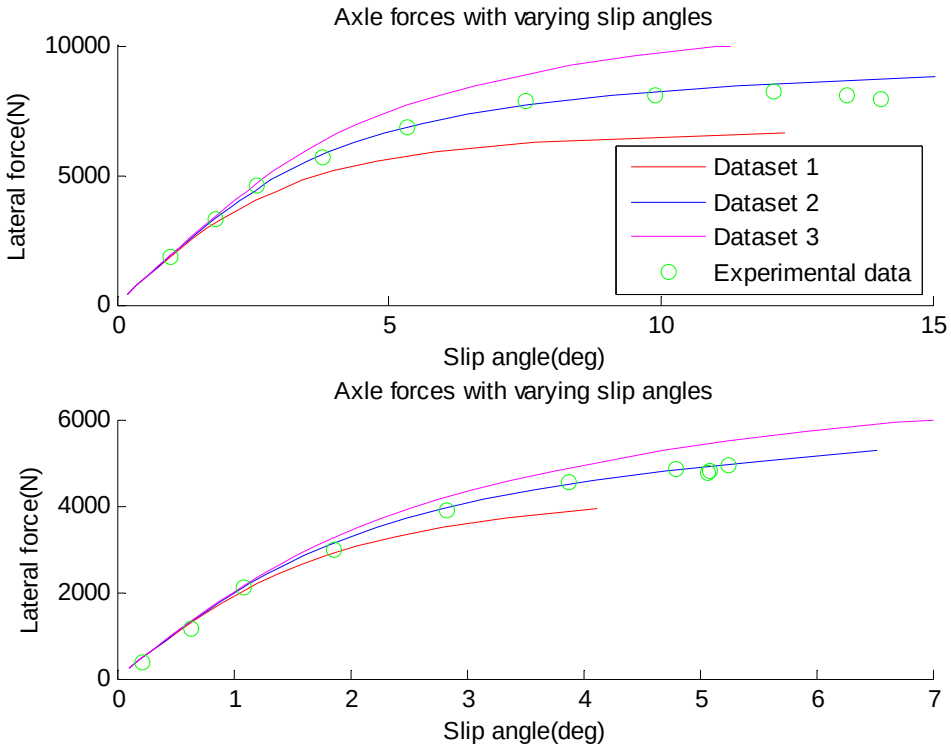

Figure 27 Influence of $\lambda_{\mu y}$ on front and rear axle curve

- λ_{Ey}, has no big influence on the curve. It may come true that changing this parameter is not proficient for the fitting of the experimental data. The usefulness of this parameter is further discussed in section 6.3.
- When the λ_{Ky} scaling factor is changed the lateral stiffness factor is changed. This happens in the same way as for the p_{Ky1} coefficient.

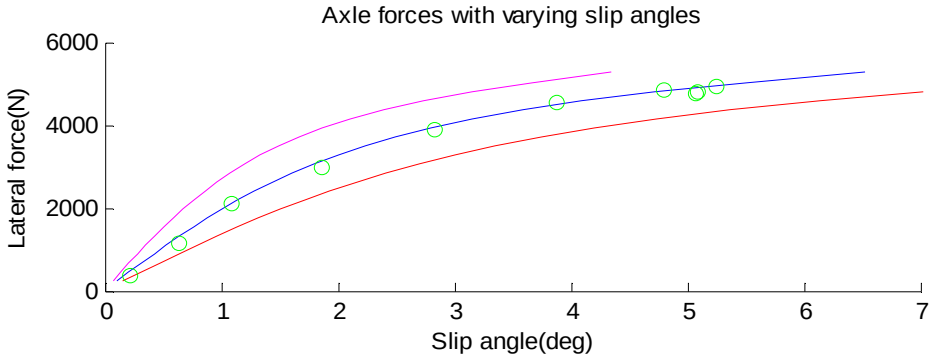

Figure 28 Influence of λ_{Ky} on rear axle curve

6.3 Consideration of E

The TyreEstimator application, which is written for the optimization process, contains the option whether to consider the parameters related to the lateral curvature factor (E_y), to keep them constant or to set them to zero. The parameters related to E_y influence the shape of the peak of the curve for a given condition. If the maximum lateral force can not be built up during the experimental tests, no saturation of the tyres will take place. The maximum lateral force is therefore not reached and the parameters that relate to E_y will not be reliable. To be able to handle this type of experimental data this option is added to the application.

6.4 Evaluation of parameters

From the analysis on coefficients and scaling factors it can be presumed that both parameter sets are suitable to be used in the optimization process, for they should both be able to fit the data correctly. The sets of parameters modify the curve in approximately the same way. The advantage of the scaling factors is that only four parameters are considered, which causes the optimization to operate quicker. Nevertheless, by acting only on the scaling factors, the cornering stiffness variation with the vertical load can not be altered (p_{Ky2}).

Because both design variables are presumably able to fit the experimental data an option is built in. The application then uses the chosen parameter set to perform the optimization. When the choice is made to optimize the coefficients the scaling factors will remain constant and vice versa.

Furthermore, the p_{Ey2} coefficient will no longer be considered because of its small influence on the vehicle model results. Also, because tyre saturation isn't necessarily reached during experimental testing, an option for evaluating the parameters related to E_y is implemented in the application.

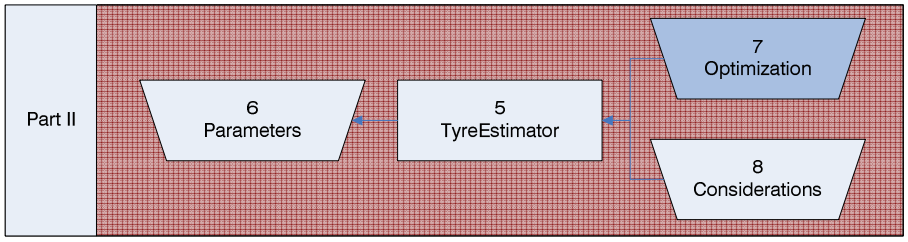

7 Optimization

Optimization is a tool to obtain the best results from a calculation. This calculation is based on how the difference between experiment and model is defined and how this difference can be minimized.

The optimization process is based on two crucial elements, which are important for every optimization. These elements are: The objective function and the algorithm. The sections 7.1and 7.2 treat these elements subsequently.

7.1 Objective function

The input for the TyreEstimator application is called the objective function or cost function. The application minimizes the optimization problem that may be described analytically by the simple function:

$$f(p_0, \lambda_0) = \sum_{i=1}^{n} \left| F_{yi} - F_y(F_{zi}, \alpha_i, p_0, \lambda_0) \right| \qquad \textbf{(7-1)}$$

With i representing every point of the experimental data and n representing the total number of data points. F_{yi} is the lateral force coming from the experimental data, while F_y stands for the lateral force calculated using a vehicle model. The lateral force of the simulation model depends on four variables. Among these α_i refers to the slip angle for every point of the experimental data and F_{zi} is the vertical tyre force, which is directly related to the lateral acceleration. For the Two-DOF model the calculation of F_{zi} is shown in subsection 2.1.1. This formula is validated using more detailed (multibody) models and with the experimental data, as was the F_{zi} of the Fourteen-DOF model. The other two variables in the function are the design variables; p_0 and λ_0. They represent respectively the coefficients and the scaling factors of the Magic Formula on which this optimization is based. Resulting from Chapter 2, these are defined as:

$$[p_0] = \begin{bmatrix} p_{Cy} \\ p_{Dy1} \\ p_{Dy2} \\ p_{Ey1} \\ p_{Ky1} \\ p_{Ky2} \end{bmatrix} \qquad [\lambda_0] = \begin{bmatrix} \lambda_{Cy} \\ \lambda_{\mu y} \\ \lambda_{Ey} \\ \lambda_{Ky} \end{bmatrix}$$

In order to calculate the differences between the lateral forces of the experimental data and the model, the values of the lateral forces of the model at the slip angles of the experimental data are evaluated. This process is shown in Figure 29 and is executed by means of linear interpolation and extrapolation. The considered errors in lateral force for the summation in the objective function are taken in the slip angle domain. If the errors were considered in the lateral force domain, due to the decay of the curve, a lateral force could correspond to two slip angle values. This is not desirable.

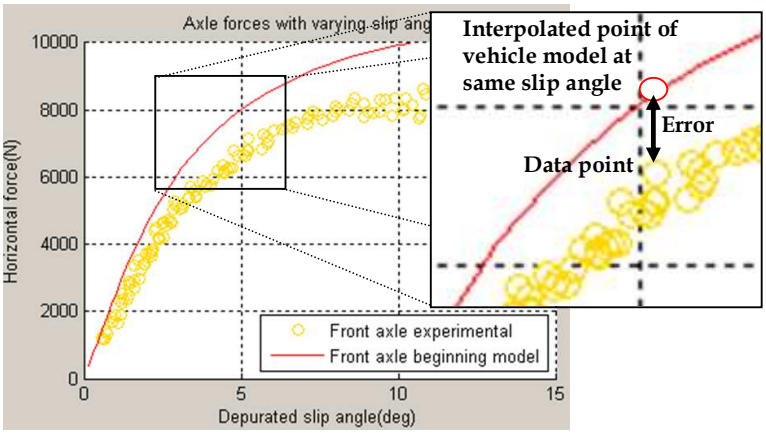

Figure 29 Graphic representation of error calculation

The errors on both axles are summed, though the lateral forces on both axles are different. Considerations made on this topic are written in section 8.3. The measurement data is randomly distributed over the front- and rear slip angle domain. Writing out the error using the Magic Formula, the calculation of F_y becomes:

$$F_y(F_{zi}, \alpha_i, p_0, \lambda_0) = D_y(F_{zi}, p_0, \lambda_0)\sin \left[C_y(p_0, \lambda_0)\arctan \left\{ \begin{matrix} \alpha_i B_{yi}(F_{zi}, p_0, \lambda_0) - \\ E_{yi}(F_{zi})\left(\alpha_i B_{yi}(F_{zi}, p_0, \lambda_0) - \arctan\left(\alpha_i B_{yi}(F_{zi}, p_0, \lambda_0)\right)\right) \end{matrix} \right\} \right] \quad \textbf{(7-2)}$$

The previously described objective function (7-1) is used to explain the principle. In this objective function simply the sum of the errors is calculated. It is not explicitly necessary to use this function. Another, more complicated function could be to divide the absolute errors by the respective interpolated lateral forces of the errors. By taking the mean value thereof, a ratio is obtained which enables the comparison of values from different optimizations in a proper way. The objective function is then given by:

$$f(p_0, \lambda_0) = \frac{1}{n} \sum_{i=1}^{n} \frac{\left| F_{yi} - F_y(F_{zi}, \alpha_i, p_0, \lambda_0) \right|}{F_y} \tag{7-3}$$

Another option, if a part of the curve does not match the experimental data, is the possibility to take that part more into consideration. Applying a weight function, by multiplying the errors with a triangular weight profile that starts at 0.5 and ends at 1.5 in the slip angle domain, changes the contributions of the errors to the total sum. This function gives more importance to the high slip angles, where the correlation is generally worse. The errors at small slip angles will then contribute less to the total error then the errors at high slip angles. One of the problems of adding weight to a function is that there is no longer a uniform method to compare the results. The formula with weight function used is written as:

$$f(p_0, \lambda_0) = \sum_{i=1}^{n} \left| F_{yi} - F_y(F_{zi}, \alpha_i, p_0, \lambda_0) \right| \left(0.5 + \frac{(\alpha_i - \alpha_{\min})}{(\alpha_{\max} - \alpha_{\min})} \right) \tag{7-4}$$

Other weight functions could also be applied to this problem, though this weight function is easy to implement and the most logical in this situation.

7.2 Algorithm

For the solving of optimization problems an algorithm is needed. An algorithm is an effective method for solving a problem using a finite sequence of instructions. The optimization algorithm starts at an initial state and, through well-defined instructions which determine new states, it comes to a final state. Optimization algorithms are available in the Matlab environment. The limited amount of time to customize an optimization algorithm especially for this problem and the proven efficiency of the available algorithms is reason for using these.

From the non-linear terms in the objective function it can be deduced that this problem concerns non-linear optimization programming. Two optimization routines

are available in Matlab which can be implemented in the TyreEstimator for solving this type of problem; the fminsearch routine and the lsqnonlin routine. The working of these two methods is explained in subsection 7.2.1 and 7.2.2.

7.2.1 Fminsearch

The fminsearch algorithm is a zero order method, meaning that it doesn't use gradient information to calculate the next state. Generally this algorithm is used for unconstrained non-linear optimization problems. It can handle several variables and starts at an initial given estimate. This method is very robust, but requires generally more steps to find an optimum compared to other methods.

This algorithm incorporates the downhill simplex method or Nelder-Mead method. The routine starts with the virtual construction of a simplex, a polytope with N + 1 vertices, in N dimensions. For example a triangle in the 2D design space or a tetrahedron in the 3D space. N is related to the size of the parameter set of the design variable (p_0 or λ_0). The method starts with generating N + 1 points from the initial parameters. Extrapolating the behaviour at each test point, Nelder-Mead generates a new test point. One of the test points is replaced by the new test point and so the technique progresses. The simplex can also be expanded, contracted or reflected to find a new position. The process is being repeated until the largest diagonal of the simplex is smaller than a chosen value and thus a (local) minimum is found.

7.2.2 Lsqnonlin

The lsqnonlin algorithm, which stands for least square non-linear algorithm, is a pseudo-second order method. Normally a second order method works with function evaluations and gradient information and the Hessian matrix. This algorithm estimates the Hessian matrix instead of calculating it and is therefore described as a pseudo-second order method. The routine is generally used for solving non-linear least-squares problems, including non-linear data-fitting problems. Besides, it can handle under-determined problems, where the number of equations is less then the number of variables. Combined with the robustness and speed of this method it is suitable for the optimization routine that has to be carried out for this project.

This algorithm uses the Levenberg-Marquardt method. In contrary to the fminsearch algorithm it accounts for the error between the experimental data and the vehicle

model using a square. The objective function remains the same but the algorithm squares the individual contribution of the error, so the function can be written as:

$$S(p_0 / \lambda_0) = \sum_{i=1}^{n} \left(F_{yi} - F_y \left(F_{zi}, \alpha_i, p_0, \lambda_0 \right) \right)^2 \quad \textbf{(7-5)}$$

The root of the outcome divided by n, leads to the RMS value. This value gives a statistical measure of the amplitude, which would be ideal for the comparison of different objective functions. However due to the different objective functions this value can not be used throughout the entire thesis.

For every iteration the design variable, p_0 or λ_0 depending on the chosen options in the application, is replaced by a new estimate. If the case of p_0 is analyzed, this new estimate is represented by $p_0 + \delta$. This δ is determined, by approximating the function, using a linearization this becomes:

$$f(p_0 + \delta) \approx f(x_i, p_0) + J_i \delta$$

Where the gradient of the function f with respect to the design variable is given by:

$$J_i = \frac{\partial f(x_i, p_0)}{\partial p_0}$$

When the gradient of S with respect to δ is zero, a (local) minimum is found. Differentiating S using the first order approximation $f(p_0 + \delta)$ and setting the result to zero leads to the following relation:

$$\left(J^T J \right) \delta = J^T \left[y - f(p_0) \right]$$

This is a set of non-linear equations which can be solved for δ. If a damping term is introduced into this equation, this becomes:

$$\left(J^T J + \lambda I \right) \delta = J^T \left[y - f(p_0) \right]$$

λ represents the non-negative damping term and I is the identity matrix. The damping term is adjusted for each iteration.

$$\left(J^T J + \lambda diag\left(J^T J \right) \right) \delta = J^T \left[y - f(p_0) \right]$$

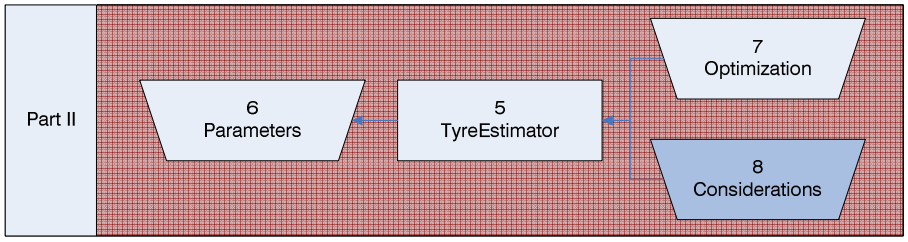

8 Considerations

Apart from the standard components of an optimization process, each optimization has its own specific needs and particularities that influence the outcome of the optimization. Several options, which are special for this optimization procedure, to improve the quality of the optimization are programmed in TyreEstimator application.

In section 8.1 the starting point is considered. Section 8.2 concerns the averaging of the experimental data, while in section 8.3 the number of datasets for the optimization is discussed.

8.1 Starting point

The starting point can be changed at the beginning of the application. Therefore after clicking the 'Plot'- or 'Start optimization'-button the choice to customize the data must be made. In a new dialog box the default starting parameters are shown. These can be altered individually. By clicking 'OK' the chosen procedure is started using the implemented values. Otherwise the default initial conditions will be taken, which are given in Appendix D. The (new) starting parameters are shown in the GUI of the TyreEstimator contemporaneously with the initial error.

The starting point can be an important factor in the calculation of the tyre parameters. Different initial values can cause the algorithms to find a local minimum, while both algorithms are sensitive to this phenomenon. Using other initial parameters the finding of local minima can be prevented. In the application the initial parameters and the final parameters of the optimization are shown.

8.2 Averaging

With averaging, a way for the experimental data to be clustered to fewer points is denoted. The program divides the number of experimental data points by ten and

the mean value of these points is calculated. From this operation ten new points are obtained in which all the experimental data is contained. The error between the model data and the 'new' experimental data is now the objective function. For the fminsearch algorithm, in which the objective function is given by the sum of the errors, the averaging before or the averaging in the error function will not change the result. However, depending on the interpolation and the objective function this may lead to different results.

This way the potential influence of outliers is adaptable. The data is more consistent; especially when many outliers are present this method provides a good alternative. Less required calculations and thus the higher speed also favour the use of this principle.

8.3 Number of parameter sets

The option for different parameter sets is implemented in the TyreEstimator application to make it possible to cope with differing front- and rear-axle experimental data. When this option is selected, the optimization is first based only on the front axle. An 'optimum' set of parameters is calculated as well as an error on the front axle. Next the same procedure is completed for the rear axle.

The choice can be used to see if there are relevant differences between the behaviour of the front and rear tyres and to see which parameters differ most between the two axles. Another possibility is when different front wheels and rear wheels are mounted on the vehicle and the behaviour has to be evaluated individually.

This option makes it also possible to cope with non-saturated tyres. For example, if the rear axle does not reach saturation, the first optimization could be based on the rear axle not using parameters concerning E_y. Next a complete optimization can be done, with the rear axle parameters as a basis.

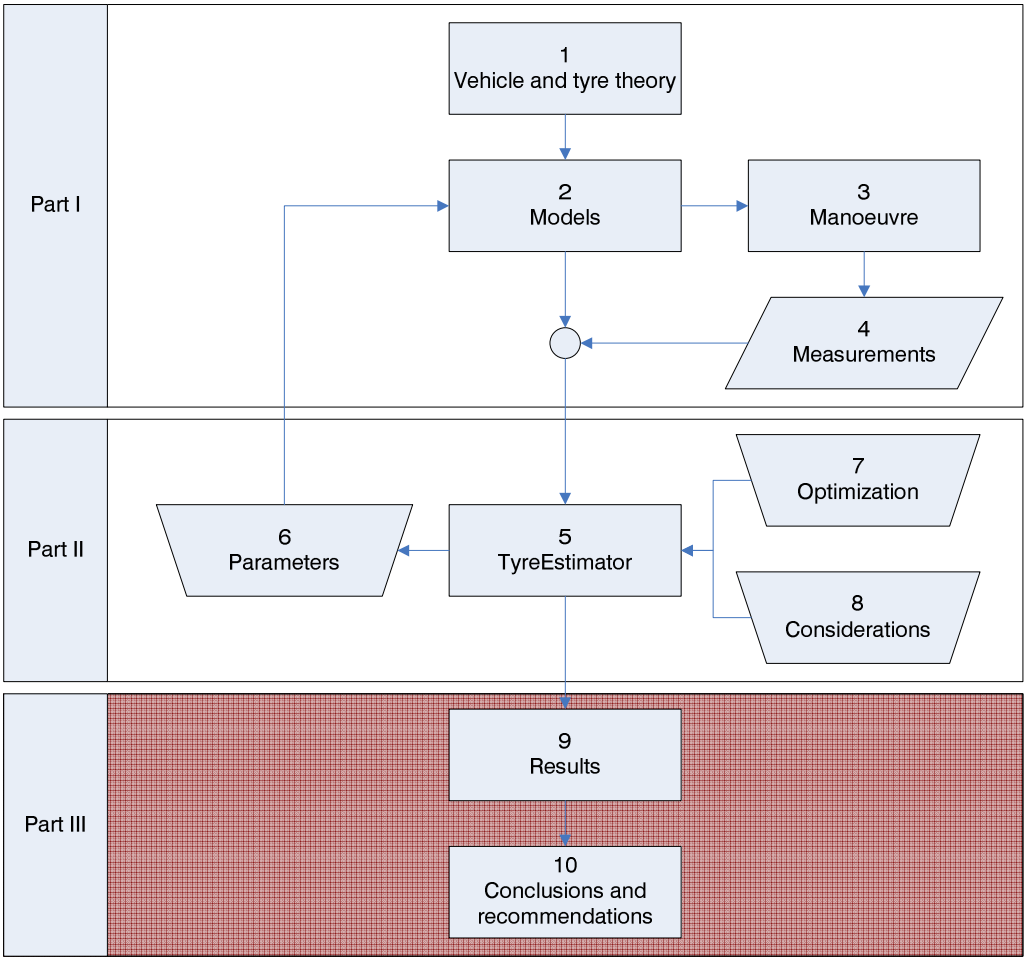

Part III Results and conclusion

"Methods and techniques that have consistently shown results superior than those achieved with other means, and which are used as benchmarks to strive for. There is, however, no practice that is best for everyone or in every situation, and no best practice remains best for very long as people keep on finding better ways of doing things." – Business dictionary.com

The multiplicity of influences on the F_y-α curve makes it difficult to define a unique configuration for the TyreEstimator application to find good parameters for the Magic Formula that correspond to the experimental data. Therefore in this thesis a 'best practice' is shown for the data provided by the CRF.

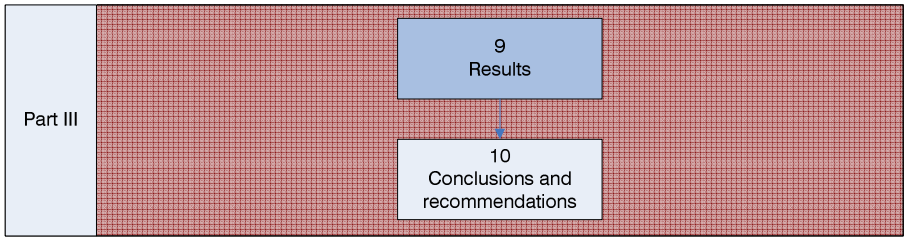

9 Results

The results of the optimizations for identifying the tyre parameters are described in this chapter. The performed optimizations are based on one set of experimental data. The identification of the tyre parameters is only valid for the part shown in the graphs. Beyond the experimental data, no reliable information can be given over the tyre behaviour using the results from the optimization.

It is possible that for a different dataset other options of the application show better results. The TyreEstimator is written with that in mind. The options built in the application have the purpose to be able to best match this set of experimental data. To find these options a 'best practice' method is used. The application options should finally be verified through optimizations using data sets of different vehicles with respective simulation models to check its quality.

In section 9.1 the results of the Two-DOF model are discussed, while in 9.2 these are discussed for the Fourteen-DOF model.

9.1 Two-DOF model

Recapitulating, the Two-DOF vehicle model is a simple and easy model that can make quick iterations. It is based on the theory of a bicycle model, where the effect of the rolling of the vehicle is compensated using the effective axle characteristics. The model calculates an equilibrium for every lateral acceleration. Its tyre model is based on the Magic Formula, but only six coefficients and four scaling factors are taken into account. A more extensive description is found in section 2.1. The purpose of this model was to help develop the application and to make a good and quick estimation of the parameters, which can be refined by making use of the Fourteen-DOF model.

In subsection 9.1.1 the standard optimization is discussed, additionally some general observations that occurred during simulation are noted. Subsection 9.1.2 treats the issues that concern the parameters, while subsection 9.1.3 treats the issues that

concern the optimization options. In subsection 9.1.4 the other options built in the application to improve the results of the simulations are discussed. The results are found in the Appendix F.

9.1.1 General comments

The graphs of Figure 30 show the initial conditions together with the optimized result using the standard conditions for the optimization with this vehicle simulation model. To make a proper comparison between the standard optimization and the manipulated optimizations only one aspect is considered per comparison. This way the improvement or deterioration can be considered well.

These standard conditions to which the errors are related for the Two-DOF model are:

- Objective function given by equation (7-3), where the errors are divided by their respective lateral forces (referred to as scaled error function)
- Fminsearch algorithm
- Optimization on coefficients
- Optimization on E_y
- Handtuned initial parameters
- No averaging
- Extrapolation
- One dataset

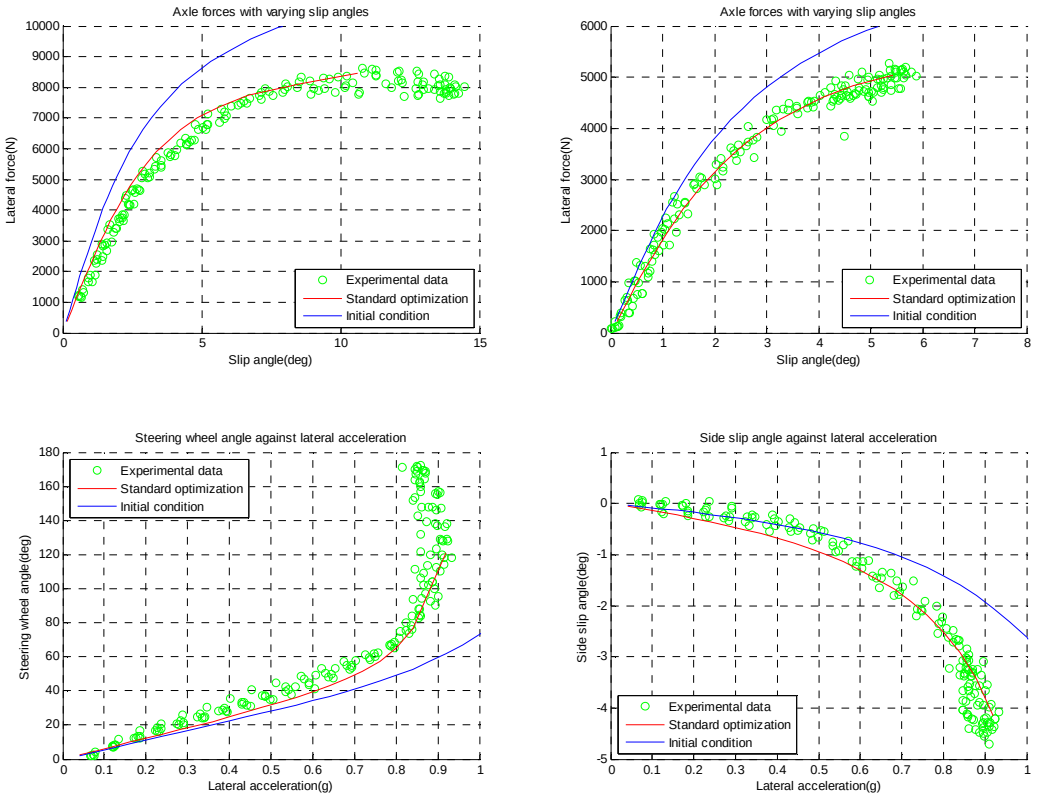

Figure 30 Two-DOF Results of standard optimization and initial condition

The quality of the optimization is based on the visual interpretation of the graphs and on a calculated error. This error takes the mean of all (front and rear) absolute differences between the experimental and the interpolated modelled data. By dividing each difference by its respective interpolated modelled data this can be expressed as a percentage.

In Figure 30 the upper left graph shows the lateral forces and slip angles at the front axle, while the upper left shows the same properties for the rear axle. This can also be deduced from the fact that lateral forces occur at the front axle. The lower graphs show from left to right two other important properties of the vehicle; the steer wheel angle vs. the lateral acceleration and the side slip angle vs. the lateral acceleration.

A similarity is noted between the F_y-α front and rear curves and respectively the steer wheel angle and side slip angle curve. These are related by the equations presented in Appendix C. In (C-5) the relation for the steer wheel angle is given by:

$$\delta_1 = -\alpha_2 + \alpha_1 + \frac{L}{R}$$

The relation (C-8) gives the relation between side slip angle and rear axle slip angle, which reads:

$$\beta = \frac{x_2}{R} - \alpha_2$$

F_y and a_y for front and rear axle are also directly related by the formulas:

$$F_{y1} = a_y m_1$$
$$F_{y2} = a_y m_2$$

Therefore if one of the curves matches the experimental data, the other curve should match the data as well. Figure 30 corresponds to this theory.

9.1.2 Parameters

To find the best parameter set first the comparison is made between a standard optimization using coefficients and one using scaling factors. From Figure 31 it appears that the differences between these two results are minimal, although the calculated error is about 15 % higher for the scaling factors. The optimization performed on the scaling factors is about five times quicker than when performed on the coefficients. This is due to the fewer parameters that have to be optimized.

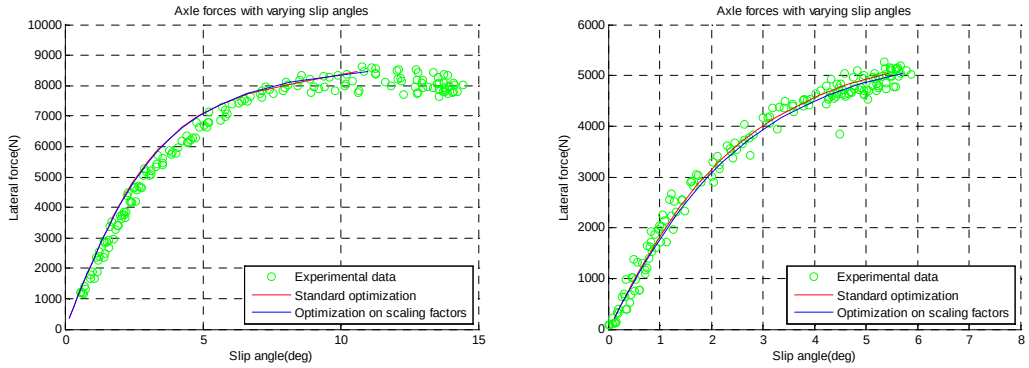

Figure 31 Two-DOF results of comparison between coefficients and scaling factors

The second comparison tests whether the parameters that compose E_y improve the results of the optimization. The outcome improves when p_{Ey1} is kept constant (p_{Ey2} is already kept constant) and even when set to zero (also p_{Ey2} is set to zero to eliminate the effect of E_y). The mean error diminishes with almost 1.5 % for both options. A visual improvement is shown especially for the result on the front axle, which can be seen in Figure 32. It centres the experimental data much better at the beginning of the curve. The difference between the two curves produces by the simulation with

constant p_{Ey1} and p_{Ey2} and the simulation with p_{Ey1} and p_{Ey2} taken as zero is minimal. Only the peak, considered in the Two-DOF model as the final simulation is located earlier for the constant E_y component.

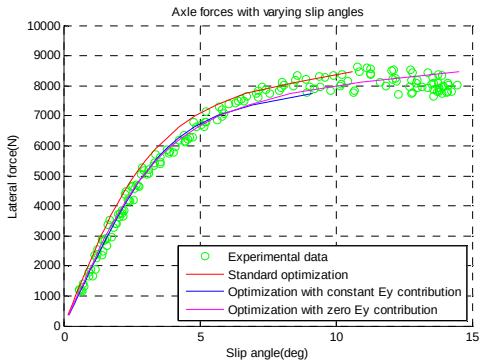

Figure 32 Two-DOF result of comparison of consideration of E_y component for front axle

9.1.3 Optimization

The objective function is evaluated using the objective functions (7-1), (7-3) and (7-4) mentioned in section 7.1. In Figure 33 the results of these optimizations are shown. The optimizations with an objective function different from the standard one result in an error of 5 to 10%. It can be concluded from the graphs that the optimization without scaling tends less to optimize on the high slip angles. In that case all differences contribute in the same way to the objective function. Considering that for low lateral forces the data is less scattered, this leads to more attention from the optimizer to the first part of the graph.

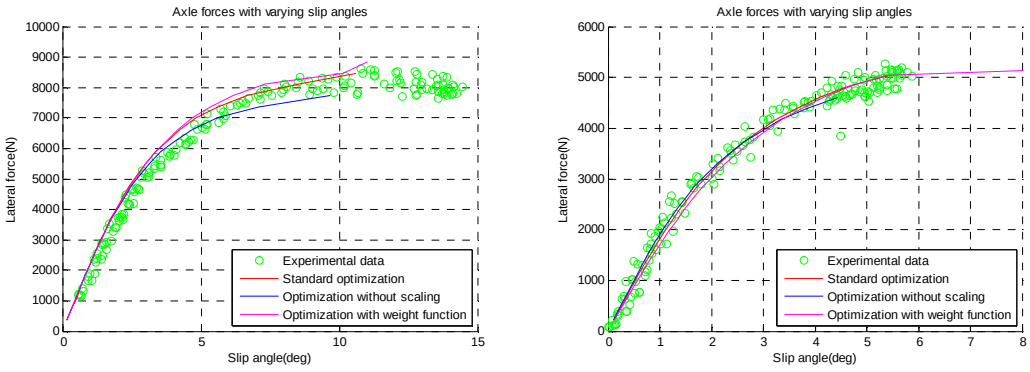

Figure 33 Two-DOF results of comparison between objective functions

During the simulations it turned out that for this system the lsqnonlin-algorithm did not work. When the lsqnonlin-algorithm was used, the following error message appeared: "Ill-conditioned matrix". This is the case when small changes in the

coefficients of the solution have drastic effects on the results. Iterating the solutions to a small residual is then a tricky operation. Numerical round-off can also cause trouble if a matrix is ill-conditioned.

9.1.4 Considerations

When the original coefficient from the tyre manufacturer is used as different starting point, it is not possible to find the same or better results than with the original initial conditions. Although the experimental data for the front axle is matched better for low slip angles, for higher slip angles the difference between the experimental data and the simulation is clearly present. The effects on the rear axle are even worse, noticeable in Figure 34, leading to a total error that is 25% higher with respect to the standard optimization. The different behaviour is due to a local minimum found using the coefficients from the tyre manufacturer. If the starting curve is located closer to the objective curve the chance to find local minima is smaller.

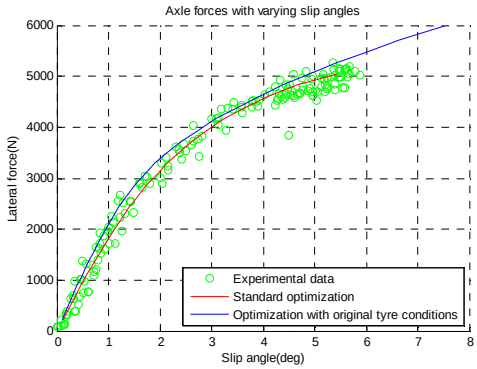

Figure 34 Two-DOF result of comparison between different initial conditions for rear axle

Looking at the results using the averaging option in the TyreEstimator application, the difference for the rear axle is negligible. When considering the averaged points, the curve produced by the standard optimization lies closer to the averaged points. This is deduced from Figure 35 and confirmed by the calculated error. The averaging option does not improve the results of the optimization in this case. The difference between the averaged curve and the curve produced by the standard optimization is explained by the fact that the averaging is performed before the interpolation and the objective function.

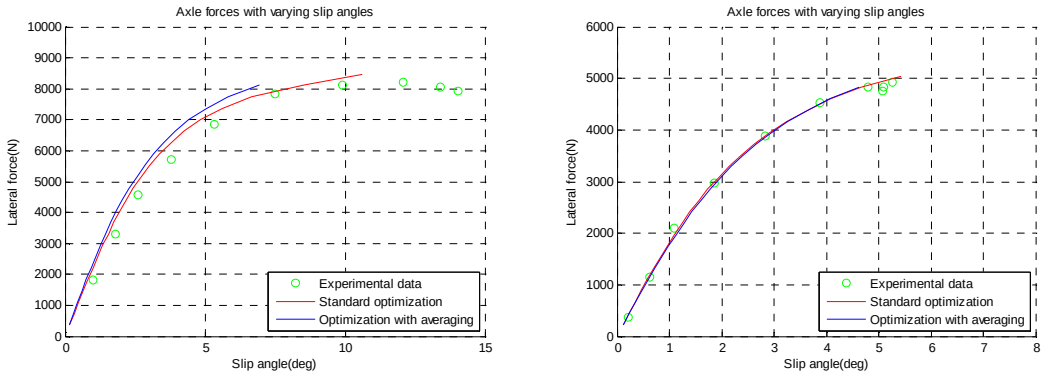

Figure 35 Two-DOF results of comparison using averaged datapoints

The last option of the application that is considered is whether or not to use different parameter sets to discriminate the tyre parameters. The results are reproduced in Figure 36. The errors found using two parameter sets are smaller than for the standard optimization. Therefore the optimization procedure has to be performed two times. It is questionable if this is worth it. When the two resulting parameter sets are compared the largest difference is viewed for the p_{Ey1}. It can therefore be assumed that the tyres are alike but because saturation is only reached for the front axle the E_y parameter can only be found using the front axle curve.

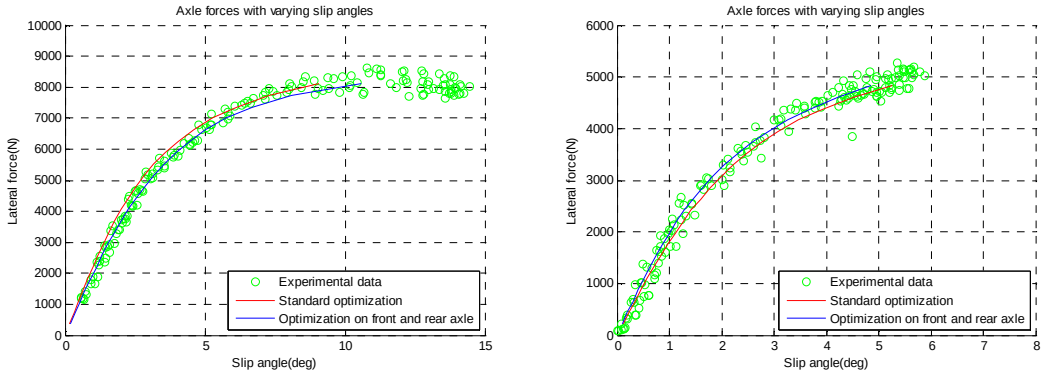

Figure 36 Two-DOF results of comparison for different datasets on front and rear axle

9.2 Fourteen-DOF model

The Fourteen-DOF vehicle model is a complex vehicle model developed by CRF. The model performs a dynamic simulation by using look-up table based models of vehicle components to simulate a certain vehicle. One of these component models is the tyre model; represented by the Magic Formula. In this model all parameters are used, however only six coefficients and four scaling factors are used for the

optimization. For a more extensive description of the model it is advisable to read section 2.2. The purpose of this model was to refine the results from the Two-DOF model and get the coefficients that correspond best to the experimental data.
In subsection 9.2.1 the standard optimization is described and a comparison between the two and the fourteen DOF model is made. The topic concerning the parameters is treated in subsection 9.2.2. The options related to the optimization procedure are treated in subsection 9.2.3. Finally, in subsection 9.2.4, all other options involved in the application are commented. The results can be found in Appendix G.

9.2.1 General comments

The initial conditions for the optimization with this vehicle model are slightly different with respect to the Two-DOF vehicle model. Only the starting parameters and the optimization algorithm are changed to improve the basic quality of the results. The standard conditions for optimization, shown in Figure 37, with the Fourteen-DOF model are now given by:

- Objective function given by equation (7-3), where the errors are divided by their respective lateral forces (referred to as scaled error function)
- Lsqnonlin algorithm
- Optimization on coefficients
- Optimization on E_y
- Original initial parameters
- No averaging
- Extrapolation
- One dataset

For this model the quality of the results is based on the visual aspect of the optimizations as well as on the results. The third aspect is based on the optimization time, because this aspect plays an important role for this vehicle model.

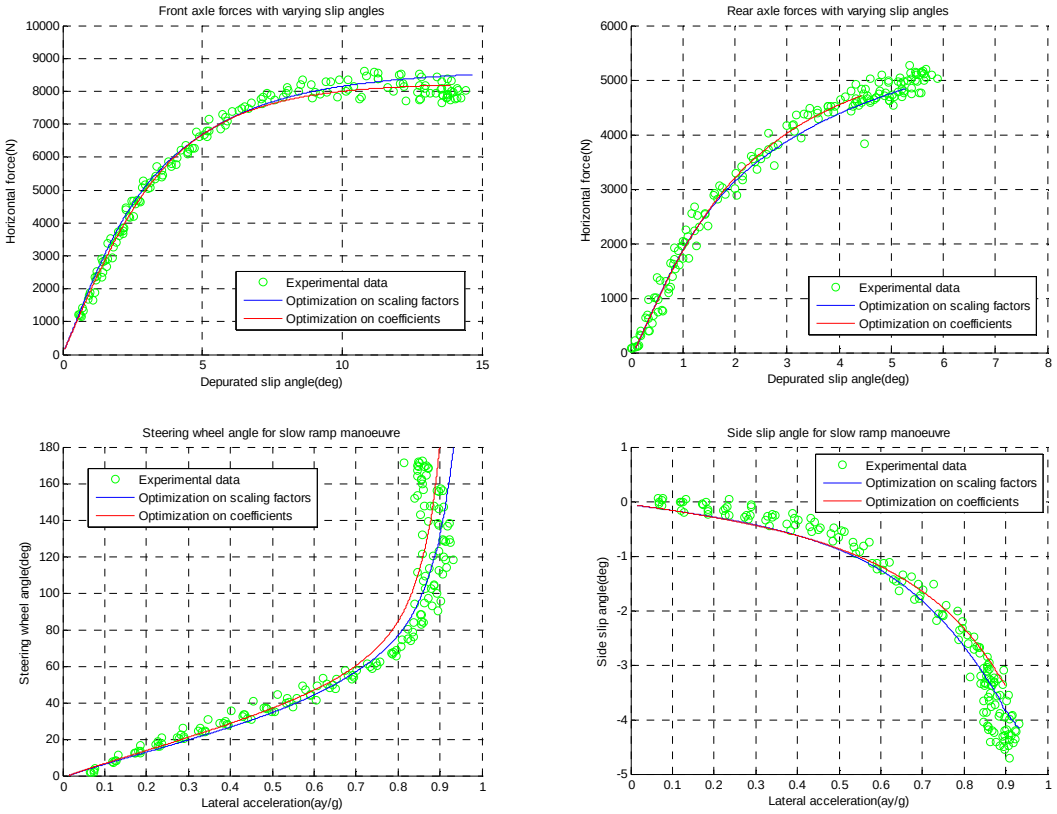

Figure 37 Fourteen-DOF results of comparison between coefficients and scaling factors

Also for this vehicle model the relationship between the F_y-α curves and the steer wheel angle and side slip angle curves is noted from Figure 37.

The p_{Ey2} coefficient was initially considered for this model, therefore the complete results in the Appendix show also p_{Ey2}. Along the way the limited influence of p_{Ey2} was noted, but due to the limited amount of time to use this model it was not possible to generate the results without considering p_{Ey2}. The small influence of p_{Ey2} on the simulations, though the results can still be considered reliable.

The complex vehicle model did not show the same results with the same parameters of the simple vehicle model. This is shown in Figure 38, where the results of the standard optimization with the Fourteen-DOF model is plotted using the Two-DOF model and compared with the results of the optimization with the Two-DOF model. The difference is due to the Magic Formula tyre parameters used as input of the two models. For the simple model these are only the ones that were described earlier, while the complex model makes use of all other parameters of the Magic Formula as well. Although the other parameters for the Fourteen-DOF model are kept constant during the optimization they influence the tyre behaviour noticeably.

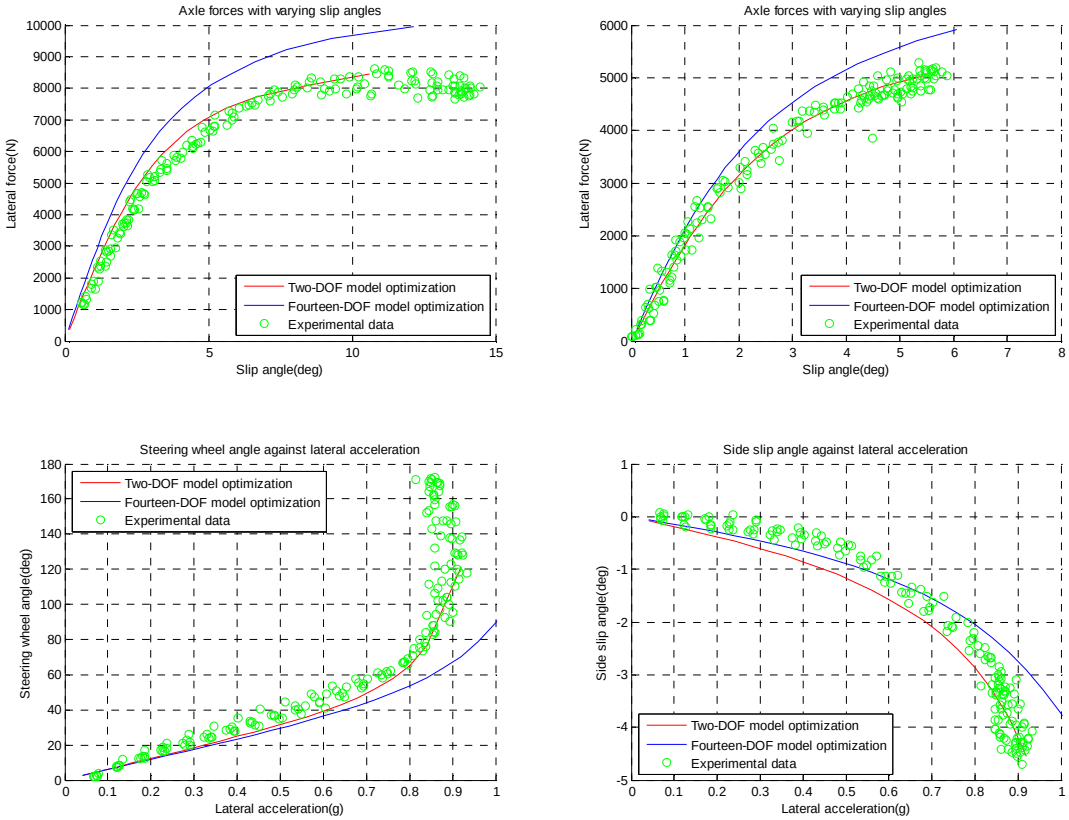

Figure 38 Comparison of results of optimization Two-DOF model and Fourteen-DOF model

9.2.2 Parameters

The optimization of the coefficients is compared with the optimization of the scaling factors in Figure 37. The optimization of the coefficients shows the best results, although the mean error difference is only 0.5%. For the front axle it can be seen that the peak is reached nicely using this optimization. The optimization time doesn't differ much, although one optimization uses six parameters and the other optimization uses four.

Setting the E_y component to zero is not an option for this model, because of the many parameters involved with E_y. The optimization where p_{Ey1} and p_{Ey2} are kept constant shows in this case no difference compared to the standard optimization, as can be deduced from Figure 39. The error is very similar, moreover the optimization time is longer.

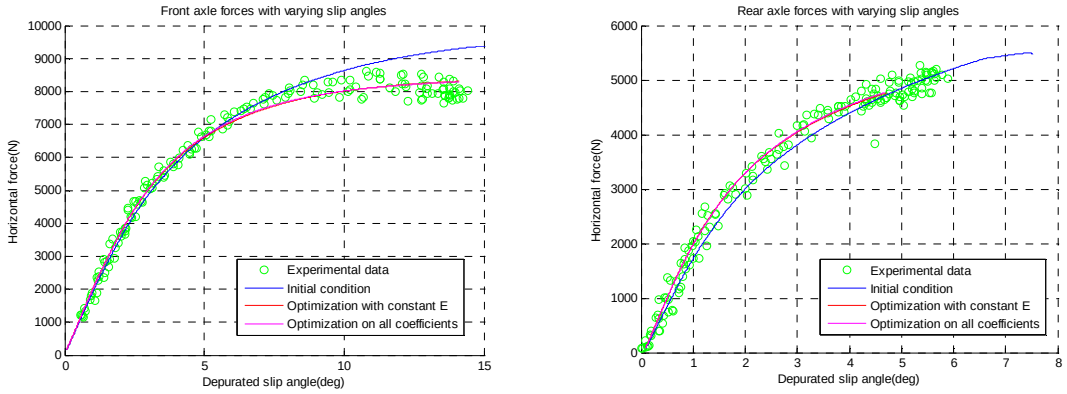

Figure 39 Fourteen-DOF model results of comparison of consideration of E_y

9.2.3 Optimization

In Figure 40 it is visible that the differences for the objective functions options are minimal. From the results can be derived that the option with scaling matches the experimental data best, notwithstanding that the other optimizations give good results as well. The optimization time with the error function multiplied by the respective slip angle is 1.5 times longer than the optimization time of the other two that are almost equal.

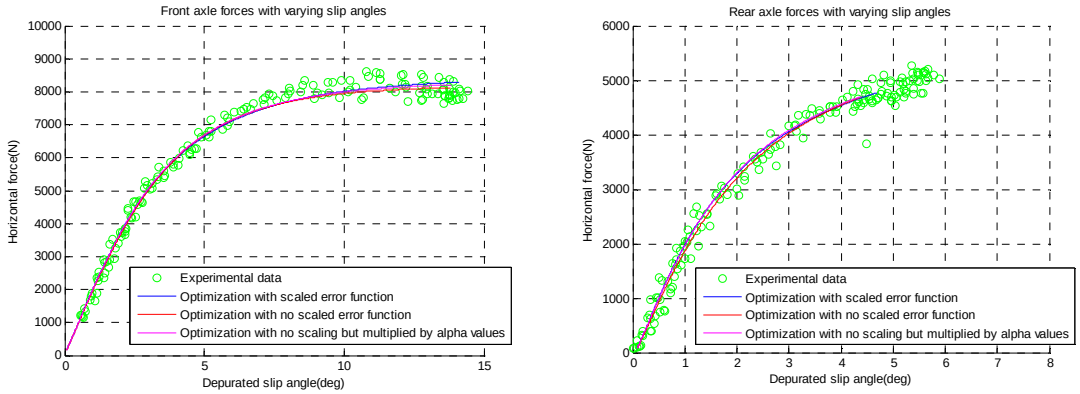

Figure 40 Fourteen-DOF model results of comparison between different objective functions

The optimization using the fminsearch-algorithm is more than two times quicker than the lsqnonlin-algorithm. This speed counteracts the quality of the optimization. Since the lsqnonlin-algorithm considers the first order gradient, the chance of finding local minima is considerably reduced. This can be seen particularly well for the fminsearch optimization results on the rear axle characteristics. In Figure 41 the first part of the model is too high with respect to the experimental data. The peak of the

front axle of the fminsearch optimization is located beyond the maximum slip angle, which is also undesirable.

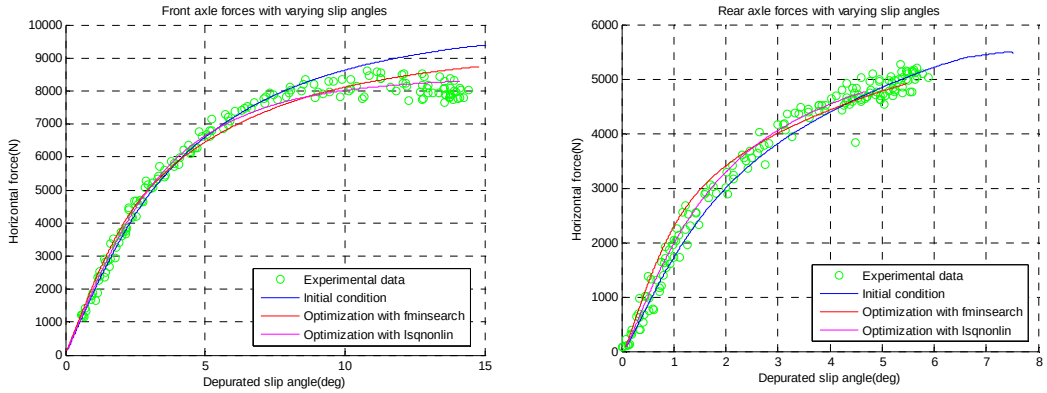

Figure 41 Fourteen-DOF model results of comparison between the two algorithms

9.2.4 Considerations

Altering the starting point can prevent the algorithm from getting stuck in a local minimum. The resulting coefficients of the two optimizations differ from each other but are of the same order. Visually the result is about the same (Figure 42).

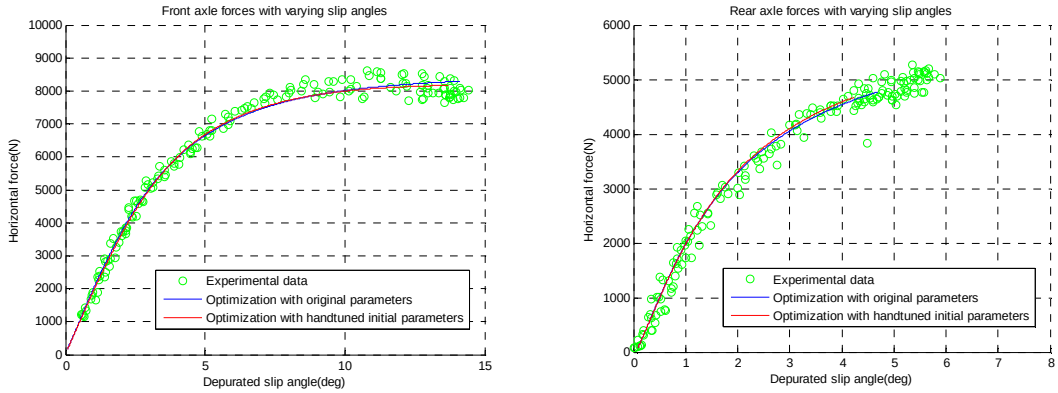

Figure 42 Fourteen-DOF model results of comparison between different initial conditions

The result on the front axle of the optimization using averaged datapoints compared with the results of the optimization using the normal datapoints is shown in Figure 43. The averaged results are slightly better. The optimization time is about the same as are the resulting coefficients.

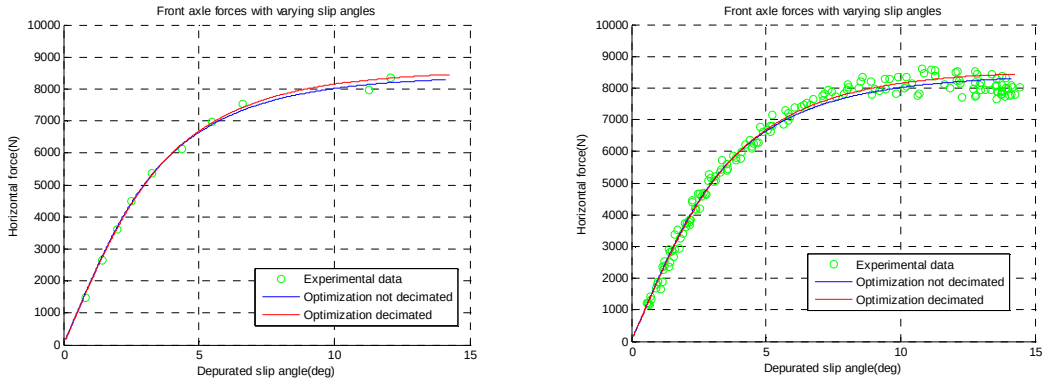

Figure 43 Fourteen-DOF model results of comparison using averaged datapoints for front axle

For this case the optimization is first performed considering the front axle and then a new optimization is performed considering the rear axle. The results are presented in Figure 44. When these results are combined a 'perfect' match is obtained for front and rear axle curves, although the C_y, the D_y and the E_y components have different parameter sets. Not reaching saturation at the rear axle is an unsatisfactory explanation for the difference between these components. Reflecting that the same tyres were used, probably these showed different behaviour due to other causes, like wear or temperature differences.

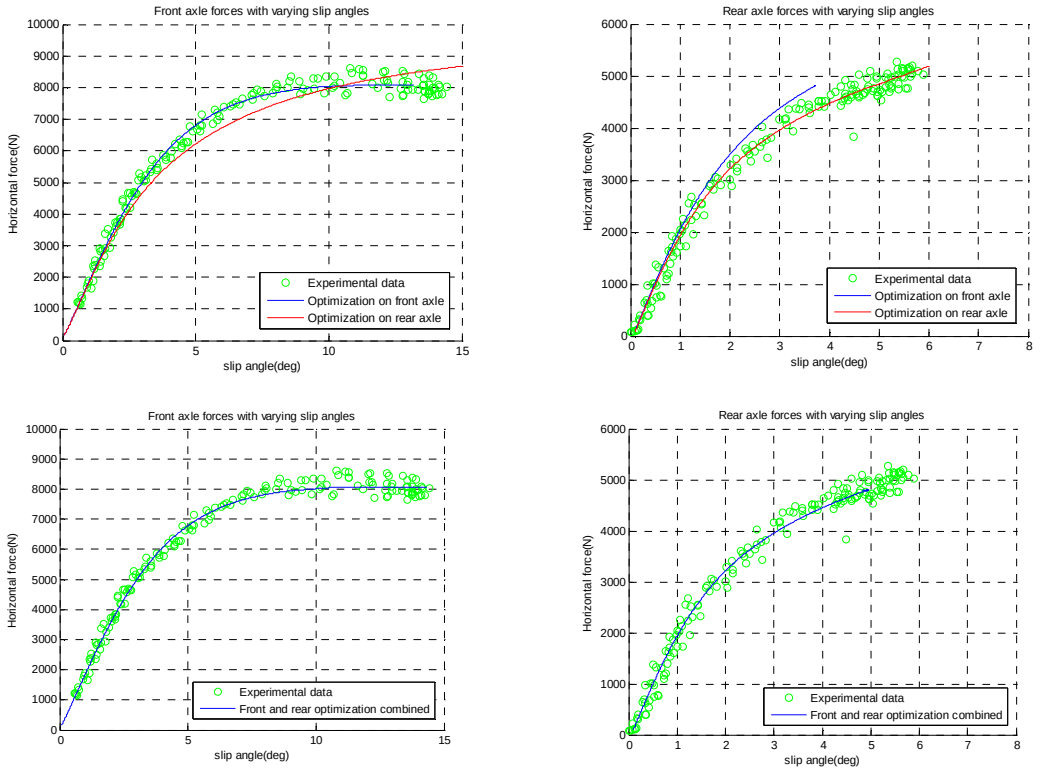

Figure 44 Fourteen-DOF model results of comparison for different datasets on front and rear axle

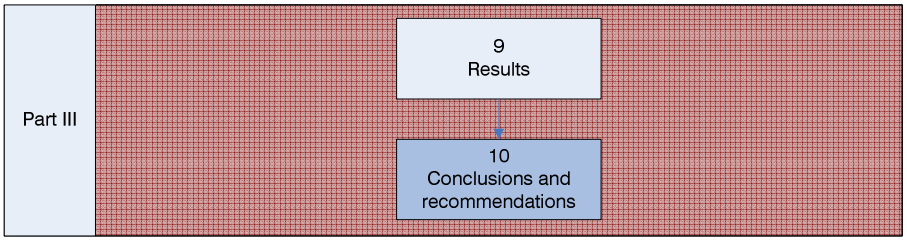

10 Conclusions and recommendations

The goal was to create an application that identifies automatically the tyre parameters from tests on a complete vehicle. Meanwhile, computation of the selected parameters to identify is a complex problem. The different dependencies of the parameters on components, methods and initial conditions complicate finding one optimal set of options that solves the problem. To make it possible to deal with the different properties an application was created to find the best results. This way the options that result in the best fit can be adapted for any data set and for any purpose.
Using the TyreEstimator application, optimizations were performed employing the two vehicle models discussed in this thesis. The models vary from each other not only in approach and complexity, but also the tyre model used is different. Although both make use of the Magic Formula, the implementation is different. This leads to different results in terms of parameters. In terms of visual results these are similar.
In the consideration of the results the option with two parameter sets is not taken into account. All tyres have been assumed to be equal, so the behaviour at the front and rear axle should be alike. This is not in accordance with the results and therefore this option is not acknowledged.
The conclusions for the two vehicle models are given in section 10.1 and 10.2. Finally some recommendations are given in section 10.3.

10.1 Two-DOF model

The vehicle model with two degrees of freedom has the advantage to perform cheap optimizations because of the simplicity of this model. The drawback consists in the poor applicability of these results and the low accuracy, due to the small amount of parameters involved.
All in all the 'best practice' for the Two-DOF vehicle model is given by the optimization that uses the scaling factors and does not consider the E_y components.

10.2 Fourteen-DOF model

The vehicle model with fourteen degrees of freedom has the advantage to discriminate the parameters with much more accuracy than the simple model. A shortcoming for the higher accuracy is the larger computation time.

The 'best practice' for the Fourteen-DOF model is the standard optimization, optimizing on coefficients and considering the E_y components. Overall the options used in this optimization with the complex vehicle model are preferable when the time factor is not crucial, because of the accuracy and the fact that the results describe the tyre behaviour using the complete Magic Formula tyre model.

10.3 Recommendations

It has been shown that with the use of the TyreEstimator application it is possible to calculate parameters of the Magic Formula that match the experimental data. Although the application works, more research is required to improve and expand the working field of the application. This research has to look into the following issues:

- Local minima: The two algorithms used for this thesis regularly find local minima. To avoid this problem another optimization algorithm should be implemented. The Monte Carlo method should be more suitable. This method relies on random sampling to compute its results. It is favourable especially when deterministic algorithms can not find exact results. However this algorithm is more expensive than the used algorithms
- Parameters to optimize: By reducing the design space and thus the number of dimensions of the solution space, the possibility to find local minima is also reduced. It has been showed that this could be done for the p_{Ey2} coefficient, this leads to the conclusion that this could be extended to other insensitive parameters as well.

  On the other hand the fact that the optimization is done only on six coefficients or four scaling factors reduces the possibility for the optimization to compensate for certain phenomena that occur during the manoeuvres. To manage that, the camber angle equations should be introduced in the loop of the optimization. It implies more parameters for the optimization, which could cause more uncertainties and inaccuracies, but if done well the

reliability of the parameters improves significantly. Finding the right balance between useful 'old' parameters and 'new' parameters to implement is therefore an important issue.

- Computation time of Fourteen-DOF model: The 14-DOF model is preferred for finding the parameters that match the experimental data. This model has the disadvantage that the optimization takes a lot of time. By reducing this optimization time significantly the identification would be even more useful. This could be done by simplifying this vehicle model or try to implement the complete Magic Formula tyre model in the Two-DOF model.

Furthermore, TNO showed interest in this thesis and would like to read it. This implies that the TyreEstimator application could be a good basis for further development of the identification of the Magic Formula tyre coefficients.

Literature

Abe, M. (2009). Vehicle Handling Dynamics: Theory and Application. Oxford: Butterworth-Heinemann.

Arosio, D., Braghin, F., Cheli, F., Sabbioni, E. (2005). Identification of Pacejka's scaling factors from full-scale experimental tests. *Vehicle dynamic systems*, Volume 43 (1), pages 457-474

Bakker, E., Nyborg, L., Pacejka, H.B. (1987). Tire modelling for use in vehicle dynamics studies. *SAE paper*, Number 870421

Bakker, E., Pacejka, H.B., Lidner, L. (1989). A New Tire Model with Application in Vehicle Dynamic Systems. *SAE paper*, Number 890087

Bayle, P., Forissier, J.F., Lafon, S. (1993) A New Tyre Model for Vehicle Dynamics Simulation. *Automotive Technology International*

Best, M.C., Newton, A.P. (2008). Vehicle Tyre and Handling Model Identification using an Extended Kalman Filter. *International Journal of Vehicle Autonomous Systems,* Volume 5 (3-4), pages 256-273.

CRF. (2005). Basics of Vehicle Dynamics. Turin: CRF

Genta, G. (2006). Motor Vehicle Dynamics: Modelling and Simulation. Singapore: World Scientific Publishing

Gillespie, T.D. (1992). Fundamentals of Vehicle Dynamics. Warrendale: Society of Automotive Engineers

Guiggiani, M. (2007). Dinamica del Veicolo. Biella: Città Studi

Papalambros, P.Y., Wilde, D.Y. (2000). Priciples of Optimal Design: Modelling and Computation. Cambridge: Press syndicate of the Cambridge University

Pacejka, H.B., Bakker, E. (1993). The Magic Formula tyre model. Proceedings of 1st Colloquium on Tyre Models for Vehicle Analysis. *Vehicle Dynamic Systems, 21*

Pacejka, H.B. (2002). Tyre and Vehicle Dynamics. Oxford: Butterworth-Heinemann.

Reccia, L., Pesce, M., Data, S. (2004). Identification of steering system parameters by experimental measuring processing. *Journal of Automobile Engineering*, Volume 218 (8), pages 783-792

Vries, E.J.H. de. (2008). Course Notes Voertuigdynamica A. Delft : Delft University of Technology

Figures

Figure 1 – Photo by Dario Lo Conte

Figure 2 – Schematical drawing Visio

Figure 3 – Tyre and Vehicle Dynamics, H. B. Pacejka, 2002

Figure 4 - http://www.virtualcar.it/public/media0a/fulvia_coupe_brt_.jpg

Figure 5 – Course Notes Voertuigdynamica, E.J.H. de Vries, 2008

Figure 6 – http://www.motortrend.com/roadtests/convertibles/

Figure 7 – Excel plot courtesy of CRF

Figure 8 – Excel plot courtesy of CRF

Figure 9 – Excel plot courtesy of CRF

Figure 10 – http://www.gumitra.com/home/img/liner.jpg

Figure 11 – Delft Tyre user manual

Figure 12 – http://www.clarks-garage.com/shop-manual/susp-15.htm

Figure 13 – jbtirefactory.com/services/837-alignment

Figure 14 – Tyre and Vehicle Dynamics, H. B. Pacejka, 2002

Figure 15 – http://www.tut.fi/plastics/tyreschool/moduulit/moduuli_10/hypertext/8/kuvat/

Figure 16 – Schematical drawing Visio

Figure 17 –Vehicle Handling Dynamics: Theory and Application, M. Abe, 2009

Figure 18 – Courtesy of Google Maps

Figure 19 – Courtesy of CRF

Figure 20 – Courtesy of CRF

Figure 21 – http://en.wikipedia.org/wiki/Maxima_and_minima

Figure 22 to Figure 24 – Screenshots of TyreEstimator application

Figure 25 to Figure 28 – Plots of parameter variations with Two-DOF model

Figure 29 – Schematical drawing

Figure 30 to Figure 36 – Plots of TyreEstimator results with Two-DOF model

Figure 37 to Figure 44 – Plots of TyreEstimator results with Fourteen-DOF model

Appendix

A. Original assignment formulated by CRF

(This text has been summarized in English in the 'Introduction' of this thesis)

Identificazione dati pneumatico da prove strada su veicolo completo
Non si tratta di sviluppare modelli di pneumatico ma di sviluppare e mettere a punto una procedura che permetta di identificare in modo automatico i dati di input di modelli pneumatico già presenti in letteratura (in particolare i coefficienti principali del modello di Pacejka, comunemente utilizzato per simulazioni di dinamica longitudinale /llaterare). La procedura dovrà prevedere l'utilizzo di prove sperimentali in pista su veicoli strumentati e di modelli di veicolo (disponibili in CRF, non da sviluppare) in cui l'unica incognita a livello di dati di input sia rappresentata dai dati del pneumatico. Come punto di partenza si utilizzerebbero i dati di pneumatico che sono forniti dai costruttori di pneumatici e che generalmente necessitano di un tuning per riprodurre il comportamento del veicolo in curva e/o in frenata/accelerata.
Si considerano modelli veicolo comprendenti i seguenti sottosistemi: cassa, sistema di sterzo, sospensioni anteriori e posteriori, ruote e pneumatici anteriori e posteriori.
L'approccio normalmente seguito nella validazione di un modello veicolo per analisi handling consiste anzitutto nel validare i modelli delle sospensioni rispetto a dati sperimentali ottenuti da prove elasto-cinematiche al banco: si effettua una correlazione numerico-sperimentale considerando le curve caratteristiche che descrivono la posizione della ruota rispetto alla cassa sotto l'azione degli input che arrivano dal terreno attraverso il pneumatico (forza verticale, longitudinale, laterale e momento autoallineante).
Una volta validati i modelli delle sospensioni, si procede con la validazione del modello di veicolo completo rispetto a prove sperimentali in pista, prove in cui si misurano i segnali fondamentali per la valutazione della dinamica laterale: steering wheel angle, lateral acceleration, yaw rate, sideslip angle, vehicle speed, roll angle.
Validare il modello di veicolo significa effettuare una messa a punto del modello agendo principalmente sui dati di input del modello di pneumatico. Noi utilizziamo generalmente la formulazione Pac2002 del modello interpolativo di Pacejka quindi i dati di input sono i coefficienti della Magic Formula di Pacejka. Per quanto riguarda i dati pneumatico di partenza, generalmente ci troviamo in uno dei due casi seguenti:

1. Il costruttore dei pneumatici montati sul veicolo fornisce i coefficienti di Pacejka ottenuti a partire da prove sperimentali sui pneumatici: generalmente questi coefficienti non sono pienamente rappresentativi del comportamento del pneumatico su strada per cui devono essere modificati in modo tale da migliorare la correlazione numerico-sperimentale a livello dei segnali indicati sopra.
2. I coefficienti relativi ai pneumatici montati sul veicolo non sono disponibili: in questo caso partiamo dai coefficienti di un pneumatico simile a nostra disposizione e poi seguiamo un approccio analogo a quello precedente.

Normalmente la modifica dei coefficienti si effettua "a mano" seguendo il flusso descritto sotto:

- Si inizia a verificare ed eventualmente modificare i coefficienti che descrivono il comportamento del pneumatico in condizioni quasi-stazionarie e che influiscono sul comportamento stazionario lineare e non lineare del veicolo: in questa prima fase si considerano sia in simulazione sia dal punto di vista sperimentale manovre a dinamica lenta con livelli di accelerazione laterale via via cresenti.
- Si estende poi la verifica e l'eventuale tuning ai coefficienti che descrivono il comportamento transitorio del pneumatico e che influiscono solo sul comportamento transitorio del veicolo.
- Infine se necessario si può estendere la verifica / validazione al comportamento in combinato ossia alla presenza contemporanea di carichi longitudinali e laterali significativi (condizione che si ha per esempio in una frenata in curva).

L'intero flusso viene appunto effettuato "a mano" ovvero chi valida il modello modifica per tentativi i coefficienti del modello pneumatico basandosi sull'esperienza, sulla conoscenza del modello di pneumatico e sulla conoscenza teorica della dinamica laterale del veicolo.
L'obiettivo del lavoro è quello di rendere il più possibile automatico e robusto questo processo di validazione modellistica.
Sempre partendo da una buona conoscenza del modello di pneumatico e dei fondamenti di dinamica laterale del veicolo, bisogna arrivare a definire una procedura che consenta di effettuare in modo automatico la messa a punto del pneumatico, utilizzando opportunamente degli algoritmi di ottimizzazione. Sarà parte del lavoro il valutare quale sia il modo migliore di fare ciò: ad esempio se sia meglio mantenere una flusso "in cascata", che parte con lo stazionario per poi affrontare il transitorio a stazionario definito, oppure mettere a punto tutti i coefficienti assieme.

B. Parameter sensitivity analysis of vehicle model

This sensitivity analysis consists of analyzing the responses of the simulation of a full vehicle model on parameter changes. The Fourteen-DOF simulation model and the application that was used for this sensitivity analysis were provided by CRF. In the simulation a basic manoeuvre is performed in almost steady-state conditions while in every simulation different parameters are varied. For example, the height and place (front/back) of the centre of gravity, the stiffness of the suspensions and the pneumatic parameters are varied. Several responses are considered, among which; the understeer gradient, the sideslip gradient, the roll angle gradient and the load transfer. The terms considered in this analysis are explained in chapter 1.

First the standard vehicle is simulated. The manoeuvre considered in this simulation is the slow ramp steer. During this manoeuvre the longitudinal speed remains constant (100 km/h) and the steer angle will be increased slowly with 10 degrees/s up to 180 degrees. The slow dynamics are reason enough to consider this as a steady state manoeuvre. In the next performed simulation one parameter is changed with regard to the standard vehicle.

Table 1 on the next page shows the results of this analysis. The changed parameters are listed in the left column of the table together with their variation. On the upper row the response parameters of the vehicle are denoted. In the rest of the table the plus, equal and minus signs show the variation of the individual parameter with respect to the value obtained with the basic vehicle. If the original parameter was negative a plus indicates that the value increased in negative direction.
For the understeer and the sideslip a distinction is made. This distinction consists in a gradient for the lateral accelerations below 0.4 g and a numerical value at 0.7 g. This is due to the linearity of the first part and the non-linearity of the last part. The non-linear behaviour of the tyre can cause different results for these parameters.

	Understeer gradient Kδvol (linear part)	Sideslip gradient Kβ (linear part)	Roll angle gradient Kθ	Angle δvol @ 0.7g (non-linear)	Angleβ @ 0.7g (non-linear)	Total load transfer	Load transfer on front axle	Load transfer on rear axle
10% raise height centre of mass (Hcg)	=	=	+	+	=	+	=	=
10% raise nominal load on front wheels	+	=/-	=	+	-	=	=	=
10% raise nominal load on rear wheels	-	=/+	=	-	+	=	=	=
50% raise of anti-symmetric stiffness front	=	=	-	+	-	=	+	-
50% raise of anti-symmetric stiffness rear	=	=	-	-	+	=	-	+
20% raise cornering stiffness of front tyres	-	=	=	-	=	=	=	=
20% raise cornering stiffness of rear tyres	+	-	=	=/+	-	=	=	=
10% raise of peak value of front tyres	-/=	=	=	-	=	=	=	=
10% raise of peak value of rear tyres	=	-/=	=	=/+	-	=	=	=
50% raise of camber stiffness front	=	=	=	-	=	=	=	=
50% raise of camber stiffness rear	=	=/-	=	=/+	-	=	=	=

Table 1 Results of sensitivity analysis

Table 1 shows that the parameter variations to the vehicle only influence a few properties at the time. When there are two signs in the table the first one gives the found value by the analysis while the second shows the theoretical variation. This is explained in the next lines together with the most important influences on the vehicle.

- The height of the centre of mass contributes specifically to the roll coefficient and the total load transfer. When cornering with a higher centre of mass the moment about the x-axis of the ground will increase, so more load is transferred to the outer side and thus to the tyres. Therefore the tyres have 'to work harder', and the saturation point of the tyres is reached earlier then with the basic vehicle. In other words, the load on the front outer wheel is higher and, because of the non-linear behaviour of the tyre, the total force to keep the vehicle in line can not be recuperated by the front inner wheel, so sliding over the front wheels takes place. This causes an increase of understeer in the non-linear part of the δvol graph.
- The higher mass distribution at the front of the vehicle causes obviously more load on the front tyres. This results in a higher understeer gradient and higher non-linear values of δvol. Due to the different mass distribution the preloading condition of the front and rear suspension springs will be altered as well. The roll-centre height and the spring response due to the non-linear behaviour in an extreme case can therefore be influenced. By adjusting the preloading condition these effects can be compensated as well. Also the roll gradient is dependent on these characteristics of the vehicle. In theory the sideslip gradient decreases due to the lower vertical load at the rear axle. If the sensibility of the rear tyre is low for the variation of vertical load this effect can not be observed. The reduction of the sideslip angle is more visible in the non-linear range.
- In contrary to the higher mass distribution at the front of the vehicle, the higher mass distribution on the back shows a lower understeer gradient and theoretical a higher sideslip gradient. In the non-linear part lower values of steer wheel angle as well as higher values of sideslip are obtained. The reason for that is exactly opposite to the previous configuration. The other parameters remain the same, like in the previous analysis.
- When the increase of the front anti-symmetric suspension stiffness is considered the rolling gradient goes down because more force has to be applied to let the vehicle roll especially over de front. The increase of the load on the front wheels can be explained with the fact that more force is given through because of the stiffer front suspension. This then causes the numerical value of the sideslip to decrease and the numerical value of the understeer coefficient to increase. For the increase of the back anti-symmetric suspension stiffness, the opposite reasoning applies.
- The cornering stiffness of the tyres doesn't change the vehicle's body configuration. So the load transfer and the rolling gradient won't change. For the linear part the tyres slide less because of the higher cornering stiffness, diminishing the understeer for a higher front cornering stiffness and increasing understeer for a higher rear cornering stiffness. The changes in cornering stiffness influences also the sideslip gradient, but due to the formulation which includes only the cornering stiffness of the rear tyres, this is only seen with the increase of the cornering stiffness of the rear tyres. In the

non-linear part of the graphs there is a lower understeer gradient for the higher cornering stiffness of the front tyres and a lower sideslip angle for the higher cornering stiffness of the back tyres. This shows that the linear trend is confirmed. The higher non-linear understeer for the increase of the rear cornering stiffness should also be visible but again this is not seen.

- An increase of the peak value of the cornering stiffness for the front tyres only influences δvol, especially in the non-linear range. Because of this higher peak value the saturation of the tyres will happen later than normal and the sliding over the front wheels will be less. The change of peak value of the rear tyres results in a diminishing β in the non-linear range, again because saturation of the tyres happens at a later time then in the original model. Also a higher δvol is expected but is not perceptible.
- The change in camber stiffness has only little influence on the vehicle. When the camber of the front suspension is increased the understeer in the non-linear part will be lowered. The wheel is more straight up than the vehicle itself, therefore the grip will be better and the cornering stiffness increased. The higher camber stiffness of the rear suspension diminishes the non-linear sideslip angle. The change of camber stiffness is in total quite small and the expected change in understeer for the change of rear stiffness is not seen. This phenomenon is mainly dependent on the type of suspension used for the vehicle and the vehicle geometry.

C. Calculation of δ and β

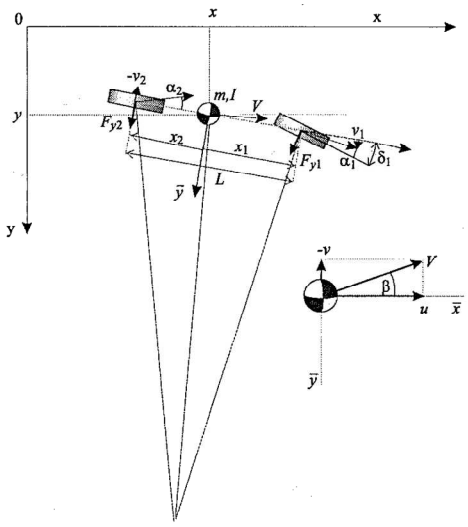

With the use of the figure above it can be determined that:

$$L = R\cos\beta\sin\alpha_2 + R\cos\beta\sin\left(\delta_1 - \alpha_1\right) \quad \textbf{(C-1)}$$

To simplify this relation, the trigonometry is linearized by assuming that $\cos\beta \approx 1$ and sin α = α, which is true for small sideslip angles, the formula becomes:

$$L = R\alpha_1 + R\left(\delta_1 - \alpha_1\right) \quad \textbf{(C-2)}$$

Grouping the α-terms results in:

$$L = R\left(\alpha_2 - \alpha_1\right) + R\delta_1 \quad \textbf{(C-3)}$$

From this it can be concluded that:

$$\frac{L}{R} = \alpha_2 - \alpha_1 + \delta_1 \quad \textbf{(C-4)}$$

With this δ_1 can be defined as:

$$\delta_1 = -\alpha_2 + \alpha_1 + \frac{L}{R} \quad \textbf{(C-5)}$$

For which the following relation holds for R:

$$R = \frac{V^2}{a_y}$$

Where a_y, defined as lateral acceleration, is the component of the acceleration in the horizontal direction in the picture. The linearized trigonometry can also be applied to calculate the sideslip angle of the model. Below the different steps of this process are shown:

$$x_2 = R\cos\beta\sin\alpha_2 + R\cos\beta\sin\beta \quad \textbf{(C-6)}$$

Where again the linearizations $\cos\beta \approx 1$ and sin α = α hold, therefore:

$$x_2 = R\alpha_2 + R\beta \quad \textbf{(C-7)}$$

The relation for β can now be described:

$$\beta = \frac{x_2}{R} - \alpha_2 \quad \textbf{(C-8)}$$

The definition of R is the same as in the previous calculation.

D. Matlab program

Description of the program TyreEstimator2, that calculates automatically the parameters according to the options selected in the program.
The original initial parameters are:

```
pcy  = 1.318409;        % Shape factor Cfy for lateral forces
pdy1  = 1.307495;       % Lateral friction Muy
pdy2  = 0.335312;       % Variation of friction Muy with load
pey1  = 1.1549;         % Lateral curvature Efy at Fznom
pky1  = -23.0708979;    % Maximum value of stiffness Kfy/Fznom
pky2  = 1.664681;       % Load at which Kfy reaches maximum value
LCY    = 1;             % Scale factor of Fy shape factor
LMUY   = 1;             % Scale factor of Fy peak friction coefficient
LEY    = 1;             % Scale factor of Fy curvature factor
LKY    = 1;             % Scale factor of Fy cornering stiffness
```

The handtuned initial parameters are:

```
pcy  = 1.6;             % Shape factor Cfy for lateral forces
pdy1  = 1.3;            % Lateral friction Muy
pdy2  = -0.1;           % Variation of friction Muy with load
pey1  = 1.15;           % Lateral curvature Efy at Fznom
pky1  = -21.8;          % Maximum value of stiffness Kfy/Fznom
pky2  = 1.35;           % Load at which Kfy reaches maximum value
LCY    = 1;             % Scale factor of Fy shape factor
LMUY   = 1;             % Scale factor of Fy peak friction coefficient
LEY    = 1;             % Scale factor of Fy curvature factor
LKY    = 1;             % Scale factor of Fy cornering stiffness
```

Next; Run TyreEstimator2.m

- Initializes the user interface with 4 figures, 11 checkboxes and 5 pushbuttons
- Sets pushbutton2, pushbutton3 and pushbutton4 off
- Set in Workspace Base, continueOptimization to 0 and exitOptimization to 0 and update structure

Options
Optimization method
Checkbox 1: fminsearch (default)
Checkbox 2: lsqnonlin

Consideration of parameter E
Checkbox 3: Yes (default)
Checkbox 4: Yes, but keep it constant
Checkbox 5: No

Number of datasets to use
Checkbox 6: One (default)
Checkbox 7: Two, one for front and one for rear

Optimization parameters

Checkbox 8: Consider coefficients (default)
Checkbox 9: Consider scaling factors

Implement decimation
Checkbox 10: Yes
Checkbox 11: No (default)

Use extrapolation
Checkbox 12: Yes (default)
Checkbox 13: No

Actions
Pushbutton 1: Plot

- ClearFigures; Clears all figures and textboxes and disables pushbutton2, pushbutton3 and pushbutton4
- Choice of dataset; Original or Customized
- Set in Workspace Base, continueoptimization to 0
- GetHandles; Gets handles from checkboxes
- InitializationOptimizationforGUI; Run simulation for initial data
    - SetOptions;Set initial options
    - Starting_Pacejka; Get initial (original or customized) tyre coefficients and scaling factors
    - Choice_Dataset; Original or customized initial coefficients
    - Slow_Ramp_Steer_Manoeuvre; Perform simulation of manoeuvre
        - Initialize counter
        - Set speed
        - Change lateral acceleration for every iteration
        - Vehicle_model; Provided by CRF
            - Vehicle_data; Input of basic vehicle parameters
            - rollio; Calculation of stiffness and displacements of suspensions as well as roll stiffness
            - trasferimento_di_carico; Load transfer is calculated, vertical force on every tyre
            - careffaxle; Calculate front and rear slip angles that correspond to the necessary F_y
                - Get values for Pacejka_Equation
                - Pacejka_Equation_F; Calculates slip angle that provides the necessary lateral force for the front axle using simplified Magic Formula, if errors occur these will be displayed
                - Pacejka_Equation_R; Calculates slip angle that provides the necessary lateral force for the rear axle using Magic simplified Magic

Formula, if errors occur these will be displayed
        - rigidezza_complessiva; Total slip angle for front and rear axle, steering wheel angle and sideslip angle are calculated
    - Data_Experimental_Simulation; Load data from experimental file
        - Get Experimental data
        - Sort on AlfaF
        - If decimate option is on; Decimate; Reduces Data points
            - Divide in parts and sum values of the parts together
            - Calculate values for all the parts
        - CheckError; Calculates initial error
- PlotInitial; Plot results from simulation with experimental data, complete figures
- CheckError; Calculates initial error(s)
- DisplayText; Displays initial error(s) and initial parameters and saves them for optimization
- Sets pushbutton2 and pushbutton4 on
- Update handles structure

Pushbutton 2: Start optimization

- Check if a new optimization must start or one has to be continued
- If a new optimization has to start, with which dataset? Original or Customized
- Unable pushbutton2 and able pushbutton3
- Set in Workspace Base, stopOptimization to 0
- GetHandles; Gets handles from checkboxes
- ModulatedOptimizationforGUI; Run simulation for initial data
    - SetOptions; Set initial options
    - Starting_Pacejka_Optimization; Get initial (saved, original or costumized) tyre coefficients and scaling factors
    - Choice_Dataset; Original or customized initial coefficients
    - Slow_Ramp_Steer_Manoeuvre; Perform simulation of manoeuvre
        - Initialize counter
        - Set speed
        - Change lateral acceleration for every iteration
        - Vehicle_model; Provided by CRF
            - Vehicle_data; Input of basic vehicle parameters
            - rollio; Calculation of stiffness and displacements of suspensions as well as roll stiffness
            - trasferimento_di_carico; Load transfer is calculated, vertical force on every tyre

        - careffaxle; Calculate front and rear slip angles that correspond to the necessary F_y
            - Get values for Pacejka_Equation
            - Pacejka_Equation_F; Calculates slip angle that provides the necessary lateral force for the front axle using simplified Magic Formula, if errors occur these will be displayed
            - Pacejka_Equation_R; Calculates slip angle that provides the necessary lateral force for the rear axle using Magic simplified Magic Formula, if errors occur these will be displayed
        - rigidezza_complessiva; Total slip angle for front and rear axle, steering wheel angle and sideslip angle are calculated
- Data_Experimental_Simulation; Load data from experimental file
    - Get Experimental data
    - Sort on AlfaF
    - If decimate option is on; Decimate; Reduces Data points
        - Divide in parts and sum values of the parts together
        - Calculate values for all the parts
- If the optimization is continued;
    - PlotInitial; Plot results from simulation with experimental data, complete figures
    - CheckError; Calculates initial error(s)
    - DisplayText; Displays initial error(s) and initial parameters and saves them for optimization
- Optimization_SQRforGUI; Run optimization
    - PrepareForOptimization; Set variables and constants for optimization
    - Set optimization options
    - Run optimization with fminsearch or lsqnonlin on the basis of errorfunc6b
        - GetParameters; Prepare parameters for optimization
        - Run Slow_Ramp_Steer_Manoeuvre; Simulation manoeuvre as described above
        - If no decimation takes place don't consider experimental values higher than the highest slip angle from the simulation
        - Interpolate values from simulation to compare with experimental data

        - Calculate errors
    - Show_resultsforGUI; Plot results in GUI figures
        - SetParameters; Prepare optimized parameters for simulation manoeuvre
        - Clear old values
        - Run Slow_Ramp_Steer_Manoeuvre; Simulation manoeuvre as described above with optimized parameters
        - If no decimation takes place don't consider experimental values higher than the highest slip angle from the simulation
        - PlotFinal; Plot results in GUI figures and complete figures
        - Display of final error and parameters
        - Recapitulate and save coefficients
- Unable pushbutton3 and able pushbutton2
- Set in Workspace Base, stopOptimization to 1 and continueOptimization to 1
- Update handles structure

Pushbutton 3: Stop optimization

- Set in Workspace Base, continueOptimization to 1 and stopOptimization to 1
- myoutput; Makes sure to stop optimization at current iteration and proceeds to Show_resultsforGUI (see previous pushbutton)
- Unable pushbutton3 and able pushbutton2
- Update handles structure

Pushbutton 4: Clear figures

- ClearFigures; Clears all figures and textboxes and disables pushbutton2, pushbutton3 and pushbutton4
- Update handles structure

Pushbutton 5: Cancel

- Set in Workspace Base, stopOptimization to 1 and exitOptimization to 1 and update structure to stop current optimization if necessary
- Update handles structure
- Close TyreEstimator2

E. Results influence coefficients and scaling factors

Experimentation on front and rear axle curves with following initial parameters:

pcy	= 1.4137	LFZ0	= 1
pdy1	= 1.3229	LCY	= 1
pdy2	= -0.3976	LMUY	= 1
pey1	= 0.9991	LEY	= 1
pey2	= 1.5771	LKY	= 1
pky1	= -15.2575		
pky2	= 0.7569		

E-1 Coefficients

p_{Cy} = [1.0 1.4137 1.8]

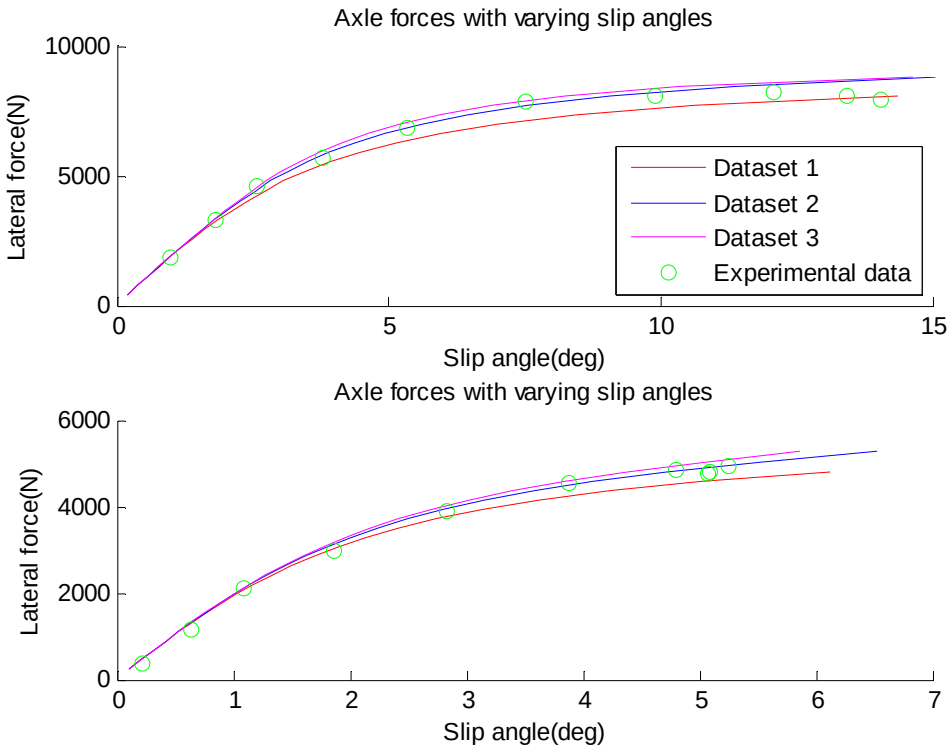

p_{Dy1}= [0.8 1.3229 1.8]

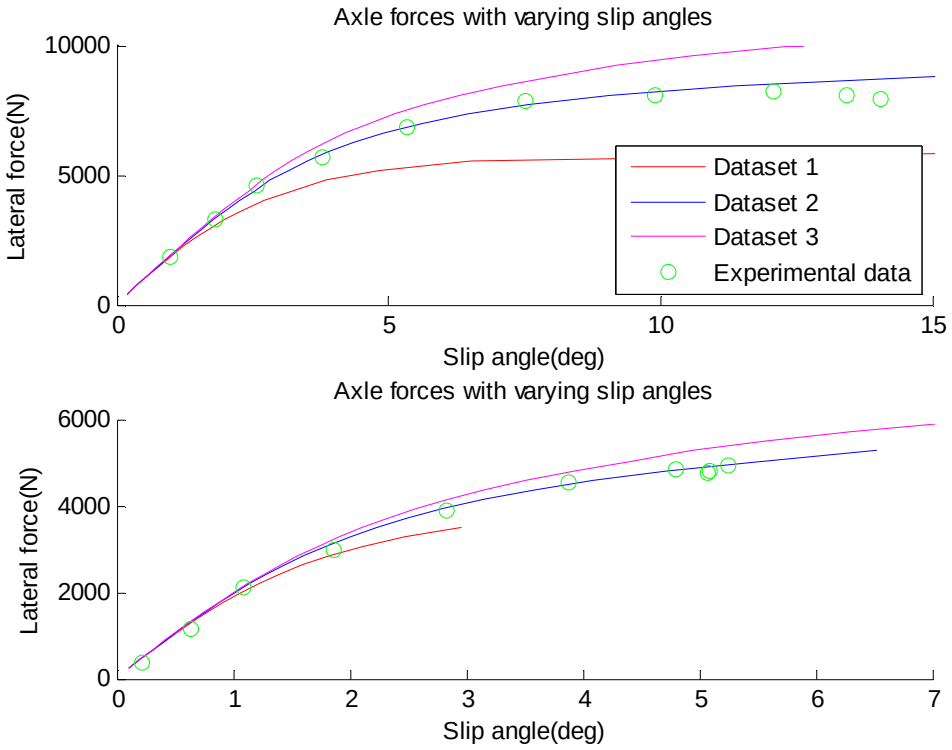

p_{Dy2}= [-0.8 -0.3976 0]

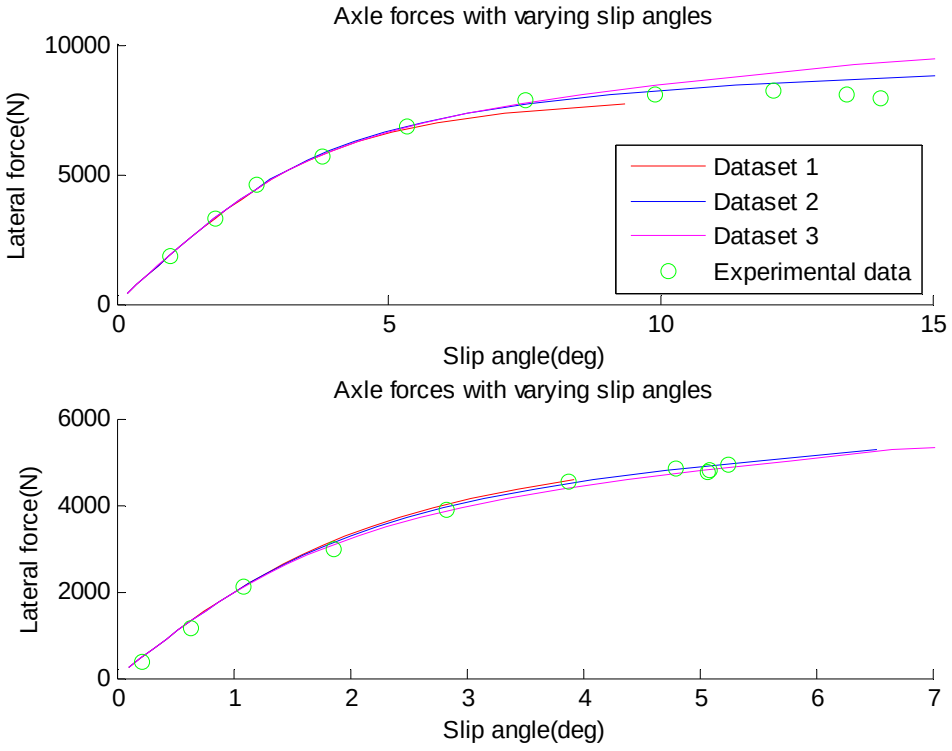

p_{Ey1}= [-1 0.9991 3]

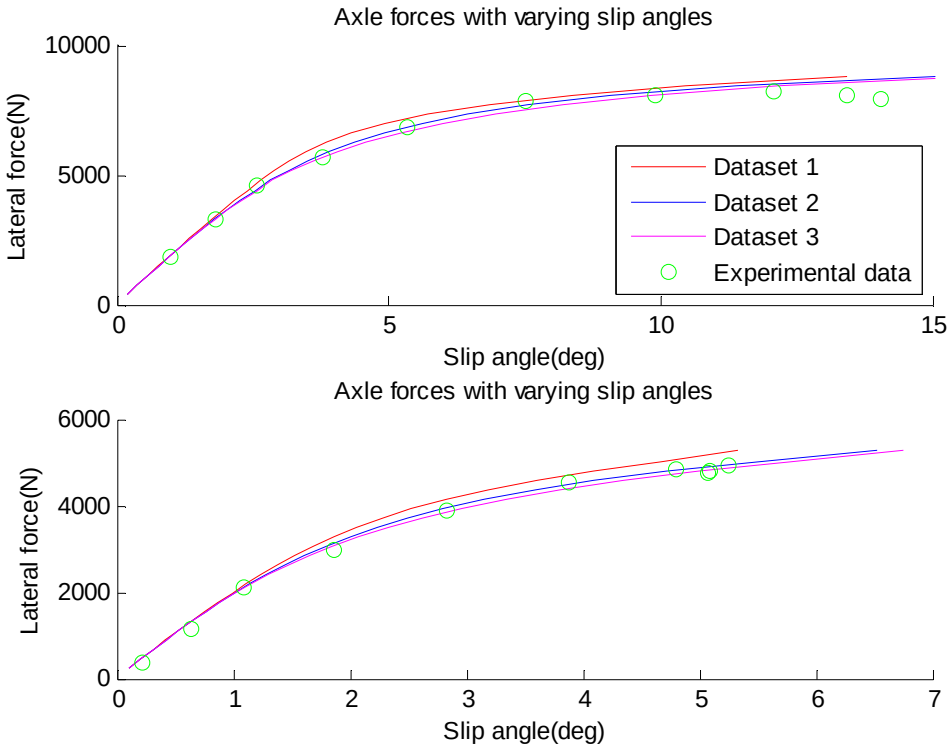

p_{Ey2}= [0 1.5771 3]

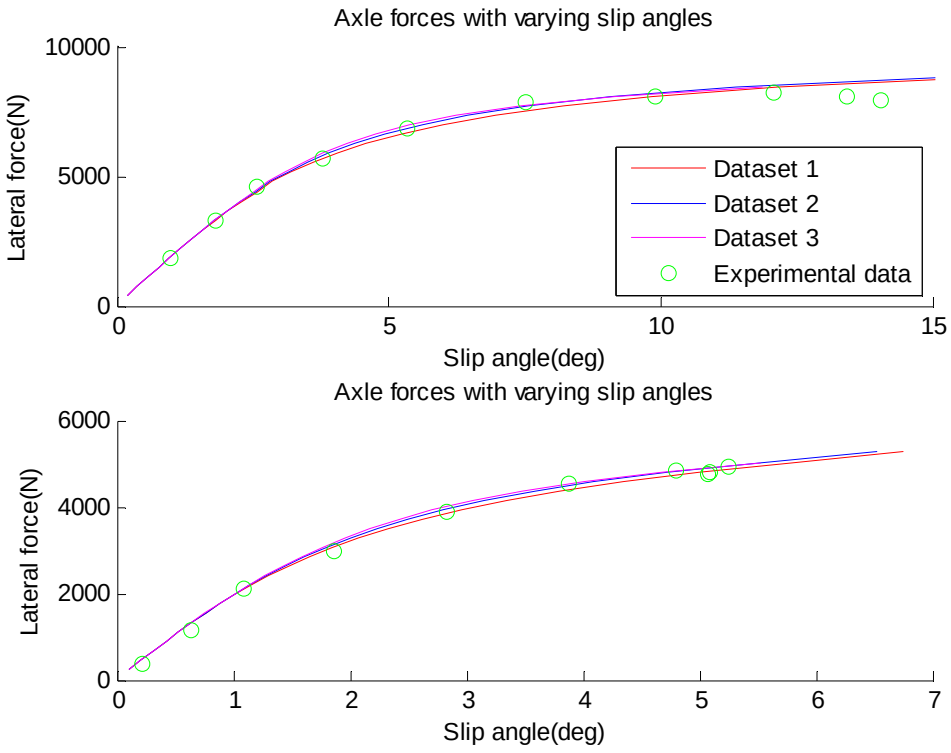

p_{Ky1} = [-20 -15.2575 -10]

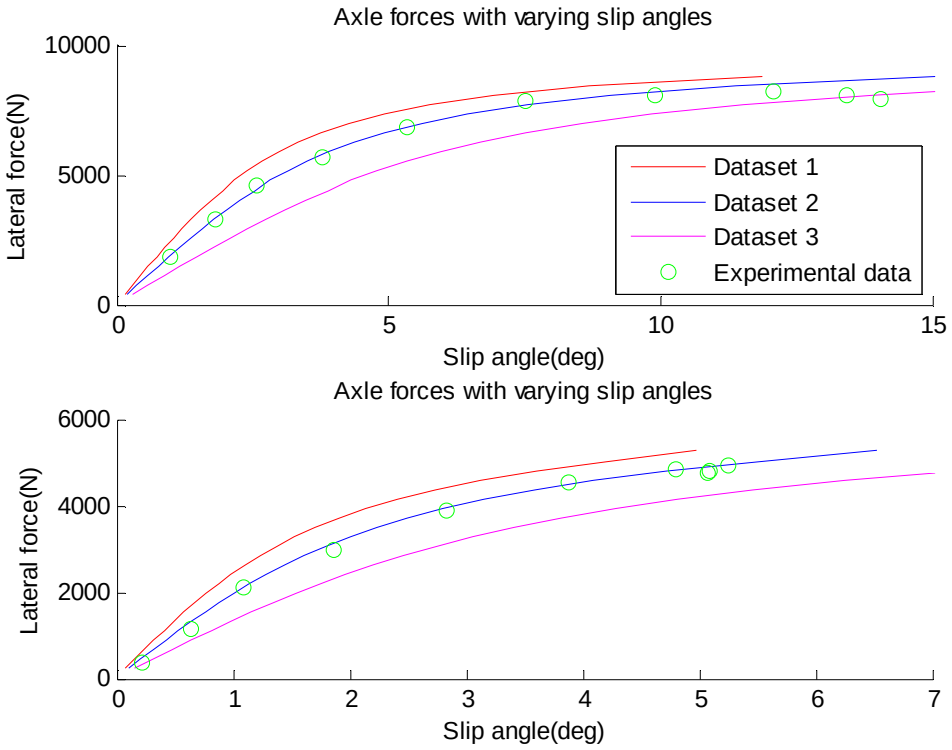

p_{Ky2}= [0.5 0.7569 1]

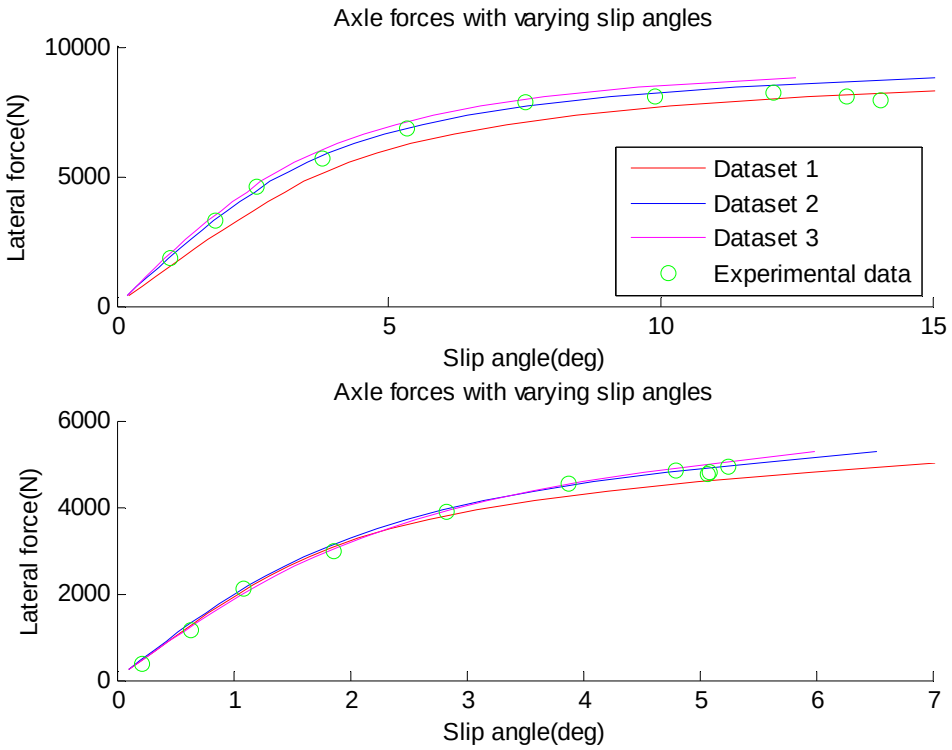

E-2 Scaling factors

λ_{Cy} = [0.667 1.0 1.5]

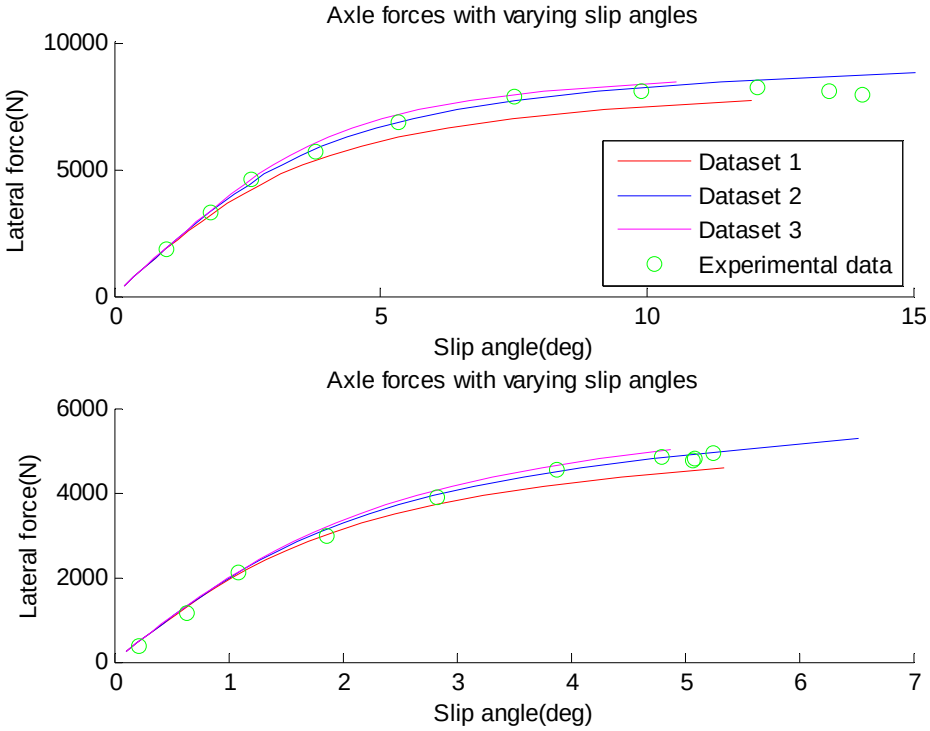

$\lambda_{\mu y}$ = [0.667 1.0 1.5]

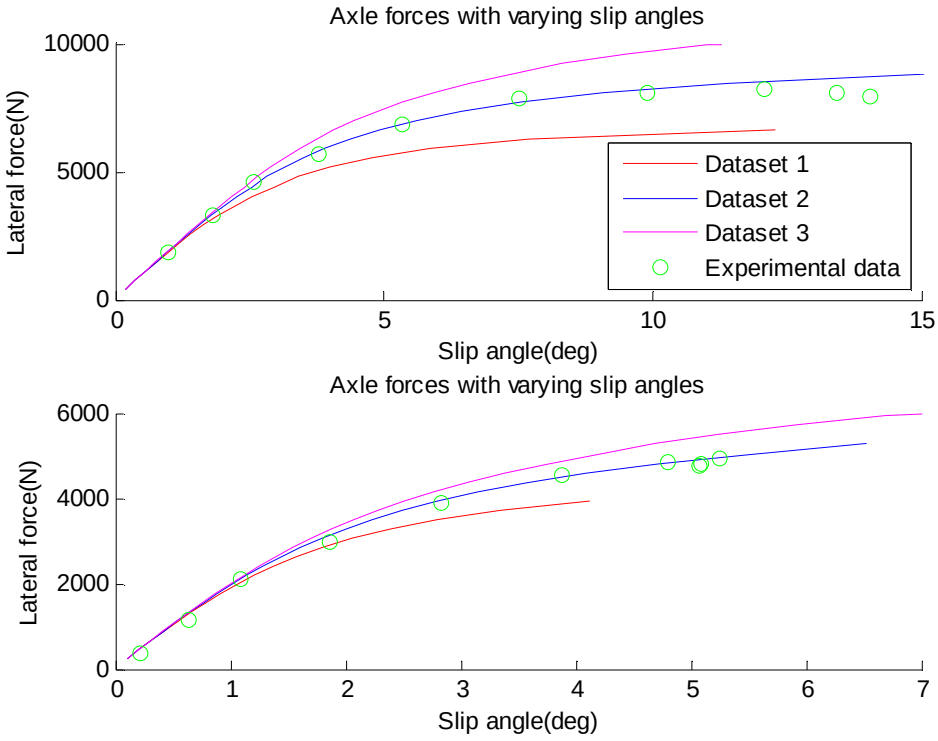

λ_{Ey} = [0.667 1.0 1.5]

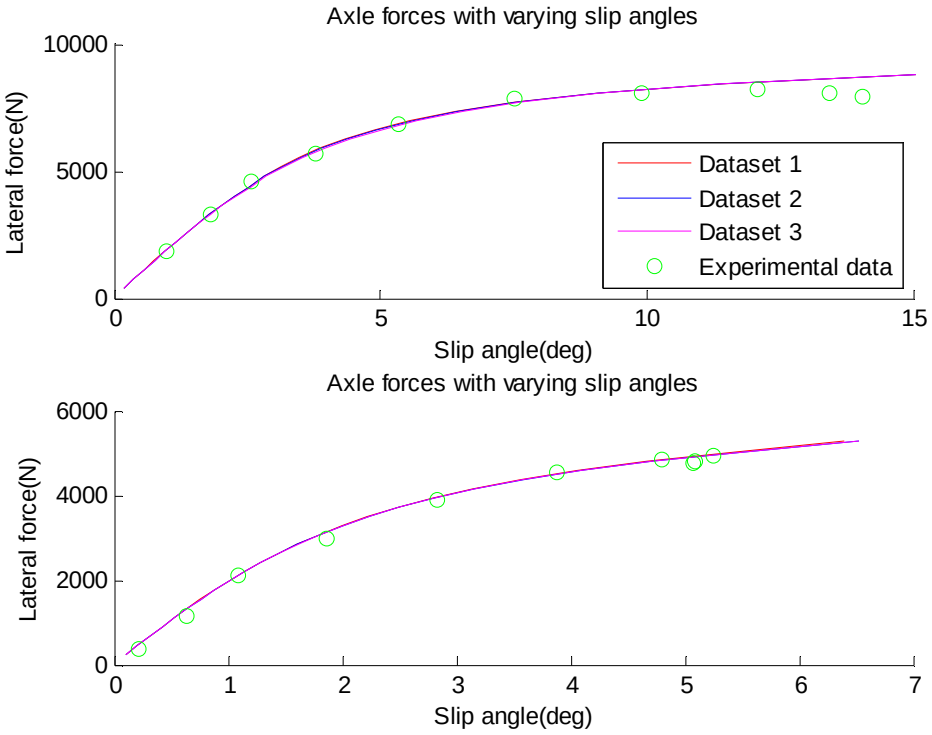

λ_{Ky} = [0.667 1.0 1.5]

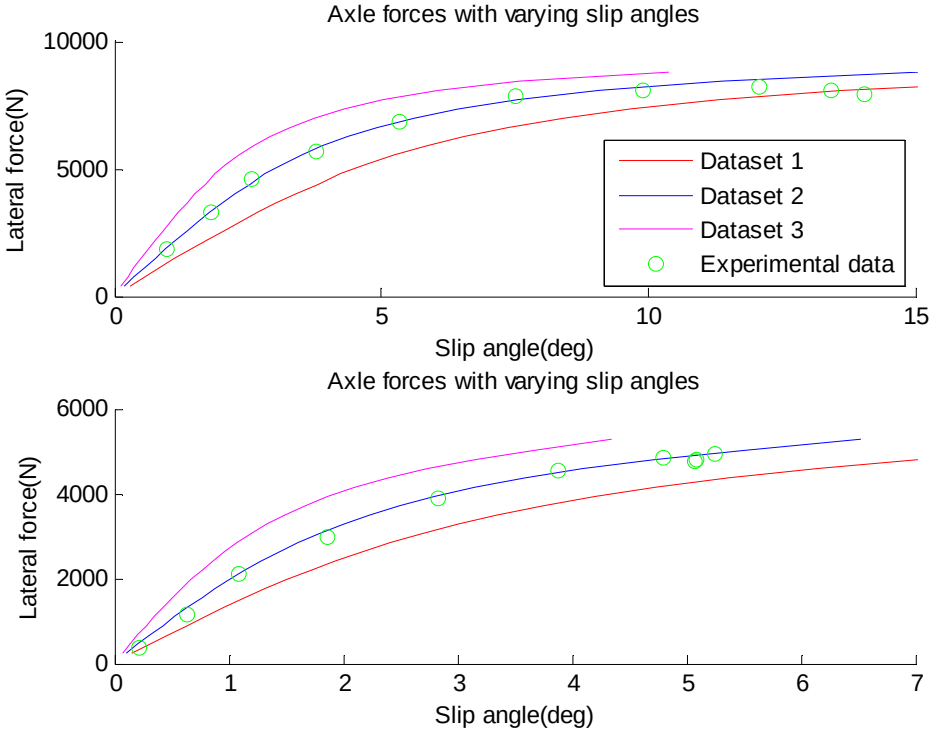

F. Results optimizations Two-DOF model

Simulation 1.1, Standard optimization with fminsearch

Algorithm	Fminsearch					
Target	Coefficients					
Decimation	No					
Parameter E	Considered					
Nr. Of sets	One					
Duration	317.0251 s					
Result	0.0802					
Coefficients	p_{Cy}	p_{Dy1}	p_{Dy2}	p_{Ey1}	p_{Ky1}	p_{Ky2}
Initial	1.6000	1.3000	-0.1000	1.1500	-21.8000	1.3500
Optimized	2.0068	0.9944	-0.0952	1.3423	-16.5179	1.2484
Scaling factors	λ_{Cy}	$\lambda_{\mu y}$	λ_{Ey}	λ_{Ky}		
	1.0000	1.0000	1.0000	1.0000		

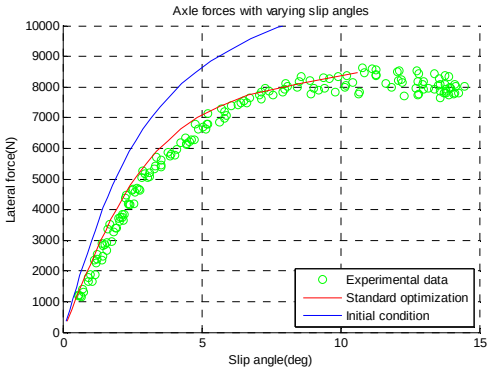

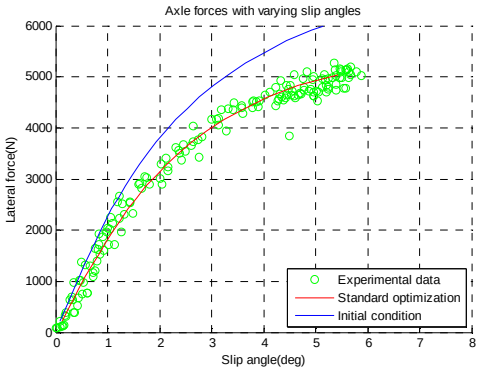

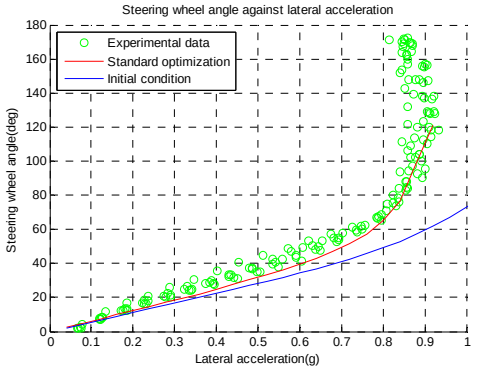

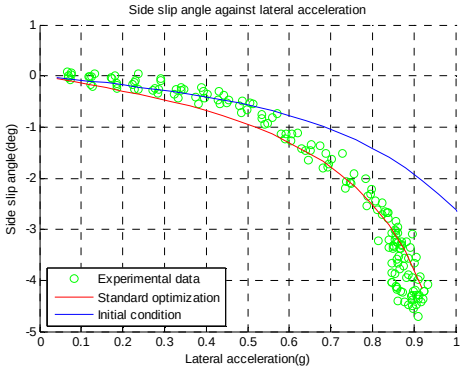

Simulation 1.2.1 Optimization with fminsearch on scaling factors

Algorithm	fminsearch					
Target	Scaling factors					
Decimation	No					
Parameter E	Considered					
Nr. Of sets	One					
Duration	60.2663 s					
Result	0.0920					
Coefficients	p_{Cy}	p_{Dy1}	p_{Dy2}	p_{Ey1}	p_{Ky1}	p_{Ky2}
Constant	1.6000	1.3000	-0.1000	1.1500	-21.8000	1.3500
Scaling factors	λ_{Cy}	$\lambda_{\mu y}$	λ_{Ey}	λ_{Ky}		
Initial	1.0000	1.0000	1.0000	1.0000		
Optimized	1.1679	0.7537	1.2583	0.7638		

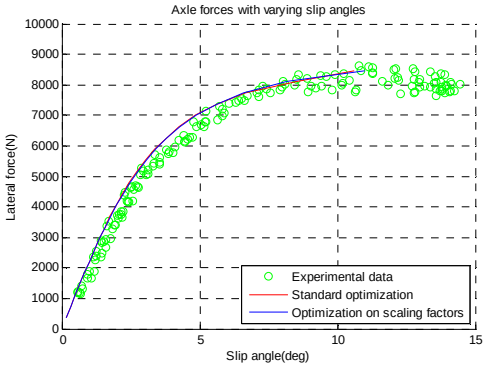

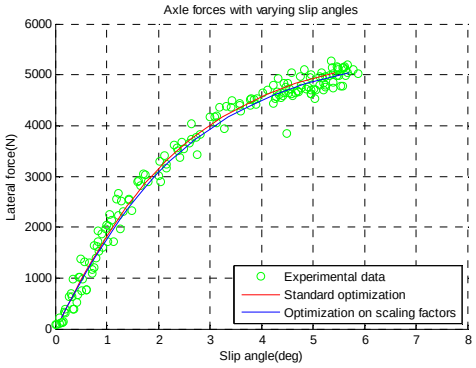

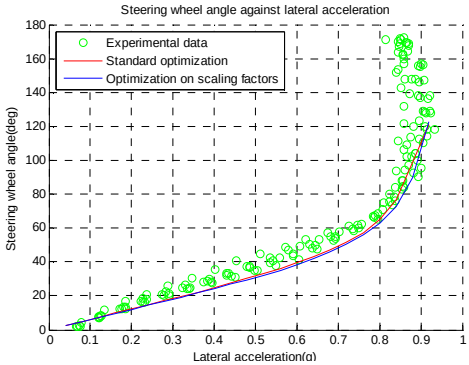

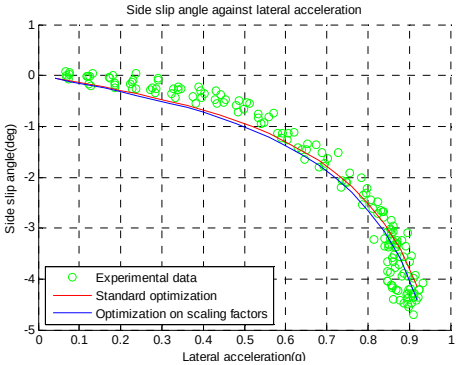

Simulation 1.2.2, Optimization with fminsearch with constant E

Algorithm	fminsearch					
Target	Coefficients					
Decimation	No					
Parameter E	Constant					
Nr. Of sets	One					
Duration	276.7710 s					
Result	0.0675					
Coefficients	p_{Cy}	p_{Dy1}	p_{Dy2}	p_{Ey1}	p_{Ky1}	p_{Ky2}
Initial	1.6000	1.3000	-0.1000	1.1500	-21.8000	1.3500
Optimized	2.5314	1.2142	-0.0928	1.1500	-15.2837	0.7069
Scaling factors	λ_{Cy}	$\lambda_{\mu y}$	λ_{Ey}	λ_{Ky}		
Constant	1.0000	1.0000	1.0000	1.0000		

Simulation 1.2.3, Optimization with fminsearch with no E

Algorithm	fminsearch					
Target	Coefficients					
Decimation	No					
Parameter E	Not considered					
Nr. Of sets	One					
Duration	98.7711 s					
Result	0.0680					
Coefficients	p_{Cy}	p_{Dy1}	p_{Dy2}	p_{Ey1}	p_{Ky1}	p_{Ky2}
Initial	1.6000	1.3000	-0.1000	1.1500	-21.8000	1.3500
Optimized	1.9816	1.0745	-0.1541	0	-14.9326	0.8707
Scaling factors	λ_{Cy}	$\lambda_{\mu y}$	λ_{Ey}	λ_{Ky}		
Constant	1.0000	1.0000	1.0000	1.0000		

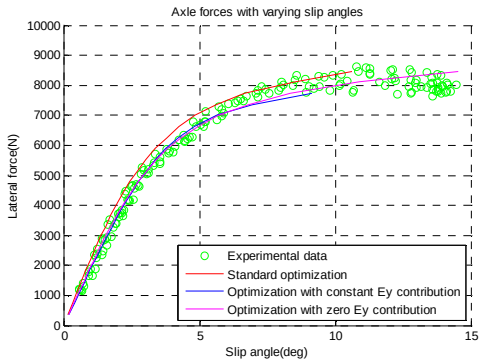

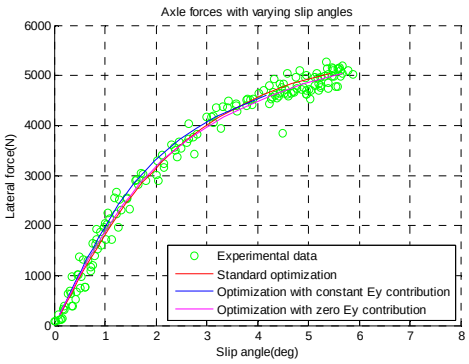

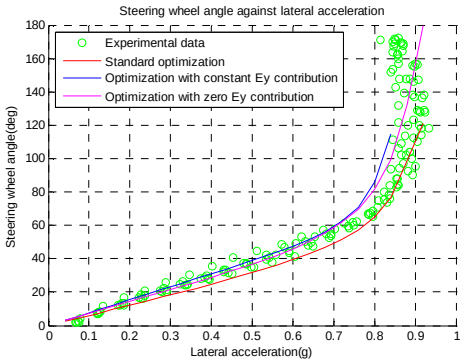

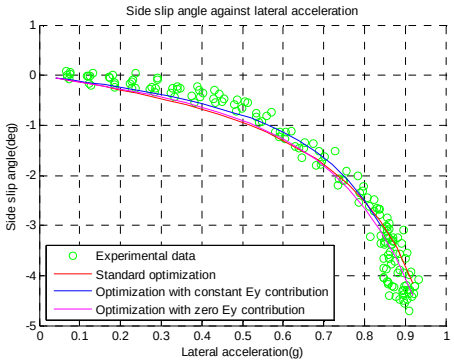

Simulation 1.3.1, Optimization with fminsearch with no scaling

Algorithm	fminsearch					
Target	Coefficients					
Decimation	No					
Parameter E	Constant					
Nr. Of sets	One					
Duration	330.5717 s					
Result	0.0811					
Coefficients	p_{Cy}	p_{Dy1}	p_{Dy2}	p_{Ey1}	p_{Ky1}	p_{Ky2}
Initial	1.6000	1.3000	-0.1000	1.1500	-21.8000	1.3500
Optimized	2.2784	0.9433	-0.0488	1.3825	-16.1832	1.0652
Scaling factors	λ_{Cy}	$\lambda_{\mu y}$	λ_{Ey}	λ_{Ky}		
Constant	1.0000	1.0000	1.0000	1.0000		

Simulation 1.3.2, Optimization with fminsearch with no scaling but mult. Alpha

Algorithm	fminsearch					
Target	Coefficients					
Decimation	No					
Parameter E	Not considered					
Nr. Of sets	One					
Duration	500.5702 s					
Result	0.0876					
Coefficients	p_{Cy}	p_{Dy1}	p_{Dy2}	p_{Ey1}	p_{Ky1}	p_{Ky2}
Initial	1.6000	1.3000	-0.1000	1.1500	-21.8000	1.3500
Optimized	1.8741	1.0111	-0.1094	1.0644	-16.7029	1.4523
Scaling factors	λ_{Cy}	$\lambda_{\mu y}$	λ_{Ey}	λ_{Ky}		
Constant	1.0000	1.0000	1.0000	1.0000		

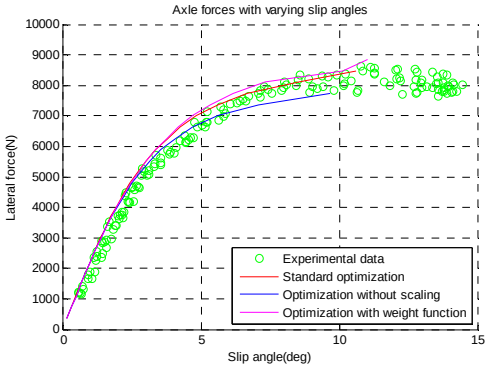

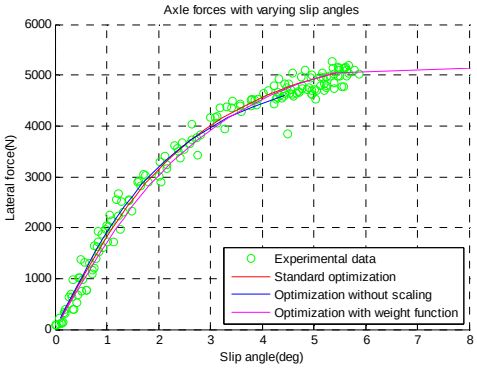

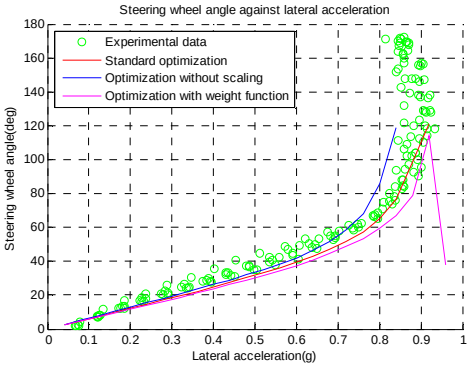

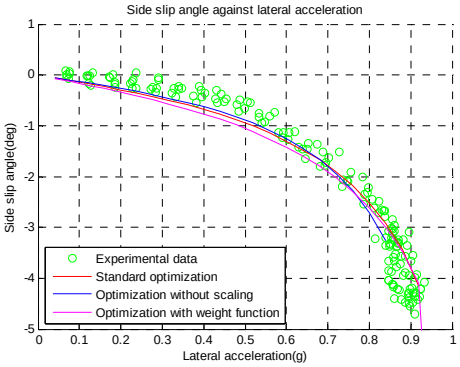

Simulation 1.4.1, Optimization with fminsearch on initial tyre conditions

Algorithm	Fminsearch					
Target	Coefficients					
Decimation	No					
Parameter E	Considered					
Nr. Of sets	One					
Duration	168.3750 s					
Result	0.101					
Coefficients	p_{Cy}	p_{Dy1}	p_{Dy2}	p_{Ey1}	p_{Ky1}	p_{Ky2}
Initial	1.3184	1.3075	0.3353	1.1549	-23.0709	1.6647
Optimized	0.9726	1.8692	0.4121	1.7491	-16.3826	0.6251
Scaling factors	λ_{Cy}	$\lambda_{\mu y}$	λ_{Ey}	λ_{Ky}		
	1.0000	1.0000	1.0000	0.8500		

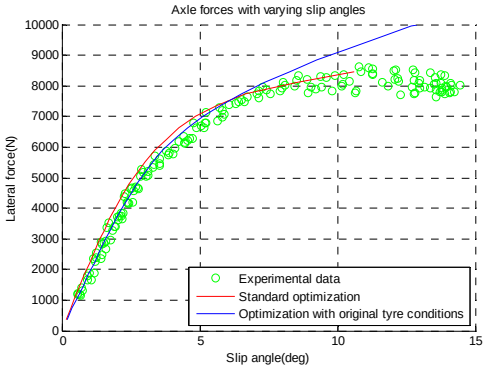

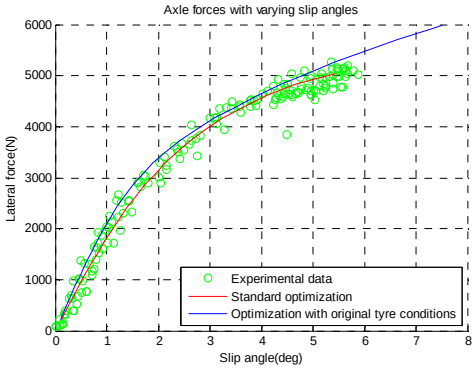

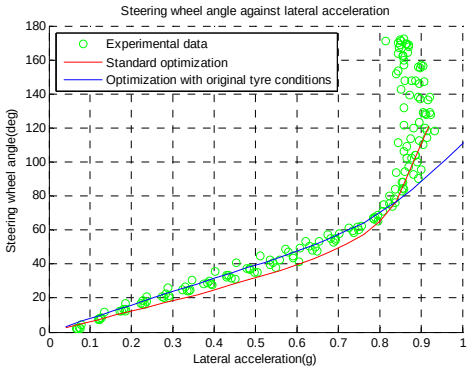

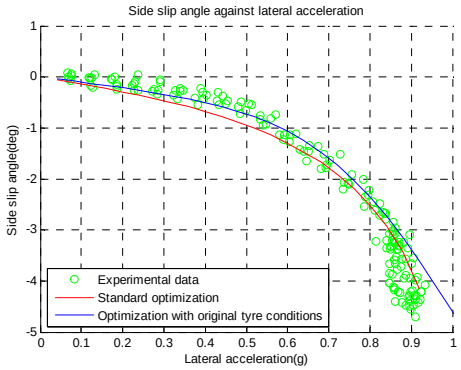

Simulation 1.4.2, Optimization with averaging

Algorithm	Fminsearch					
Target	Coefficients					
Decimation	Yes					
Parameter E	Considered					
Nr. Of sets	One					
Duration	125.6834 s					
Result	0.0569/0.0939					
Coefficients	p_{Cy}	p_{Dy1}	p_{Dy2}	p_{Ey1}	p_{Ky1}	p_{Ky2}
Initial	1.6000	1.3000	-0.1000	1.1500	-21.8000	1.3500
Optimized	1.5299	1.0122	-0.1231	1.2063	-18.6963	1.6174
Scaling factors	λ_{Cy}	$\lambda_{\mu y}$	λ_{Ey}	λ_{Ky}		
	1.0000	1.0000	1.0000	1.0000		

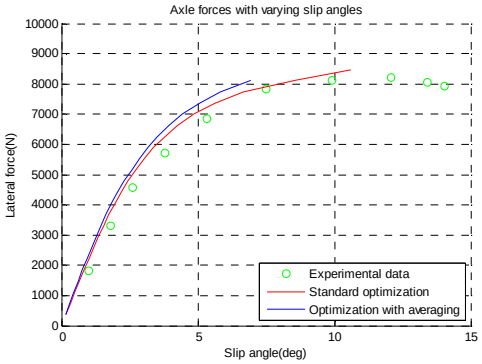
Axle forces with varying slip angles
Lateral force(N)
Slip angle(deg)
Experimental data
Standard optimization
Optimization with averaging

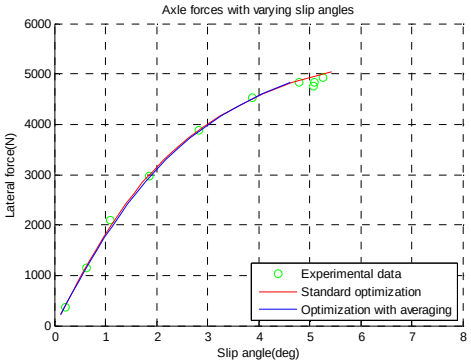
Axle forces with varying slip angles
Lateral force(N)
Slip angle(deg)
Experimental data
Standard optimization
Optimization with averaging

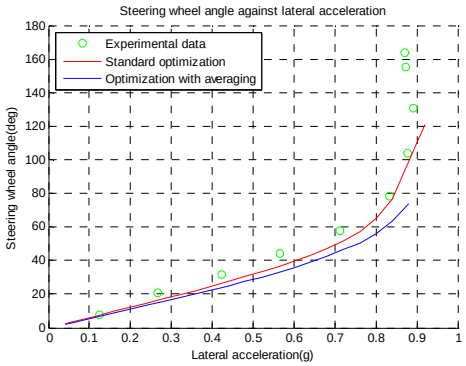
Steering wheel angle against lateral acceleration
Steering wheel angle(deg)
Lateral acceleration(g)
Experimental data
Standard optimization
Optimization with averaging

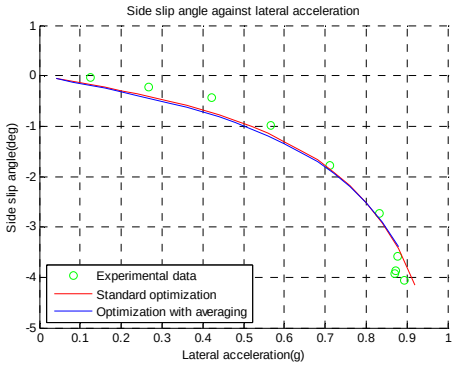
Side slip angle against lateral acceleration
Side slip angle(deg)
Lateral acceleration(g)
Experimental data
Standard optimization
Optimization with averaging

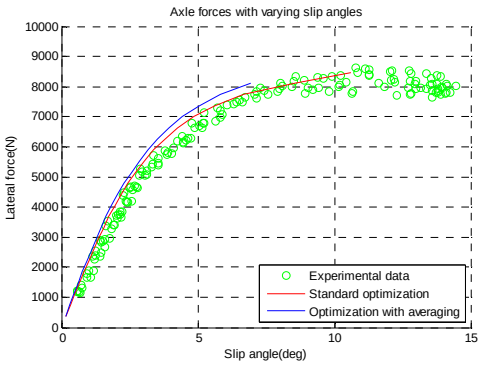
Axle forces with varying slip angles
Lateral force(N)
Slip angle(deg)
Experimental data
Standard optimization
Optimization with averaging

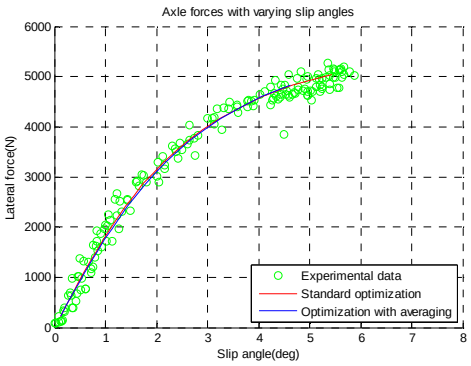
Axle forces with varying slip angles
Lateral force(N)
Slip angle(deg)
Experimental data
Standard optimization
Optimization with averaging

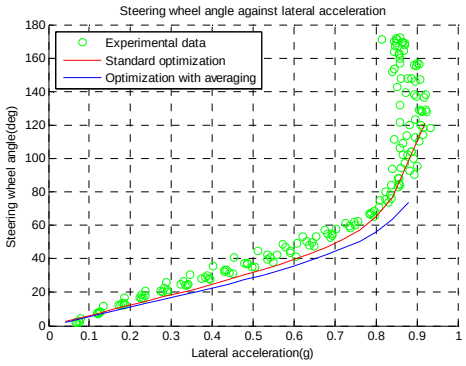
Steering wheel angle against lateral acceleration
Steering wheel angle(deg)
Lateral acceleration(g)
Experimental data
Standard optimization
Optimization with averaging

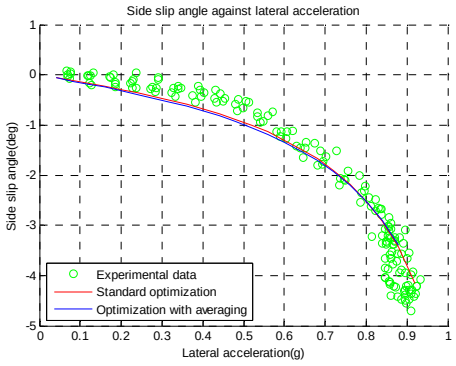
Side slip angle against lateral acceleration
Side slip angle(deg)
Lateral acceleration(g)
Experimental data
Standard optimization
Optimization with averaging

Simulation 1.4.3, Optimization on front and rear axle

Algorithm	Fminsearch					
Target	Coefficients					
Decimation	Yes					
Parameter E	Considered					
Nr. Of sets	One					
Duration	385.2789 s/147.9028 s					
Result	0.036885/0.092361/0.068					
Coefficients front	p_{Cy}	p_{Dy1}	p_{Dy2}	p_{Ey1}	p_{Ky1}	p_{Ky2}
Initial front	1.6000	1.3000	-0.1000	1.1500	-21.8000	1.3500
Optimized front	1.4481	1.0266	-0.1237	0.5658	-17.6390	2.1520
Coefficients rear	p_{Cy}	p_{Dy1}	p_{Dy2}	p_{Ey1}	p_{Ky1}	p_{Ky2}
Initial rear	1.6000	1.3000	-0.1000	1.1500	-21.8000	1.3500
Optimized rear	1.1858	1.2815	-0.1436	1.3437	-17.1933	1.0707
Scaling factors	λ_{Cy}	$\lambda_{\mu y}$	λ_{Ey}	λ_{Ky}		
	1.0000	1.0000	1.0000	1.0000		

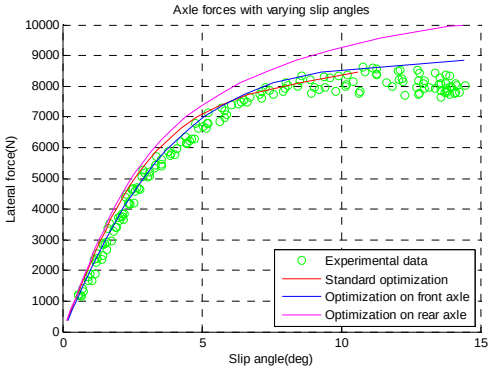

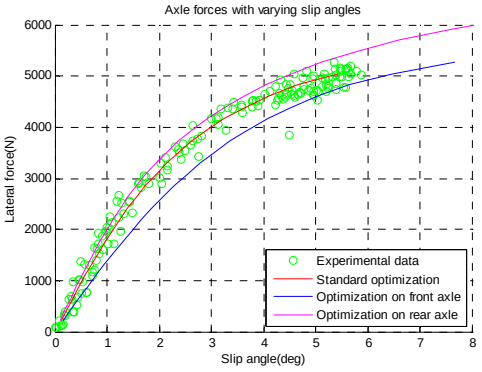

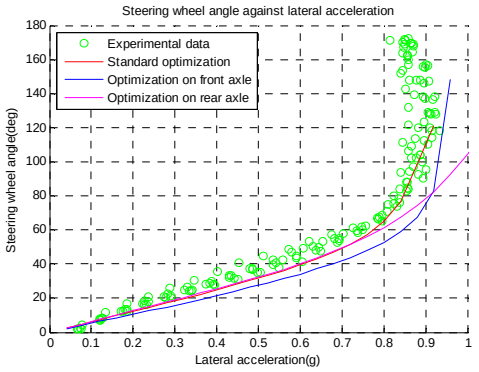

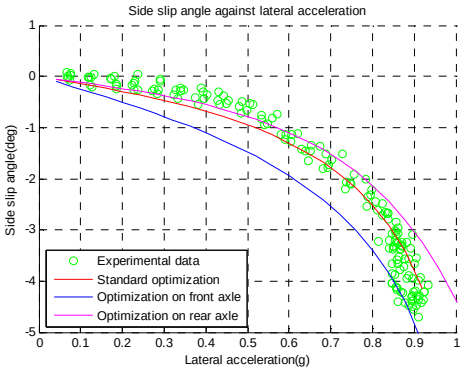

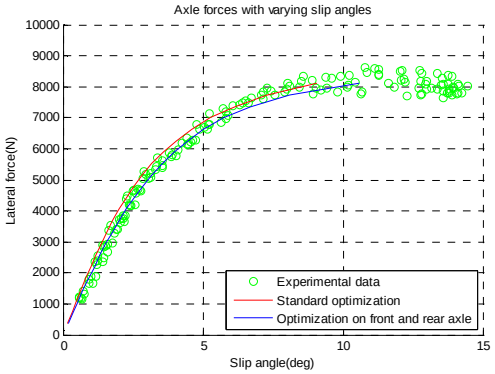
Axle forces with varying slip angles
Lateral force(N)
Slip angle(deg)
Experimental data
Standard optimization
Optimization on front and rear axle

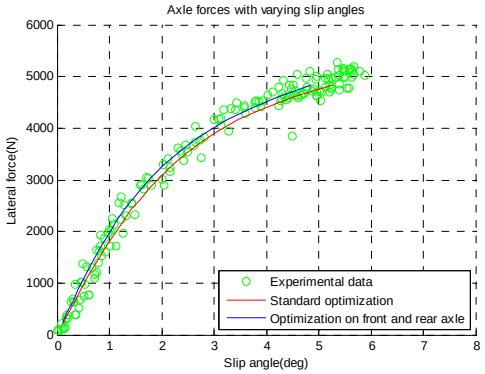
Axle forces with varying slip angles
Lateral force(N)
Slip angle(deg)
Experimental data
Standard optimization
Optimization on front and rear axle

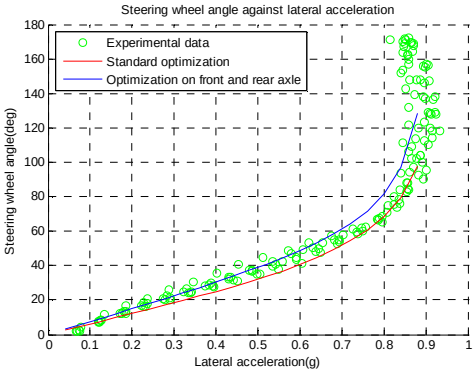
Steering wheel angle against lateral acceleration
Steering wheel angle(deg)
Lateral acceleration(g)
Experimental data
Standard optimization
Optimization on front and rear axle

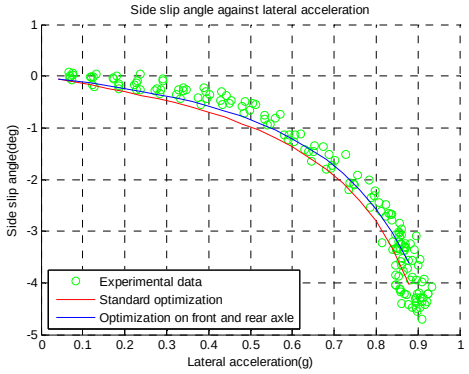
Side slip angle against lateral acceleration
Side slip angle(deg)
Lateral acceleration(g)
Experimental data
Standard optimization
Optimization on front and rear axle

G. Results optimizations Fourteen-DOF model

Simulation 2.1, Standard optimization with lsqnonlin

Algorithm	Lsqnonlin						
Target	Coefficients						
Decimation	No						
Parameter E	Considered						
Nr. Of sets	One						
Duration	2.2194e+004 s						
Result	0.0514						
Coefficients	p_{Cy}	p_{Dy1}	p_{Dy2}	p_{Ey1}	p_{Ey2}	p_{Ky1}	p_{Ky2}
Initial	1.3184	1.3075	0.3353	1.1549	0.9802	-23.0709	1.6647
Optimized	1.4233	1.2708	-0.2304	1.0190	0.9956	-23.1263	1.2740
Scaling factors	p_{Ky2}	λ_{Cy}	$\lambda_{\mu y}$	λ_{Ey}	λ_{Ky}		
Constant	1.0000	1.0000	1.0000	1.0000	0.8500		

Simulation 2.2.1, Optimization with lsqnonlin on scaling factors

Algorithm	Lsqnonlin						
Target	Scaling factors						
Decimation	No						
Parameter E	Not considered						
Nr. Of sets	One						
Duration	2.1771e+004 s						
Result	0.0582						
Coefficients	p_{Cy}	p_{Dy1}	p_{Dy2}	p_{Ey1}	p_{Ey2}	p_{Ky1}	p_{Ky2}
Constant	1.3184	1.3075	0.3353	1.1549	0.9802	-23.0709	1.6647
Scaling factors	λ_{Fz0}/p_{Ky2}	λ_{Cy}	$\lambda_{\mu y}$	λ_{Ey}	λ_{Ky}		
Initial	1.0000	1.0000	1.0000	1.0000	0.8500		
Optimized	1.0833	1.3141	0.7609	1.0029	0.9292		

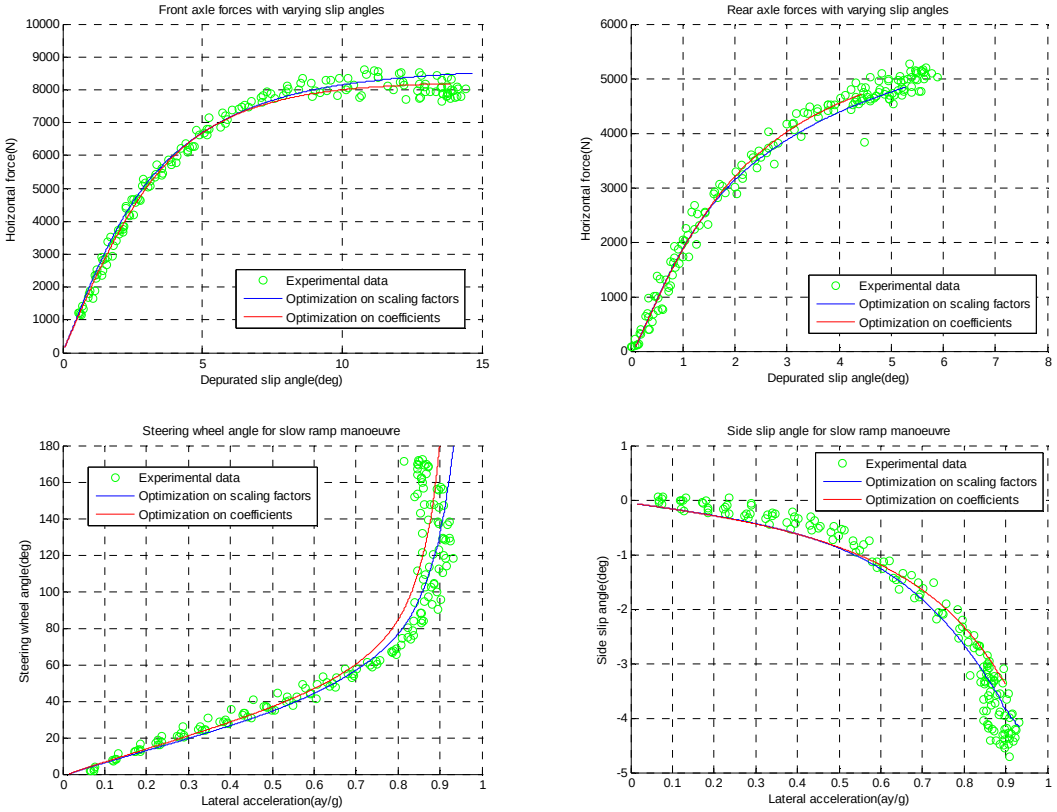

Simulation 2.2.2, Optimization with lsqnonlin with constant E

Algorithm	Lsqnonlin						
Target	Coefficients						
Decimation	No						
Parameter E	Not considered						
Nr. Of sets	One						
Duration	4.6349e+003 s						
Results	0.0521						
Coefficients	p_{Cy}	p_{Dy1}	p_{Dy2}	p_{Ey1}	p_{Ey2}	p_{Ky1}	p_{Ky2}
Initial	1.3184	1.3075	0.3353	1.1549	0.9802	-23.0709	1.6647
Optimized	1.5028	1.2247	-0.1626	1.1549	0.9802	-23.1243	1.2577
Scaling factors	p_{Ky2}	λ_{Cy}	$\lambda_{\mu y}$	λ_{Ey}	λ_{Ky}		
Constant	1.0000	1.0000	1.0000	1.0000	0.8500		

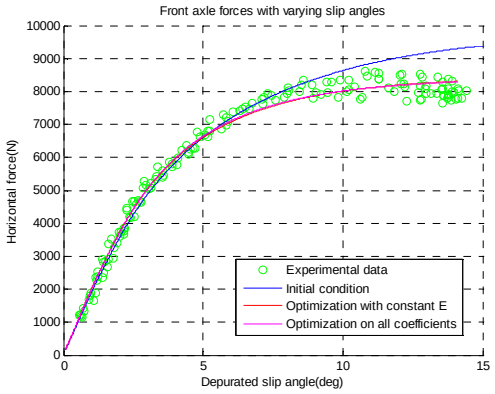

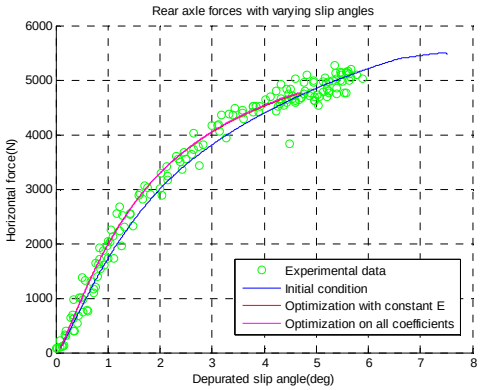

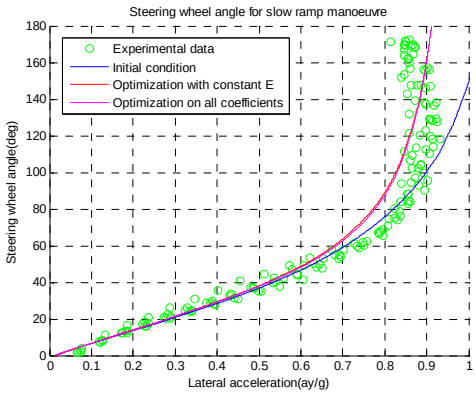

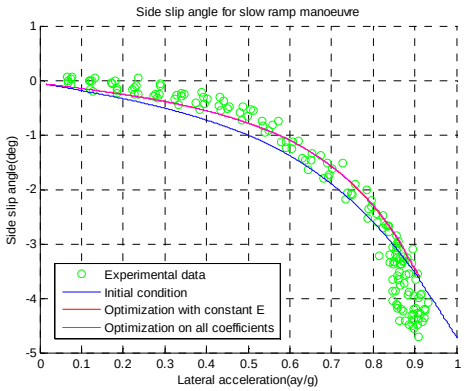

Simulation 2.3.1, Optimization with scaled error function

Algorithm	Lsqnonlin						
Target	Coefficients						
Decimation	No						
Parameter E	Not considered						
Nr. Of sets	One						
Duration	2.0921e+004 s						
Result	0.0531						
Coefficients	p_{Cy}	p_{Dy1}	p_{Dy2}	p_{Ey1}	p_{Ey2}	p_{Ky1}	p_{Ky2}
Initial	1.3184	1.3075	0.3353	1.1549	0.9802	-23.0709	1.6647
Optimized	1.5851	1.2474	-0.3044	0.9955	1.0587	-23.1237	1.4696
Scaling factors	p_{Ky2}	λ_{Cy}	$\lambda_{\mu y}$	λ_{Ey}	λ_{Ky}		
Constant	1.0000	1.0000	1.0000	1.0000	0.8500		

Simulation 2.3.2, Optimization with error function multiplied by slip angles

Algorithm	Lsqnonlin
Target	Coefficients
Decimation	No
Parameter E	Not considered
Nr. Of sets	One
Duration	3.3448e+004 s

Result	0.0524						
Coefficients	p_{Cy}	p_{Dy1}	p_{Dy2}	p_{Ey1}	p_{Ey2}	p_{Ky1}	p_{Ky2}
Initial	1.3184	1.3075	0.3353	1.1549	0.9802	-23.0709	1.6647
Optimized	1.5536	1.2430	-0.2553	0.9979	1.0592	-23.1178	1.2888
Scaling factors	p_{Ky2}	λ_{Cy}	$\lambda_{\mu y}$	λ_{Ey}	λ_{Ky}		
Constant	1.0000	1.0000	1.0000	1.0000	0.8500		

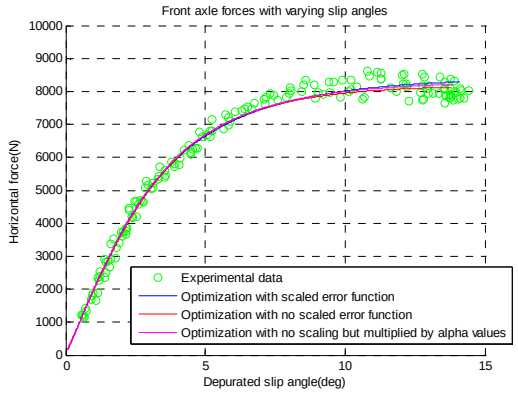

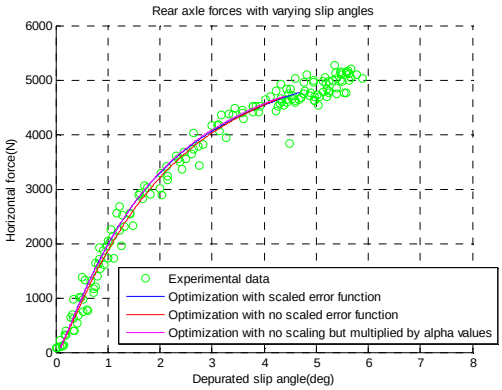

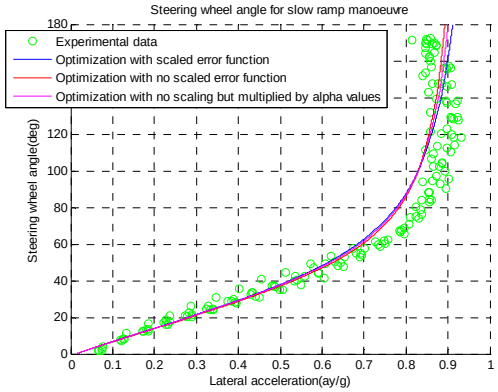

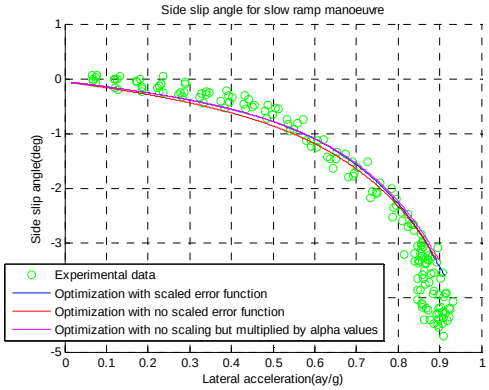

Simulation 2.3.3, Optimization with fminsearch

Algorithm	Fminsearch						
Target	Coefficients						
Decimation	No						
Parameter E	Considered						
Nr. Of sets	One						
Duration	9.8230e+003 s						
Result	0.0723						
Coefficients	p_{Cy}	p_{Dy1}	p_{Dy2}	p_{Ey1}	p_{Ey2}	p_{Ky1}	p_{Ky2}
Initial	1.3184	1.3075	0.3353	1.1549	0.9802	-23.0709	1.6647
Optimized	1.3422	1.1672	0.3219	1.3086	1.2178	-25.8676	0.9226
Scaling factors	p_{Ky2}	λ_{Cy}	$\lambda_{\mu y}$	λ_{Ey}	λ_{Ky}		
	1.0000	1.0000	1.0000	1.0000	0.8500		

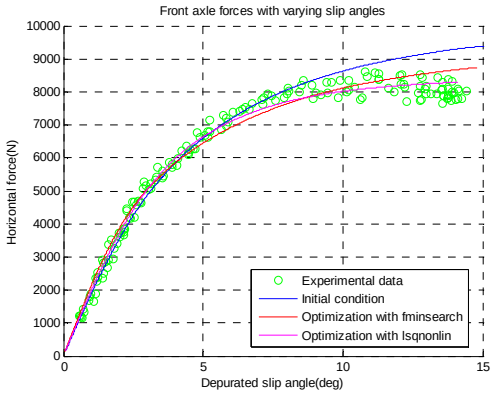

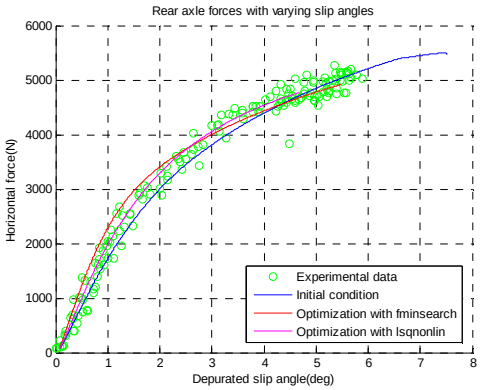

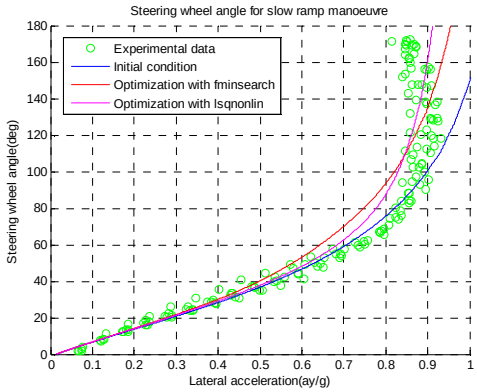

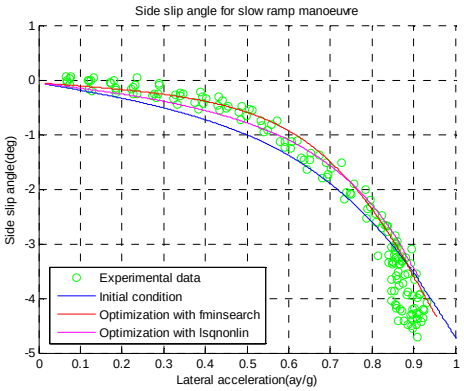

Simulation 2.4.1, Optimization with lsqnonlin handtuned initial conditions

Algorithm	Lsqnonlin						
Target	Coefficients						
Decimation	No						
Parameter E	Considered						
Nr. Of sets	One						
Duration	5.7126e+004 s						
Result	0.0530						
Coefficients	p_{Cy}	p_{Dy1}	p_{Dy2}	p_{Ey1}	p_{Ey2}	p_{Ky1}	p_{Ky2}
Initial	1.6	1.3075	-0.1	1.1549	0.9802	-21.8	1.35
Optimized	1.7980	1.2623	-0.3129	0.8687	0.8658	-21.8415	1.1458
Scaling factors	p_{Ky2}	λ_{Cy}	$\lambda_{\mu y}$	λ_{Ey}	λ_{Ky}		
Constant	1.0000	1.0000	1.0000	1.0000	0.8500		

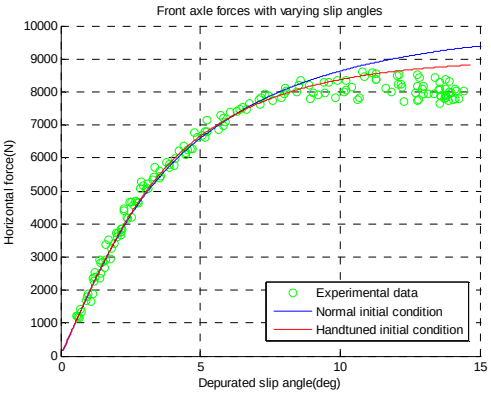
Front axle forces with varying slip angles
Horizontal force(N)
Depurated slip angle(deg)
Experimental data
Normal initial condition
Handtuned initial condition

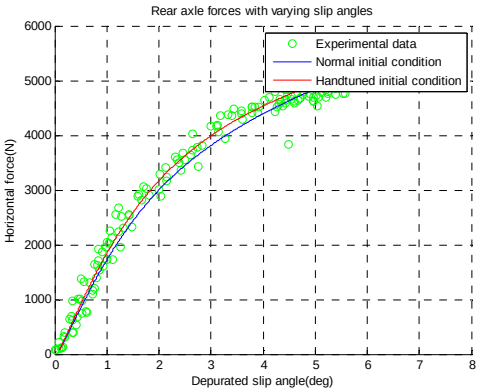
Rear axle forces with varying slip angles
Horizontal force(N)
Depurated slip angle(deg)
Experimental data
Normal initial condition
Handtuned initial condition

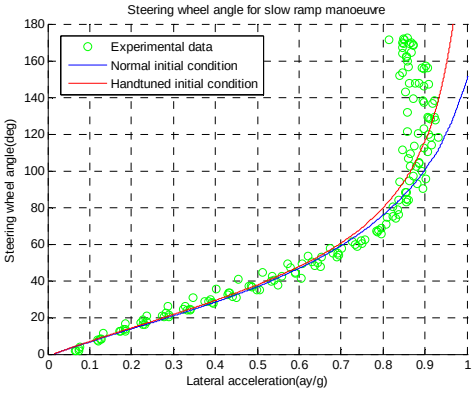
Steering wheel angle for slow ramp manoeuvre
Steering wheel angle(deg)
Lateral acceleration(ay/g)
Experimental data
Normal initial condition
Handtuned initial condition

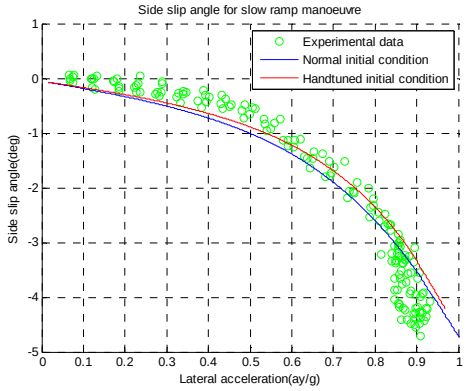
Side slip angle for slow ramp manoeuvre
Side slip angle(deg)
Lateral acceleration(ay/g)
Experimental data
Normal initial condition
Handtuned initial condition

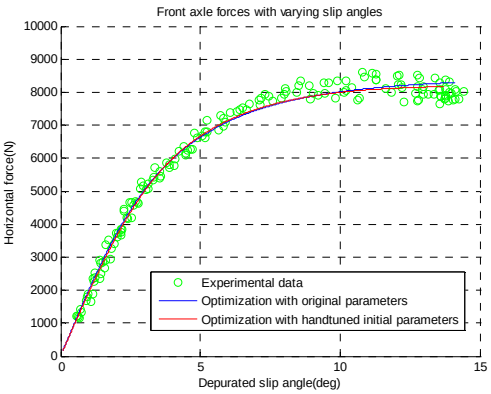
Front axle forces with varying slip angles
Horizontal force(N)
Depurated slip angle(deg)
Experimental data
Optimization with original parameters
Optimization with handtuned initial parameters

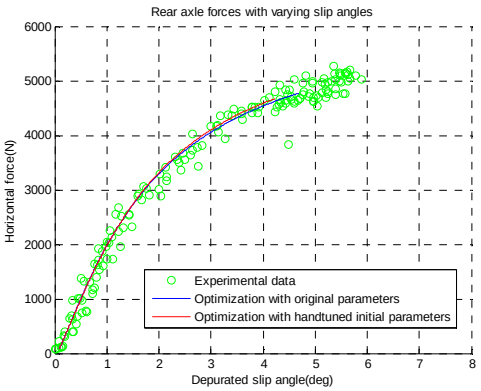
Rear axle forces with varying slip angles
Horizontal force(N)
Depurated slip angle(deg)
Experimental data
Optimization with original parameters
Optimization with handtuned initial parameters

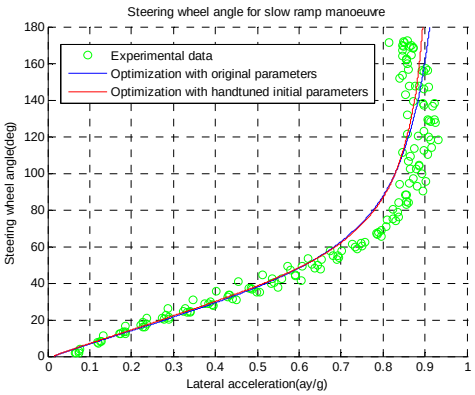
Steering wheel angle for slow ramp manoeuvre
Steering wheel angle(deg)
Lateral acceleration(ay/g)
Experimental data
Optimization with original parameters
Optimization with handtuned initial parameters

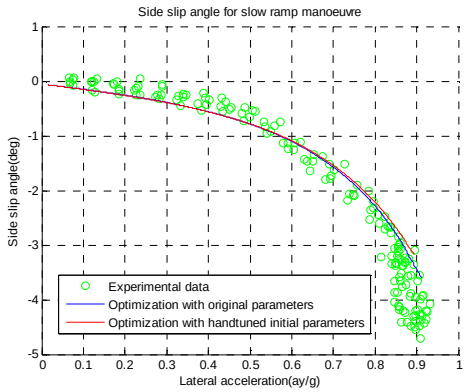
Side slip angle for slow ramp manoeuvre
Side slip angle(deg)
Lateral acceleration(ay/g)
Experimental data
Optimization with original parameters
Optimization with handtuned initial parameters

Simulation 2.4.2, Optimization with decimation

Algorithm	Lsqnonlin						
Target	Coefficients						
Decimation	Yes						
Parameter E	Considered						
Nr. Of sets	One						
Duration	1.6492e+004 s						
Result	0.0575						
Coefficients	p_{Cy}	p_{Dy1}	p_{Dy2}	p_{Ey1}	p_{Ey2}	p_{Ky1}	p_{Ky2}
Initial	1.3184	1.3075	0.3353	1.1549	0.9802	-23.0709	1.6647
Optimized	1.4925	1.2738	-0.1981	1.0553	1.0331	-22.9850	1.4025
Scaling factors	p_{Ky2}	λ_{Cy}	$\lambda_{\mu y}$	λ_{Ey}	λ_{Ky}		
Constant	1.0000	1.0000	1.0000	1.0000	0.8500		

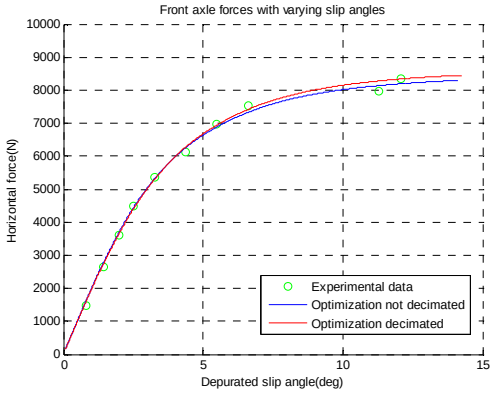

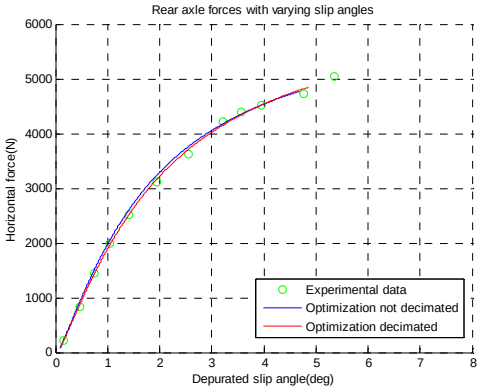

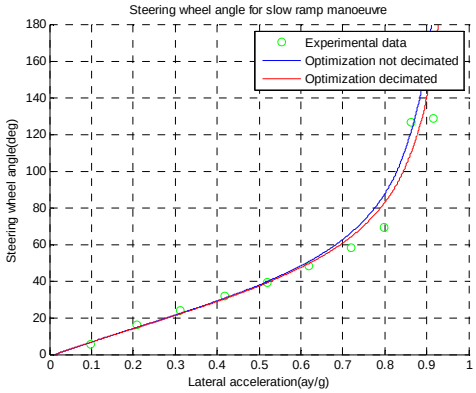

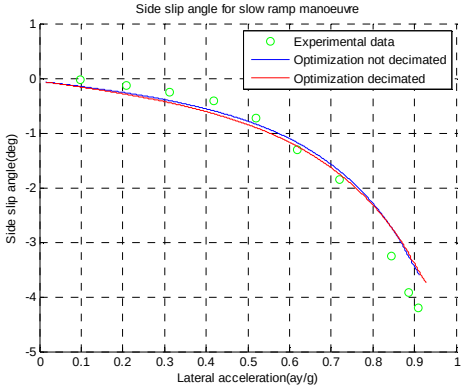

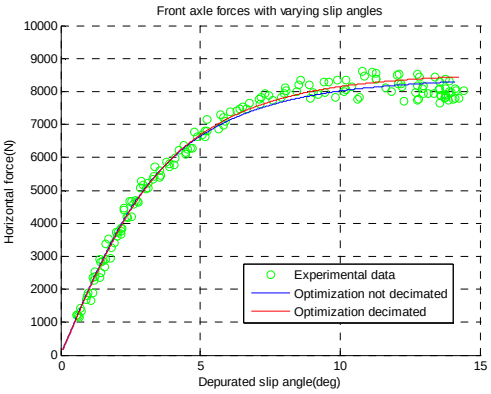

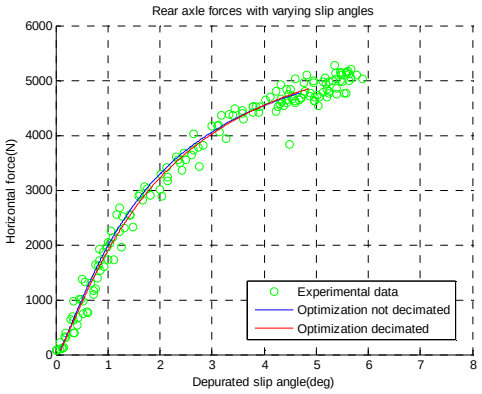

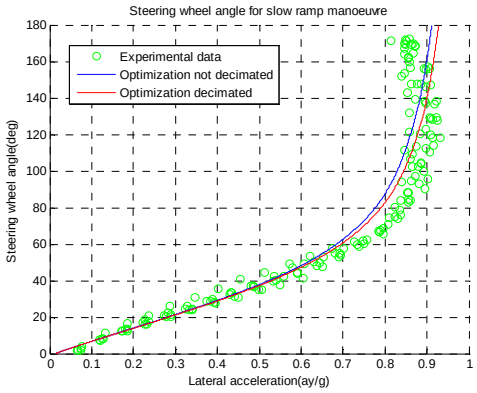

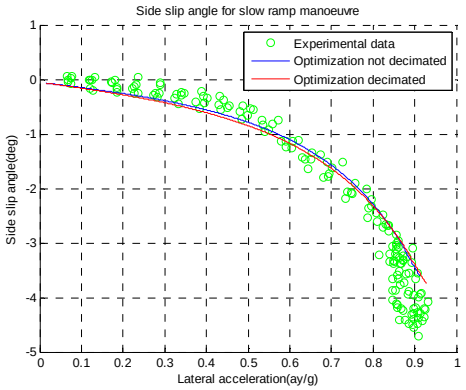

Simulation 2.4.3, Optimization with different datasets

Algorithm	Lsqnonlin						
Target	Coefficients						
Decimation	Yes						
Parameter E	Considered						
Nr. Of sets	One						
Duration	2.4721e+004 s/3.3512e+004						
Result	0.0234/0.0776/0.0444						
Coef. front	p_{Cy}	p_{Dy1}	p_{Dy2}	p_{Ey1}	p_{Ey2}	p_{Ky1}	p_{Ky2}
Initial	1.3184	1.3075	0.3353	1.1549	0.9802	-23.0709	1.6647
Optimized	2.0496	1.3009	-0.4748	0.8187	1.1353	-23.2097	1.4243
Coef. rear	p_{Cy}	p_{Dy1}	p_{Dy2}	p_{Ey1}	p_{Ey2}	p_{Ky1}	p_{Ky2}
Initial	1.3184	1.3075	0.3353	1.1549	0.9802	-23.0709	1.6647
Optimized	1.2379	1.1920	0.2117	1.1417	0.9900	-23.0874	1.4901
Scaling factors	p_{Ky2}	λ_{Cy}	$\lambda_{\mu y}$	λ_{Ey}	λ_{Ky}		
Constant	1.0000	1.0000	1.0000	1.0000	0.8500		

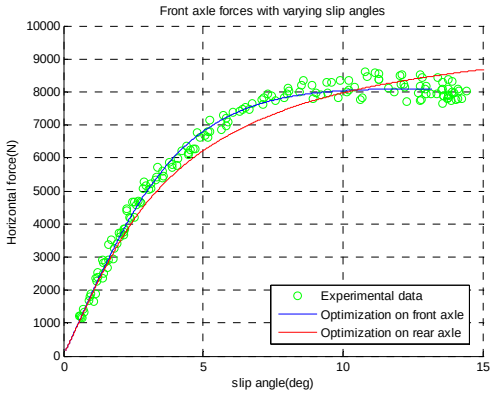
Front axle forces with varying slip angles
Horizontal force(N)
slip angle(deg)
Experimental data
Optimization on front axle
Optimization on rear axle

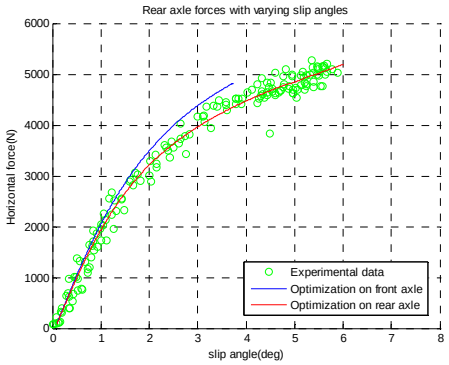
Rear axle forces with varying slip angles
Horizontal force(N)
slip angle(deg)
Experimental data
Optimization on front axle
Optimization on rear axle

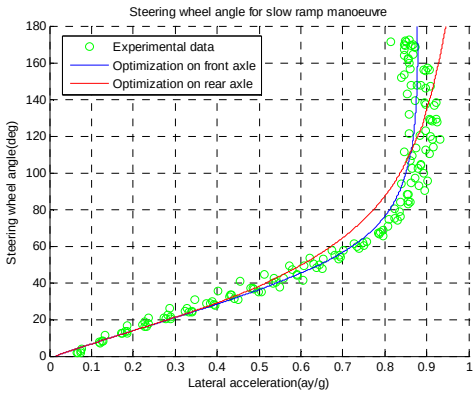
Steering wheel angle for slow ramp manoeuvre
Steering wheel angle(deg)
Lateral acceleration(ay/g)
Experimental data
Optimization on front axle
Optimization on rear axle

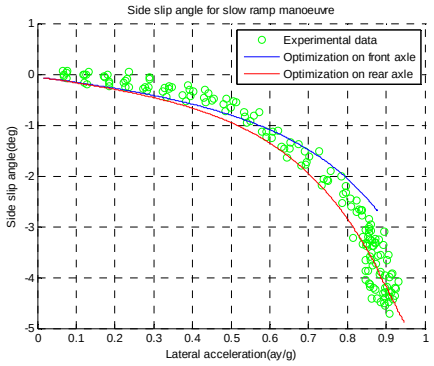
Side slip angle for slow ramp manoeuvre
Side slip angle(deg)
Lateral acceleration(ay/g)
Experimental data
Optimization on front axle
Optimization on rear axle

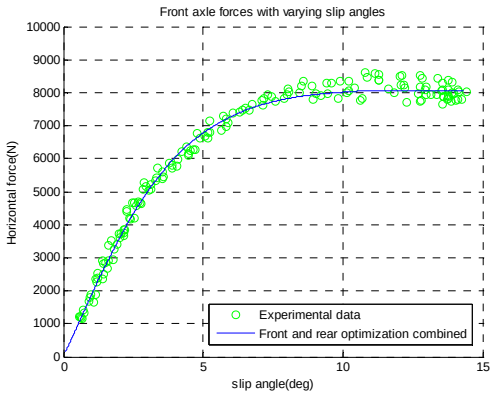
Front axle forces with varying slip angles
Horizontal force(N)
slip angle(deg)
Experimental data
Front and rear optimization combined

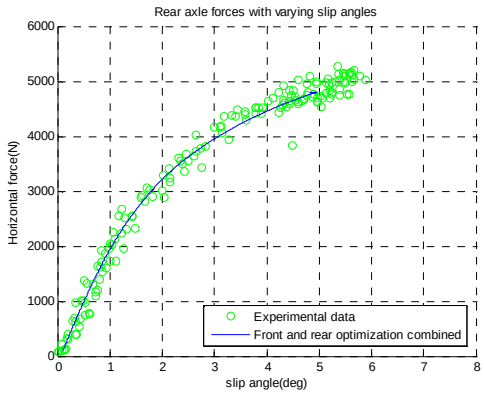
Rear axle forces with varying slip angles
Horizontal force(N)
slip angle(deg)
Experimental data
Front and rear optimization combined

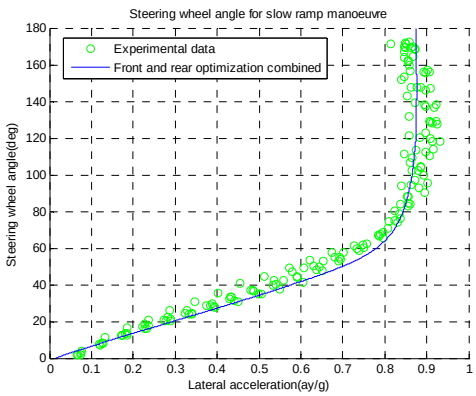
Steering wheel angle for slow ramp manoeuvre
Steering wheel angle(deg)
Lateral acceleration(ay/g)
Experimental data
Front and rear optimization combined

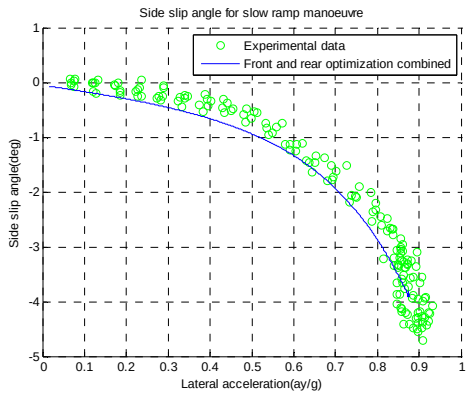
Side slip angle for slow ramp manoeuvre
Side slip angle(deg)
Lateral acceleration(ay/g)
Experimental data
Front and rear optimization combined